Master's thesis

NTNU
Norwegian University of Science and Technology
Faculty of Natural Sciences
Department of Physics

Karl Kristian Ladegård Lockert

Phonon Coupled Luttinger Liquids in a Haldane Armchair Nanoribbon

Master's thesis in Physics
Supervisor: Prof. Asle Sudbø
June 2021

NTNU
Norwegian University of
Science and Technology

Karl Kristian Ladegård Lockert

Phonon Coupled Luttinger Liquids in a Haldane Armchair Nanoribbon

Master's thesis in Physics
Supervisor: Prof. Asle Sudbø
June 2021

Norwegian University of Science and Technology
Faculty of Natural Sciences
Department of Physics

NTNU
Kunnskap for en bedre verden

Abstract

Motivated by a recently proposed method of probing topology in a spin wave model coupled to phonons, I study the single particle Green's function of topologically protected fermion states coupled to quantized lattice vibrations. The system under investigation is a Haldane Chern insulator on a graphene nanoribbon with armchair edge geometry. I explicitly demonstrate that this model host highly localized edge states which can be described by a one-dimensional fermionic theory of a many-body system. The electron-phonon coupling is found by projecting phonon eigenstates onto the edges using a nearest neighbor approximation. By bosonization of the fermionic fields close to the Fermi level, the Hamiltonian can be diagonalized in an exact manner. The representation of fermionic density-waves is found to be a combination of an orthogonal projection and a symplectic Bogoliubov-transform of uncoupled quantum harmonic oscillators. I first rederive earlier results, then proceed to generalize the method to allow for a density-density interaction, which suppresses the electron phonon coupling strength if repulsive. The inclusion of spin degrees of freedom renormalizes the electron phonon coupling by a constant factor. I derive several closed form approximations of the Green's function in the presence of a single acoustic phonon branch. On the graphene nanoribbon, I numerically calculate the relative corrections to the real space correlation function. In the absence of density-density interactions, the characteristic singularity representing linear motion is reduced by the onset of a particle-hole cloud lagging behind the itinerant electron density waves. In the presence of a Coulomb-like interaction, the long distance density waves oscillate with a finite plasma frequency, and further excitations acquire a mass. The consequence of a nonzero plasma frequency is that the single electron Green's function is modulated with a precocious particle-hole cloud.

Sammendrag

Det har nylig blitt foreslått en metode for å indirekte detektere topologi i en spinnbølgemodell koblet til fononer. Motivert av dette undersøker jeg én-partikkel Green-funksjonen til topologisk beskyttet fermionske kanttilstander koblet til kvantiserte gittervibrasjoner. Systemet er en Haldane-Chern-isolator på et grafén nanobånd med "lenestol"-kantgeometri. Jeg viser eksplisitt at denne modellen gir lokaliserte kanttilstander som kan bli beskrevet av en éndimensjonal fermionteori i et mangepartikkelsystem. Elektron-fonon-koblingen blir funnet ved å projisere fonon-egentilstander på kantene gjennom en nærmeste-nabo-tilnærming. Ved å bosonisere fermionfeltene nære Ferminivået kan Hamilton-operatoren diagonaliseres nøyaktig. Elektrontetthetsbølgene kan da representeres som en kombinasjon av en ortogonal projeksjon og en symplektisk Bogoliubovtransformasjon av kvanteharmoniske oscillatorer. Jeg gjenutleder kjente resultater, og fortsetter ved å generalisere metoden til å kunne inkorporere tetthet-tetthet-interaksjoner, som reduserer elektron-fonon-koblingen i det repulsive tilfellet. Inkluderingen av spinn-frihetsgrad renormerer elektron-fonon-koblingen med en konstant faktor. Gjennom forenklinger finner jeg flere lukkede uttrykk for Green-funksjonen i nærvær av én akustisk fononogren. På nanobåndet finner jeg den relative korreksjonen til Green-funksjonen ved numeriske beregninger. I fravær av interaksjoner mellom tetthetsbølger finner jeg at den karakteristiske singulariteten i korrelasjonsfunksjonen som representerer rettlinjet bevegelse blir redusert når en skyfaktor av partikkel-hull-eksitasjoner som henger etter tetthetsbølgene blir synlig. Med en Coulomb-type interaksjon tilstede vil tetthetsbølgene oscillere med en karakteristisk plasmafrekvens, og videre eksitasjoner i denne plasmaen blir massive. Konsekvensen av en plasmafrekvens ulik null er at én-elektron Green-funksjonen blir modulert med en fremskreden skyfaktor.

Preface

This Master thesis is the culmination of research conducted in the last of a two-year Master Program in Physics at the Norwegian University of Science and Technology (NTNU). I have had the great pleasure of writing my thesis at the Center for Quantum Spintronics. This also concludes a five-year endeavor in the field of physics, which has been the source of fun and great inspiration, but also vast confusion and self-doubt. Who would have guessed that writing a Master thesis (during a pandemic) is hard? During these years, I have found great joy in attending the courses taught by Prof. Asle Sudbø, which was why I asked him to be my supervisor. I thank him for his invaluable enthusiasm and profound insights. His encouragement, guidance and support has been paramount, especially so during a demanding year. I am grateful to my fellow students for great discussions and good laughs. Finally, I thank my family and friends for kind love, support and encouragement which has helped me persist.

Karl Kristian Ladegård Lockert
Trondheim, Norway
June 2021

Contents

Chapter 1.
Introduction

1.1 Motivation and Background

Quantum states of matter known as topological insulators has been a subject of great attention in recent years. Apart from being of fundamental research interest, these materials has promising properties relevant for future devices in information technology [1–3]. They are insulators that host gapless surface states residing in the insulating bulk gap which are protected by time reversal symmetry [4]. The existence of these states is directly related to topological invariants of the bulk [5].

Using topology as a way of classifying quantum states of matter was first proven useful by Thouless et al. [6], after the discovery of a quantized Hall (QH) effect [7]. A few years later, Haldane [8] proposed a new model of the QH state, whose phases is characterized by a topological invariant called the Chern number. Thouless, Haldane and Berezinskii was awarded the 2016 Nobel Prize in Physics "for theoretical discoveries of topological phase transitions and topological phases of matter" [9].

The inclusion of spin-orbit interactions was shown to give rise to the Spin Quantum Hall (QSH) state [10], which is an insulating phase protected by time reversal symmetry exhibiting a spin polarized Hall conductance. This state was predicted [11] and shown [1] to exist in HgTe quantum wells, and has later been vastly studied both theoretically and experimentally. The QSH state is the two-dimensional rendition of a topological insulator hosting spin-polarized states localized at the edges.

Recently a method of experimentally probing topology in a spin-wave model has been proposed by measuring a chirality in observed signal output from phonon modes propagating in opposite directions at the edge of a honeycomb nanoribbon [12]. This was proposed for an "armchair" edge geometry, since these host phonon modes highly localized at the edges, contrary to the alternative "zigzag" geometry. This begs the question of what will happen when these topological magnons are replaced by itinerant fermions at the edges, and how much of the topologically protected states remain stable even in the presence of phonon-interactions.

The coupling between electrons and phonons is an important interaction, most notably because it can give rise to the condensation of Cooper pairs [13], which are bound electron states which can lower the free energy of the system. These pairs the constituent excitations in the Bardeen-Cooper-Schrieffer (BCS) theory of superconductivity [14]. In topological insulators, It has been shown that the electron-phonon coupling can drive a topological phase transition, and hence be used as a direct probing of topological invariants [15].

Motivated by this, I will in this thesis study the problem of topological edge states in a graphene nanoribbon with armchair edges, coupled to quan-

tized lattice vibrations. More specifically, I will compute corrections to the single particle Green's function caused by interactions with phonons – both in absence and presence of fermionic two-body scattering such as the Coulomb interaction. The localized edge states of a QSH insulator are effectively one dimensional, and corresponds to helical Tomonaga-Luttinger liquids [16, 17] which also has been proposed to exist at the edges of a QH graphene nanoribbon [18].

Analogous to Landau's theory of interacting fermions [19], Haldane [20] coined the term "Luttinger liquid" to the description of interacting fermions in one dimension, where the vastly successful Fermi liquid paradigm breaks down [21, 22]. This happens because single electron excitations in one dimension are not possible due to the Pauli exclusion principle and reduced kinematics. Similar to how vehicles in a traffic jam only moves as a collective unit, so does fermions in one dimension [23]. Phenomena such as separation of spin and charge degrees of freedom, and anomalous dimensions of operators leading to power-law decay of correlation functions occur [24]. Neither of which can be explained in the Landau quasiparticle picture. By linearizing the spectrum of a one dimensional many-fermion system close to the Fermi points, Tomonaga [25] showed that the fundamental excitations of the system may be described in terms of quantized fields obeying Bose statistics. Some years later, Luttinger [26] presented the exact solution of a system described by massless fermions with an infinitely filled Dirac sea. It was later shown that these models are essentially equivalent in the long distance limit [27], and is hence often called the Tomonaga-Luttinger model.

The effect of lattice vibrations in one dimension has been investigated in general terms utilizing the technique described by Tomonaga [28–30]. Using some of these results, the calculation of single particle correlation functions in the presence of a single phonon branch has been carried out by Meden et al. [31], who has authored and co-authored several papers on the spectral properties of Luttinger liquids [32–36]. A recent study by Hsieh et al. [37] presents a general theory for experimentally probing helical Luttinger liquids on QSH insulators at finite temperature, and may be employed to study the effects of phonons.

1.2 Structure of Thesis

The main body of this thesis is in chapter 6, whereas chapters 2, 3 and 5 provide theoretical preliminaries and derivations of useful identities. In chapter 4, I calculate properties of the system to set the context for subsequent chapters. Lastly I summarize in chapter 7.

In chapter 2 I recapitulate the basics of many-body quantum mechanics.

This includes a section on the second quantization formalism, boson coherent states, expectation values and Green's functions, and a section on Fermi liquids with connection to experiments.

In chapter 3, an introduction to the states of matter known as topological insulators is presented. This chapter has a particular focus on the existence of gapless one-dimensional electron states on the edges of Quantum Spin Hall insulators, the two-dimensional rendition of a topological insulator.

Chapter 4 provides explicit calculations of the Haldane model, which is a topological model for a Quantum Hall insulator. I show the existence of localized edge states on a nanoribbon with armchair edge geometry, and further compute the phonon spectrum and electron-phonon coupling matrix for the bulk and armchair geometry.

I continue in chapter 5 by introducing the Luttinger liquid phenomenology and further deriving the bosonization identity of fermionic fields in one dimension. As an introductory calculation, I calculate the single particle Green's function in absence of lattice vibrations.

Phonon corrections to the single particle Green's function are computed in chapter 6, where I derive a method of exact diagonalization for the electron-phonon Hamiltonian. This is done by utilizing the theoretical framework introduced in the preceding chapters. Multiple systems are considered, and several closed form representations of the Green's functions are explicitly calculated when only a single phonon branch is present. For the full phonon spectrum of the graphene nanoribbon, I numerically compute the absolute relative difference in the interacting and non-interacting cases.

Finally, the thesis is summarized in chapter 7, where I also mention possible extensions of the work in this thesis.

Chapter 2.
Many-Body Quantum Mechanics

Many-Body Quantum Mechanics

Finding the exact solution of the quantum mechanical problem for a single particle in an arbitrary potential is in general considered to be a hard problem, and only exactly solvable in a few cases. Solving the quantum mechanical problem for many interacting particles is thus not surprisingly an even harder problem, and it is computationally expensive to solve even a few interacting states without a further developed theory. Nevertheless, significant progress can be made in the quantum theory of solids.

2.1 Second Quantization

The theoretical framework of this thesis is the "second quantization" representation of many body quantum mechanics. In this section, I will give a short introduction to this formalism, also commonly called the "occupation number representation". There are many excellent books [38–41] describing this theoretical framework, and for brevity I will skip many details in the construction and indulge the reader to study these for their own pleasure.

2.1.1 Occupation Number Representation

As with many things quantum in nature, the Schrödinger equation is the microscopic description of the dynamics in a non-relativistic system. A one-particle quantum state is denoted by the vector $|\psi_\lambda(\mathbf{r})\rangle$ residing in a Hilbert space $\mathcal{H}$. This state is described unambiguously by a set of quantum numbers λ dependent on the Hamiltonian for which the system is modeled. These might for example be $\lambda = (n, l, m_l, m_s)$ for Hydrogen-like atoms, or $\lambda = (\mathbf{k}, \sigma)$ for translation invariant systems, as is very common in solids.

The same notation and identification of quantum states holds in a many-particle system, where the wave function of the entire ensemble

$$|\psi\rangle = |\psi(\mathbf{r}_1, \mathbf{r}_2, \ldots, \mathbf{r}_N)\rangle \tag{2.1}$$

describe the dynamics of all N particles. This state lives in a Fock-space which is a direct sum over N-particle Hilbert spaces. Since quantum mechanics deals with identical, i.e. indistinguishable particles, the total wave function has to obey certain symmetry constraints. For fermions, an exchange of coordinates between two one-particle states results in a relative minus sign in the total wave function. This has no physical significance if the coordinates are different, since

$$|\Psi(\ldots, x_i, x_j, \ldots, x_N)|^2 = |\Psi(\ldots, x_j, x_i, \ldots, x_N)|^2, \tag{2.2}$$

however if two coordinates x_i, x_j are equal, the relative minus sign appearing from the exchange $x_i \leftrightarrow x_j$ can only mean that the wave function is identical to zero, a manifestation of the Pauli exclusion principle. Here, $x_i = (\mathbf{r}, \sigma)$ is the coordinates for a one particle state with quantum numbers λ_i. This many-particle state may be constructed through a Slater determinant by N single-particle wave functions.

Second quantization is a way of representing the wave function without considering the notion of "which particle is in which state", since this is not a question of physical significance due to the indistinguishability of the particles.

This way of treating the system, also called the occupation number representation, considers only the occupancy of each quantum state in the N-particle system (as the name suggests). A normalized state in this representation is written as

$$|N\rangle = |n_{\lambda_1}, n_{\lambda_2}, \ldots, n_{\lambda_N}\rangle\,, \tag{2.3}$$

where n_{λ_i} is the occupancy number of a single particle state characterized by the quantum number(s) λ_i. For fermions, n can only take the numbers $0, 1$, but for bosons, all non-negative integers are allowed. This formalism is based on creation and annihilation operators which respectively increases or decreases the occupancy of a given single particle state. For fermions, these operators are most commonly denoted $c_\lambda^\dagger$ and c_λ. $c_\lambda^\dagger$ is an operator that creates a particle in the state described by λ, which is to say that $n_\lambda \to n_\lambda + 1$. Correspondingly, c_λ has the effect of reducing n_λ by one. Since n_λ is either 0 or 1, acting with either $c_\lambda^\dagger$ or c_λ destroys the state

$$c_\lambda c_\lambda\,|N\rangle = c_\lambda^\dagger c_\lambda^\dagger\,|N\rangle = 0. \tag{2.4}$$

The symmetries of the total wave function is taken care of by the action of these operators on the many-particle state, and one can show that the fermionic creation and annihilation operators must satisfy the anticommutation relations

$$\{c_\lambda, c_{\lambda'}\} = \{c_\lambda^\dagger, c_{\lambda'}^\dagger\} = 0 \qquad\qquad \{c_\lambda, c_{\lambda'}^\dagger\} = \delta_{\lambda,\lambda'}, \tag{2.5}$$

while bosonic operators obey the commutation relations

$$[b_\lambda, b_{\lambda'}] = [b_\lambda^\dagger, b_{\lambda'}^\dagger] = 0 \qquad\qquad [b_\lambda, b_{\lambda'}^\dagger] = \delta_{\lambda,\lambda'}. \tag{2.6}$$

So far, these operators provide a rich mathematical framework for representing many-body quantum states, and the field operators $\psi^\dagger(x,t)$ and $\psi(x,t)$ can now be introduced. These operators create or annihilate quantized excitations in a fermionic matter field at specified coordinates, and are defined by

$$\psi^\dagger(x,t) = \sum_\lambda \phi^*_\lambda(x) c^\dagger_\lambda(t) \tag{2.7a}$$

$$\psi(x,t) = \sum_\lambda \phi_\lambda(x) c_\lambda(t), \tag{2.7b}$$

where ϕ_λ is a single particle wave function. I will come back to how time appears in the operators $c^\dagger_\lambda(t), c_\lambda(t)$. The field operators are the ones that create and destroy fermions in the many-body system at specified time and coordinate.

2.1.2 Operators in Second Quantization

Single particle operators are operators that act only on individual particles. In second quantization, such operators are represented by a sum of the creation and annihilation operators for different quantum states λ. The amplitude for each combination of operators is given by the overlap between the single particle states ϕ_λ that are solutions of the time independent Schrödinger equation

$$\hat{h}_1(x_i)\phi_\lambda(x_i) = E_\lambda \phi_\lambda(x_i), \tag{2.8}$$

where $\hat{h}_1$ is a term in the many-body Hamiltonian that only considers individual particles. A general form for single particle operators in second quantization is the sum of over the amplitudes for single particle transitions, and takes the form

$$T = \sum_{\lambda,\lambda'} t_{\lambda,\lambda'} c^\dagger_\lambda c_{\lambda'}, \tag{2.9}$$

with

$$t_{\lambda,\lambda'} = \langle \lambda | T | \lambda' \rangle = \int \mathrm{d}x\, \phi^*_\lambda(x) \hat{T}(\hat{x},\hat{p}) \phi_{\lambda'}(x). \tag{2.10}$$

Here, the hat is present to discern the operator acting on a many-body state with the operator acting on distinct wave functions. Using the field operators defined in eq. (2.7), a general single particle operator takes the form [38]

$$T = \int \mathrm{d}x\, \psi^\dagger(x) \hat{T}(\hat{x},\hat{p}) \psi(x). \tag{2.11}$$

One can in a similar fashion find the second quantization representation of two-particle operators. The result is

$$V = \sum_{\lambda_1,\ldots,\lambda_4} v_{\lambda_1,\ldots,\lambda_4} c^\dagger_{\lambda_1} c^\dagger_{\lambda_2} c_{\lambda_3} c_{\lambda_4} \tag{2.12}$$

with

$$\begin{aligned} v_{\lambda_1,\ldots,\lambda_4} &= \langle \lambda_1, \lambda_2 | V(\hat{x}_1, \hat{x}_2) | \lambda_3, \lambda_4 \rangle \\ &= \int \mathrm{d}x_1 \int \mathrm{d}x_2 \, \phi^*_{\lambda_1}(x_1) \phi^*_{\lambda_2}(x_2) \hat{V}(\hat{x}_1, \hat{x}_2) \phi_{\lambda_3}(x_2) \phi_{\lambda_4}(x_1). \end{aligned} \tag{2.13}$$

Thus, the matrix element $v_{\lambda_1,\ldots,\lambda_4}$ is the overlap integral of wave functions that have been acted upon. Note for instance that if $\hat{V} = 1$, the matrix element become

$$v_{\lambda_1,\ldots,\lambda_4} = \delta_{\lambda_1\lambda_4}\delta_{\lambda_2\lambda_3}. \tag{2.14}$$

2.1.3 Boson Coherent States

I have introduced the concept of creation and annihilation operators as a useful way of representing one- or two-particle operators acting on an N-particle state $|N\rangle$. A natural question arising is what the eigenstates of such operators are. These states are called coherent states. For the creation operator $b^\dagger_\lambda$, the action of operating on a state $|\beta\rangle$ consisting of $n_\lambda = n$ particles of type λ is increasing the number to $n_\lambda = n + 1$. Therefore, there cannot exist a superposition of states whose linear combination is an eigenstate of the creation operator. For the annihilation operator b_λ, the state of affairs is disparate. The defining equation for a boson coherent state is

$$b_\lambda \, |\beta\rangle = \beta_\lambda \, |\beta\rangle \, , \tag{2.15}$$

i.e. $|\beta\rangle$ is an eigenstate of each b_λ, with eigenvalues $\beta_\lambda \in \mathbb{C}$. The construction of $|\beta\rangle$ is then [40, 41]

$$|\beta\rangle = \exp\left(\sum_\lambda \beta_\lambda b^\dagger_\lambda \right) |0\rangle \, , \tag{2.16}$$

where $|0\rangle$ is the vacuum and the exponential function is defined in terms of its Taylor series. The coherent boson state is therefore an infinite linear combination of states with arbitrary number of particles of each kind. Since $|\beta\rangle$ is an eigenstate of destruction operators, such a state will be difficult to destroy if properly manufactured in an experiment, and thus have a minimal decoherence.

2.2 Expectation Values and Green's Functions

2.2.1 Observables and Time Evolution

The expectation value of an operator $\hat{O}$ corresponding to an observable quantity O in a given state is

$$O_i = \langle \hat{O} \rangle_i = \langle \Psi_i | \hat{O} | \Psi_i \rangle \,, \tag{2.17}$$

where $|\Psi\rangle$ is an eigenstate of the system. The energy of the many particle ground state is for instance

$$E_0 = \langle H \rangle_{\mathrm{GS}} \equiv \langle \Psi_{\mathrm{GS}} | H | \Psi_{\mathrm{GS}} \rangle \,. \tag{2.18}$$

Temperature can be included in the expectation values by computing them in the canonical ensemble. The thermal density matrix is equal to the quantum mechanical density matrix $\sum_i |\Psi_i\rangle\langle\Psi_i|$ weighted with a Boltzmann factor for each projection, resulting in

$$\hat{\rho} = \sum_i \mathrm{e}^{-\beta E_i} |\Psi_i\rangle\langle\Psi_i| = \mathrm{e}^{-\beta H}. \tag{2.19}$$

The thermal partition function is then written as

$$Z = \mathrm{Tr}\, \hat{\rho}, \tag{2.20}$$

and expectation values for an observable at finite temperature is then

$$\langle \hat{O} \rangle_T = \frac{1}{Z} \mathrm{Tr}\Big(\hat{O} \hat{\rho} \Big). \tag{2.21}$$

A non-relativistic quantum mechanical state is as mentioned governed by the Schrödinger Equation

$$i \frac{\partial \, |\Psi(t)\rangle}{\partial t} = H \, |\Psi(t)\rangle \,, \tag{2.22}$$

which has a symbolic solution

$$|\Psi(t)\rangle = \mathrm{e}^{-iHt} \, |\Psi_0\rangle \,, \tag{2.23}$$

where again functions acting on a Hilbert space $\mathcal{H}$ is defined through its Taylor series [38], and $|\Psi_0\rangle$ is the initially prepared state. I have set $\hbar \equiv 1$. To see how observable quantities change over time, I insert eq. (2.17) and compute

$$O(t) = \langle \Psi(t) | \hat{O} | \Psi(t) \rangle = \langle \Psi_0 | \mathrm{e}^{iHt} \hat{O} \mathrm{e}^{-iHt} | \Psi_0 \rangle = \langle \Psi_0 | \hat{O}(t) | \Psi_0 \rangle \,, \tag{2.24}$$

where I defined the time-evolved operator

$$\hat{O}(t) = \mathrm{e}^{iHt}\hat{O}\mathrm{e}^{-iHt}. \tag{2.25}$$

This marks the transition from the Schrödinger picture (where all states are time-dependent and operators not) to the Heisenberg picture (where the state of affairs is the opposite). The explicit time dependence depends on the various systems, but can often be computed using the Baker-Hausdorff formula in eq. (A.2.3). The (thermal) expectation values of the number operator $\langle c_\mu^\dagger c_\mu \rangle$ for a fermionic field follow the Fermi-Dirac distribution $n_F(\varepsilon_k)$ if the system is diagonal in the c_μ-basis with dispersion ε_k. For the bosonic number operator, the expectation value $\langle b_\mu^\dagger b_\mu \rangle$ follow the Bose-Einstein distribution $n_B(\omega_q)$ on the same terms. These distributions are given by

$$n_F(\varepsilon_k) = \frac{1}{\mathrm{e}^{\beta\varepsilon_k} + 1} \tag{2.26a}$$

$$n_B(\omega_q) = \frac{1}{\mathrm{e}^{\beta\omega_q} - 1}, \tag{2.26b}$$

where $\beta = \frac{1}{k_B T}$ is the inverse temperature.

2.2.2 Green's Functions

Green's functions are in general the response of a system due to a unit impulse at a given space-time coordinate. Mathematically, a general Green's function of two variables is defined as the solution to

$$\mathcal{L}G(x,t;x',t') = \delta(x-x')\delta(t-t'), \tag{2.27}$$

where $\mathcal{L}$ is a linear operator. If the Green's function for a system described by a differential equation is known, one can obtain the system's response from arbitrary sources by integration over all space-time coordinates.

In solid state physics, the goal is often to compute physical quantities such as electric currents, magnetic response, spin-currents and more. To do this, the quantum mechanical version of the Green's function is needed. The linear operator in eq. (2.27) can then be replaced by the Schrödinger equation in eq. (2.22). In field theories, however, the term Green's function refers to a different definition, which is not the solution to a linear differential equation except for the case of free Fermi / Bose gas for which the term originated [38].

Consider a fermion with quantum number μ that is injected into the system at coordinate x' and at time t', and ask how likely it is that a fermion with the same label μ is ejected at position x at time t. This probability is described through the Green's function

$$G(x,t;x',t') = -i\left\langle \mathcal{T}\left(\psi(x,t)\psi^\dagger(x',t')\right)\right\rangle, \tag{2.28}$$

where $\mathcal{T}$ is a time-ordering operator. The "retarded" and "advanced" Green's functions are also convenient quantities, and are defined as

$$G^R(x,t;x',t') \equiv -i\Theta(t-t')\,\langle\{\psi(x,t),\psi^\dagger(x',t')\}\,\rangle \tag{2.29a}$$
$$G^A(x,t;x',t') \equiv i\Theta(t'-t)\,\langle\{\psi(x,t),\psi^\dagger(x',t')\}\,\rangle\,. \tag{2.29b}$$

The poles of the Green's function give information about the energy spectrum of the system, making it an important quantity for comparison between theory and experiment.

The advanced and retarded Green's function may be written in terms of "lesser" and "greater" Green's functions

$$iG^>(x,t;x',t') \equiv \langle\psi(x,t)\psi^\dagger(x',t')\rangle \tag{2.30a}$$
$$iG^<(x,t;x',t') \equiv \langle\psi^\dagger(x',t')\psi(x,t)\rangle \tag{2.30b}$$

by

$$G^R = \theta(t-t')(G^> + G^<) \tag{2.31a}$$
$$G^A = -\theta(t'-t)(G^> + G^<) \tag{2.31b}$$

The Greens's function also allows for the computation of average values of observable quantities in the ground state. By taking a one-particle operator T as in eq. (2.11), the average value in the ground state is is [38]

$$\langle\hat{T}\rangle = -i\int \mathrm{d}x \lim_{\substack{x'\to x\\ t'\to t+0^+}} T(\hat{x},\hat{p})G(x,t;x',t'). \tag{2.32}$$

2.3 Fermi Liquid Theory

The free electron gas is an exactly solvable model of a quantum many-body problem. Landau wondered how much of the pure electron excitations that continue to exist whilst slowly adding interactions between the particles. This is the basis for Fermi liquid theory [19], which considers systems of interacting particles obeying Fermi statistics [38]. In two or three dimensions, one can find an escape route to solve the many-body problem by incorporating interactions in the system parameters of new types of excitations that only resemble the free electrons [23]. Landau [19] originally developed the theory of Fermi liquids in an effort to solve the problem of interacting fermions. He argued that the classification of states in the non-interacting problem would be invariant when turning on interactions adiabatically. In this way one could associate the fundamental excitations of the interacting fermions, the Fermi liquid quasi-particles, with the excitations of the free fermionic problem in a one-to-one

correspondence. The fundamental excitations of a Fermi liquid is not individual fermions, but rather fermions dressed by particle-hole-excitations [22], with a reduced discontinuity of the occupation number at the Fermi surface for $T = 0$. This discontinuity is sometimes referred to as the "quasiparticle residue".

To see the effects of this, consider first the non-interacting Green's function. By taking the Schrödinger equation as the linear operator in eq. (2.27), the non-interacting Greens function of a system described by a Hamiltonian H_0 then satisfies

$$(i\partial_t - H_0)G_0 = \delta, \tag{2.33}$$

where the δ-function depends on the coordinates of the system. In Fermi liquid theory, the interacting Green's function can be related to the non-interacting by an injective function, meaning that for each fermionic excitation labeled by μ, there exist exactly one state in the interacting system that can be tagged with μ. Expressed in momentum space, the relation is often on the form

$$G^{-1}(k,\omega) = G_0^{-1}(k,\omega) - \Sigma(k,\omega), \tag{2.34}$$

where Σ is the fermion self-energy. This quantity describes the energy of a particle caused by changes to the system that originates from the very presence of the particle itself. The transformation from one to the other can be understood through[1]

$$\begin{aligned} \delta = (i\partial_t - H_0 - \Sigma)G \approx (G_0^{-1} - \Sigma)G \\ \implies G^{-1} \approx G_0^{-1} - \Sigma. \end{aligned} \tag{2.35}$$

Generally, a non-interacting momentum resolved Green's function $G_0(k,\omega)$ takes the form

$$G_0(k,\omega) = \frac{1}{\omega - \varepsilon_k + i0^+ \operatorname{sgn}(|\varepsilon_k| - \varepsilon_F)}, \tag{2.36}$$

where 0^+ is an infinitesimal and the Fermi level ε_F is the lowest lying unoccupied state. If this is the case, the interacting Green's function is consequently

$$G_0 \to G = \frac{1}{\omega - \varepsilon_k - \Sigma(k,\omega)} = \frac{z_k}{\omega - \tilde{\varepsilon}_k + \frac{i}{\tau_k}}, \tag{2.37}$$

where the quasiparticle residue z_k, lifetime τ_k, and excitation spectrum $\tilde{\varepsilon}_k$ can all be related to $\Sigma(k,\omega)$ by analytic functions.

[1] Although this is a non-rigorous derivation, and technically incorrect, the point in this section is not to compute the exact Green's function. The derivation serves the purpose of demonstrating how interactions appear in the propagator.

The Green's function is a very important quantity many body quantum mechanics since it gives a direct connection between theory and experiment through the spectral function

$$A(k,\omega) = -\frac{1}{\pi}\,\mathrm{Im}\,G^R(k,\omega). \tag{2.38}$$

This is the quantity one typically measures in Angle-resolved photoemission spectroscopy (ARPES). The imaginary part of the self energy $\Sigma(k,\omega)$ appears as a broadening of the peak, and the real part as a quasiparticle energy shift.

Chapter 3.
Topological Insulators

Topological Insulators

Topological insulators is a class of quantum matter with predicted properties relevant for the development of highly energy efficient information technologies such as spintronics [42, 43]. Apart from fundamental research interest in new states of matter, the possible uses also include the realms of topological quantum computing [5], and it is clear that the potential applications of these materials may be of high importance in future technological devices. These are materials that cannot be adiabatically connected to normal insulators, and are characterized by an insulating gap in the excitation spectrum coexistent with surface states that are protected by time-reversal symmetry [4]. This connection is not possible due to the Kramers' theorem which guarantees the existence of pairs of fermionic states, each of which is the time reversal of the other.

These materials are "topological" in the sense that certain quantities of the system is left invariant when it undergoes smooth transformations in the parameter space. The utilization of topological invariants as characterizations of physical states was shown to be useful by the theoretical discovery of the quantum Hall (QH) effect in 1982 [6]. The QH states explicitly break time-reversal symmetry, usually by the presence of a strong external magnetic field [44], giving rise to Landau levels with drifting motion at the edges. These states are therefore not, per definition, included in the class of topological insulators. A topologically distinct phase of matter with time-reversal symmetry was theoretically proposed by the inclusion of spin-orbit interactions [45, 46]. These two-dimensional topological insulators are synonymously called Quantum Spin Hall (QSH) insulators, due to their spin polarized edge currents analogous to those in the QH state.

3.1 Topological Invariant

Topological insulators differs from conventional insulators through Z_2 topological invariants [4, 5, 45]. The computation of these is generally not an easy task mathematically, but the presence of inversion symmetry allows for the determination by analyzing Bloch eigenstates at time-reversal invariant points in the Brillouin zone [47].

As an example of a topological invariant, consider the set of Bloch Hamiltonians $H(\boldsymbol{k})$ that can be smoothly deformed into one another without closing the insulating gap. These Hamiltonians can be classified by an integer n called the Chern invariant [5]. This number is the sum of total Berry flux through the Brillouin zone from each band α, which is given in terms of Bloch wave

functions $|u_\alpha(\boldsymbol{k})\rangle$ and the Berry connection

$$\boldsymbol{A}_\alpha(\boldsymbol{k}) = i \langle u_\alpha(\boldsymbol{k}) | \nabla_{\boldsymbol{k}} | u_\alpha(\boldsymbol{k}) \rangle \tag{3.1}$$

through

$$n_\alpha = \frac{1}{2\pi} \int_{1\mathrm{BZ}} \mathrm{d}^2\boldsymbol{k}\, \nabla_{\boldsymbol{k}} \times \boldsymbol{A}_\alpha. \tag{3.2}$$

For certain systems, the Hamiltonian may be expressed through the Pauli matrices $\boldsymbol{\sigma} = (\sigma^x, \sigma^y, \sigma^z)$ and identity matrix I as

$$H(\boldsymbol{k}) = E_{\boldsymbol{k}} I + \mathbf{d}_{\boldsymbol{k}} \cdot \boldsymbol{\sigma}, \tag{3.3}$$

where $\mathbf{d}_{\boldsymbol{k}}$ acts as a pseudospin field [48]. The energy eigenvalues of such systems are

$$\varepsilon_\pm(\boldsymbol{k}) = E_{\boldsymbol{k}} \pm |\mathbf{d}_{\boldsymbol{k}}|. \tag{3.4}$$

In this case, the Chern number can be expressed in terms of the normalized vector $\hat{\mathbf{d}}_{\boldsymbol{k}} = \mathbf{d}_{\boldsymbol{k}}/|\mathbf{d}_{\boldsymbol{k}}|$ alone, and eq. (3.2) takes the form

$$n = \frac{1}{4\pi} \int_{1\mathrm{BZ}} \mathrm{d}^2\boldsymbol{k}\, \hat{\mathbf{d}}_{\boldsymbol{k}} \cdot (\partial_{k_x} \hat{\mathbf{d}}_{\boldsymbol{k}} \times \partial_{k_y} \hat{\mathbf{d}}_{\boldsymbol{k}}). \tag{3.5}$$

The interpretation is that n counts how many times $\hat{\mathbf{d}}_{\boldsymbol{k}}$ winds around the unit sphere as $\boldsymbol{k}$ traverses the first Brillouin zone (1BZ), hence n is often called the "winding number" [49]. Haldane [8] showed that a particular model for the hexagonal lattice with next to nearest interaction exhibit a hall conductance

$$\sigma^{xy} = n \frac{2\pi e^2}{\hbar}, \tag{3.6}$$

where the Chern number $n = 0, \pm 1$ is related to the number of edge states through the bulk-boundary correspondence [45]. This model, famously called the Haldane model, will be studied in more detail in chapter 4. Although it is not a model for a topological insulator since it explicitly breaks time reversal symmetry, many of the properties are shared, and the Haldane model's simplicity justifies its frequent use as topological "toy" model. Experimental realization of the Haldane model has been achieved using cold atoms [50].

3.2 Topologically Protected States

That the quantum states are topologically protected is particularly exciting, since it means that transport properties (electric current, spin current, etc.) can be robust against impurities that can be treated as smooth perturbations

in the parameter space. Other effects may also produce gapped states in the bulk, but the classification through a topological invariant is different; The point is that in presence of impurities, the eigenstates vary continuously when the parameterization of impurities traverse the phase space if they are not susceptible to Anderson localization [51], whereas the existence of topologically protected states does not vary.

Although the eigenstates are topologically protected, the effects of interactions are of great importance. It can for instance be shown that adding a Hubbard-like interaction term to the Haldane model can drive a system through a topological phase transition for which the bulk gap closes with nonzero magnetic order [52]. Moreover, the presence of Rashba spin-orbit coupling can have the same effect, and in addition produce special edge states with large Chern numbers [53].

The QH effect has not only been shown to exist for fermions, but a similar effect exist for spin wave excitations [54], and a topological spin-model has been shown to produce magnonic edge states as in the fermionic Haldane model. In the noninteracting case, these magnons can propagate for a long time even at finite temperatures in contrast to the Ohmic resistance of electrons[55]. Moreover, they can induce coherent phonon transport along armchair edges of a graphene nanoribbon with armchair edges [12], which has been the initial motivation for the endeavor of this thesis.

3.3 The Quantum Spin Hall Insulator

The QSH state is the two-dimensional version of a topological insulator; It has an insulating electronic structure in the bulk, and gapless edge states in the bulk gap [4]. These edge states are associated with Z_2 topological invariants [45], and have the important property that the "up" and "down" spins propagate in opposite directions [44]. In contrast to normal one-dimensional conductors, for which weak disorder in the lattice can give rise to localized states [51], the QSH edge are robust even for strong disorder [5]. The QSH state was predicted to exist in HgTe quantum wells [11], which has been experimentally verified [1].

The Kane-Mele model for a QSH insulator is arguably the simplest model of a topological insulator [10]. It is a model for a honeycomb lattice described by the Hamiltonian

$$H_{\mathrm{f}} = \sum_{\langle i,j\rangle}\sum_{\sigma} t_1 c^{\dagger}_{i,\sigma} c_{j,\sigma} + \sum_{\langle\langle i,j\rangle\rangle}\sum_{\alpha,\beta} t_2 \mathrm{e}^{i\phi_{ij}} c^{\dagger}_{i,\alpha}\sigma_z^{\alpha\beta} c_{j,\beta}, \tag{3.7}$$

where α, β is indices and σ_z is the Pauli z matrix. The first term is a tight binding Hamiltonian, and the second term arises from spin-orbit interactions.

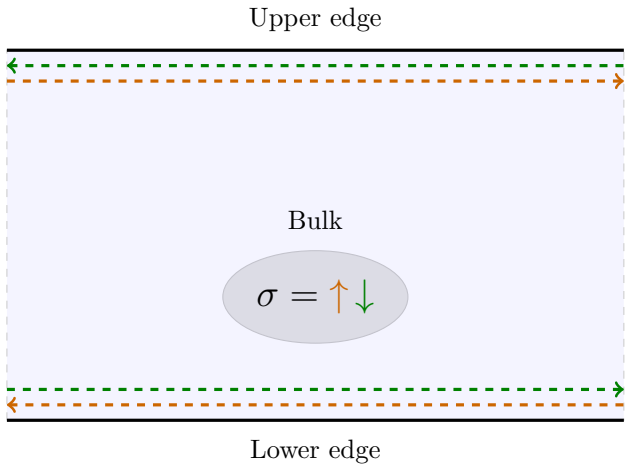

Figure 3.1: Illustration of localized edge states with spin-momentum locking. The helical edge states are highly localized close to the edges with an exponential decaying probability density into the bulk.

In contrast to the spinless Haldane model, the Kane-Mele model is protected by time reversal symmetry. The meaning of the phase factor $\exp(i\phi_{ij})$ will be clear in the discussion of the Haldane model in chapter 4, although the physical origin of its existence is different in the two models.

3.3.1 Helical Edge States and Localization

Topological insulators are unified through the bulk-boundary correspondence [5]. This is a mapping of the topological features of the bulk model to the existence of gapless boundary states residing in the insulating gap.

The edges of QSH states are Helical, which means that the projection of spin onto the direction of electron propagation is a conserved quantity, and thus serves as a good quantum number. These properties arise due to the existence of Kramers pairs, which are eigenstates of a time-reversal invariant system with opposite momentum and spin projections, thereby requiring a spin flipping interaction to allow for elastic back-scattering. The consequence of the existence of these is that spin-independent scattering at the edges are prohibited if the interaction respects time-reversal symmetry. The helical edge states of a two-dimensional topological insulator is illustrated in fig. 3.1, where the sample extends to the sides.

What is meant by the localization at the edges for these states is that the

probability density gets exponentially damped further into the sample (bulk), i.e. $\rho = |\psi|^2 \sim \exp(-\lambda x)$, where λ is some characteristic inverse length scale and x is the distance from the edge into the sample. At these edges, the most important perturbation is Rashba spin-orbit coupling, which do not break time reversal symmetry [56]. These one dimensional states are best described by bosonization of fermionic degrees of freedom through Luttinger Liquids when the Landau paradigm of Fermi liquids break down, as will be elaborated in chapter 5. In the presence of electron interactions, these Helical edge states are dubbed "Helical liquids" [57]. In the interacting system without spin-dependency, the Hamiltonian describing these helical Luttinger liquids are equal to regular Luttinger liquids with renormalized coupling constants. The same holds for the Green's functions, which is more convenient to compute in the spinless system [58].

3.3.2 Phonons in Quantum Spin Hall Insulators

The interplay between phonons and one-dimensional fermions at the edges of a QSH state is the main focus of this thesis. The initial motivation of this examination was the theoretical prediction of chiral phonon transport along the edges of a graphene nanoribbon which was induced by a magneto-elastic coupling between phonons and topological magnons [12]. It has been shown that Dirac electrons in topological insulators renormalized the velocity of surface acoustical phonons, and that the coupling leads to damping [59], but it is not well understood how much of the coherent fermion edge states remain in the presence of interactions. There are nevertheless many important results to be found in the literature, and the coupling between lattice deviations and topological fermions in topological insulators can be shown to be of great importance. Cangemi et al. [15] showed that increasing the electron phonon coupling in a Haldane Chern insulator pushes the system towards the transition to a trivial insulator. This is proposed as a method of direct measurement of topological quantum transitions. It has been proposed that the presence of phonons might induce a topological transition above a critical temperature in a system whose ground state is topologically trivial [60].

Typically one would need an inherently spin-flipping mechanism for allowing inelastic backscattering to occur at helical edge states. It has, however, been shown that long wavelength transverse phonons can give rise to an effective spin-phonon interaction [61] due to spin locking, simultaneously providing a fundamental limit to the edge conductivity in the presence of such interactions. This also shows the importance of phonons regarding the finite temperature stability of these protected states. Although the QSH state is robust against elastic backscattering due to time reversal symmetry, inelastic

and forward scattering is allowed. It has been shown that the phonons in the presence of Rashba spin orbit coupling can give rise to exactly this type of scattering, without breaking time reversal symmetry [62].

Chapter 4.
Physical System

Physical System

The physical system in consideration is presented in this chapter. A two-dimensional honeycomb lattice of tightly bound electrons in Carbon is the basis for the computation of electron phonon coupling on the edges of a finite size nanoribbon with topologically protected surface states. The Haldane model [8] will be utilized as a qualitative model for localized edge states. Mirror symmetry of the outermost electron orbitals in the system implies that, to first order in lattice deviations, out-of-plane phonon modes do not couple, and only in-plane phonon modes are considered in this work. The finite size nanoribbon is parameterized through a partial Fourier transform along one direction with periodic boundary conditions, and armchair edge geometry is considered.

4.1 Bulk Fermions and Phonons

Graphene is a single sheet of graphite. Since 2004, when Novoselov [63] described a cleavage technique for separating the atomically thin layers from the Carbon based crystal and some of its electronic properties, the material has been thoroughly studied. Graphene has been reported as the strongest material ever discovered [64], and its scope of potential applications stretches far beyond that of fundamental physics. The atoms in graphene reside on a honeycomb lattice, a lattice with a two-atom basis whose Wigner-Seitz cells are hexagons. The primitive lattice vectors are [65]

$$\mathbf{a}_1 = \frac{a}{2}(3, \sqrt{3}) \qquad \mathbf{a}_2 = \frac{a}{2}(3, -\sqrt{3}), \tag{4.1}$$

and the nearest neighbor vectors are given by

$$\boldsymbol{\delta}_1 = \frac{a}{2}(1, \sqrt{3}) \qquad \boldsymbol{\delta}_2 = \frac{a}{2}(1, -\sqrt{3}) \qquad \boldsymbol{\delta}_3 = a(-1, 0). \tag{4.2}$$

The interatomic distance is $a \simeq 1.42$Å [66]. The critical points $\mathbf{K}, \mathbf{K}'$ are the vertices on the edge of the first Brillouin zone (1BZ) and are located at

$$\mathbf{K} = \frac{2\pi}{3a}\left(1, \frac{1}{\sqrt{3}}\right) \qquad \mathbf{K}' = \frac{2\pi}{3a}\left(1, -\frac{1}{\sqrt{3}}\right). \tag{4.3}$$

These points are the locations for which the two π-bands touches, and the electronic band structure resembles that of massless fermions with a cone shaped dispersion called a Dirac cone. The symmetry point between $\mathbf{K}$ and $\mathbf{K}'$ is given by

$$\mathbf{M} = \frac{2\pi}{3a}(1, 0). \tag{4.4}$$

The band structure of Graphene can be estimated by a tight-binding approximation, neglecting Hubbard-type interactions. It can be shown that the inclusion of Hubbard interaction in the spinful Haldane model effectively renormalizes the parameters, and drives a topological transition [52].

4.1.1 Topological Graphene

Tight Binding

A tight binding model of a system is often the first step towards a qualitative understanding of a materials electronic properties. When considering materials where ions are separated by a distance much greater than the Bohr radius of the valence electrons, the wave function of the system is "tightly bound" to the ion cores, hence the name "tight binding". This is accomplished by representing the wave function in terms of Wannier states. A general tight binding Hamiltonian can be written in second quantized form as

$$H = \sum_{\alpha,\beta} \sum_{\sigma,\sigma'} \sum_{i,j} t^{\alpha\beta}_{ij,\sigma\sigma'} c^{\dagger}_{i\alpha\sigma} c_{j\beta\sigma'}, \tag{4.5}$$

where i, j represent lattice sites, σ, σ' is the spin projection, and α, β are orbital indices. The hopping amplitude is the expectation value of the single particle Hamiltonian for each orbital which can be calculated using eq. (2.10). The graphene sheet consists of sp^2-hybridized carbon atoms, by strong covalent σ-bands in the plane [41]. At zero doping of the system, it is to a good approximation only relevant to consider the π-bands formed by the p_z-orbitals in the electron structure. Thus, the orbital summation in eq. (4.5) is omitted. Since the wave functions are tightly bound to the ions, the form of the hopping parameter in the first approximation is taken to be $t_{ij} = t_1$ if i, j are neighboring atoms, and 0 else . Unless otherwise stated, I will use a nearest neighbor hopping amplitude of $t_1 \simeq -2.8\,\mathrm{eV}$ [66]. Since the lattice has two atoms in the basis, I discern the two sub-lattices as A and B, with corresponding fermionic destruction and annihilation operators. The tight binding Hamiltonian for interacting fermions is

$$H_{\mathrm{f}} = t_1 \sum_{\sigma} \sum_{i,\boldsymbol{\delta}} c^{\dagger}_{i,\sigma,A} c_{i+\boldsymbol{\delta},\sigma,B} + h.c. \tag{4.6}$$

Denoting $D \in \{\mathrm{A}, \mathrm{B}\}$, and introducing Fourier-transformed operators

$$c_{i,\sigma,D} = \frac{1}{\sqrt{N_D}} \sum_{\boldsymbol{k}} \mathrm{e}^{i\boldsymbol{k}\cdot\mathbf{r}_i} c_{\boldsymbol{k},\sigma,D}, \tag{4.7}$$

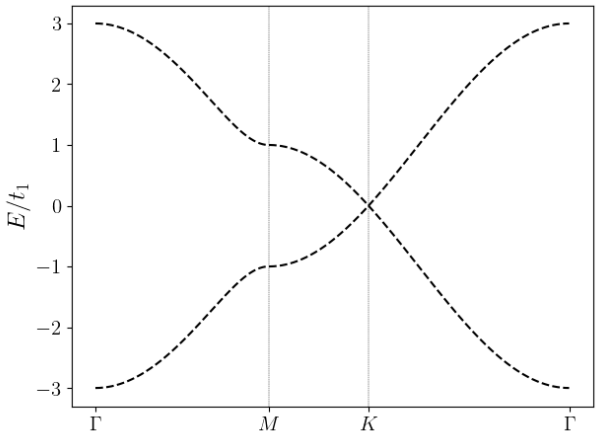

Figure 4.1: Nearest neighbor tight binding dispersion of a honeycomb lattice along straight lines in the first Brillouin zone. The Dirac cone can be seen at the high symmetry point K.

where N_D is the number of lattice sites on sub-lattice D, the resulting Hamiltonian is

$$H_{\mathrm{f}} = t_1 \sum_{\boldsymbol{k},\sigma} \gamma_1(\boldsymbol{k}) c^\dagger_{\boldsymbol{k},\sigma,A} c_{\boldsymbol{k},\sigma,B} + h.c. \tag{4.8}$$

with

$$\gamma_1(\boldsymbol{k}) \equiv \sum_{\boldsymbol{\delta}} \mathrm{e}^{i\boldsymbol{k}\cdot\boldsymbol{\delta}} = 2\mathrm{e}^{\frac{ik_x}{2}} \cos\left(k_y \frac{\sqrt{3}}{2}\right) + \mathrm{e}^{-ik_x} \tag{4.9}$$

with k_x, k_y in units of $1/a$. This Hamiltonian may now be diagonalized by introducing

$$\psi_{\boldsymbol{k},\sigma} = \begin{pmatrix} c_{\boldsymbol{k},\sigma,A} & c_{\boldsymbol{k},\sigma,B} \end{pmatrix}^T \tag{4.10a}$$

$$\psi^\dagger_{\boldsymbol{k},\sigma} = \begin{pmatrix} c^\dagger_{\boldsymbol{k},\sigma,A} & c^\dagger_{\boldsymbol{k},\sigma,B} \end{pmatrix}, \tag{4.10b}$$

and the resulting doubly degenerate energy dispersion is given by

$$\epsilon_{\boldsymbol{k}} = \pm t_1 |\gamma_1(\boldsymbol{k})|. \tag{4.11}$$

This dispersion $\epsilon_{\boldsymbol{k}}$ is plotted in fig. 4.1 along critical lines in the Brillouin zone. In addition to the Dirac cone at the K-point, the bands are essentially flat at the M-point, giving rise to Van Hove singularities in the density of states. In fig. 4.2, the two bands is shown covering the first Brillouin zone.

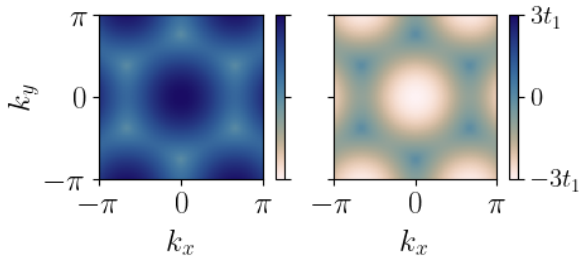

Figure 4.2: The two different energy bands of tight binding Graphene for nearest neighbor interaction. The wavenumbers are in units of $1/a$. The corners of the hexagon is the high symmetry points $\mathbf{K}, \mathbf{K}'$ and threefold rotations thereof.

Topological Fermions on Honeycomb lattices

The simplest model of an insulator with topologically nontrivial properties is arguably the spinless Haldane model, which is a well-known prototypical model of Chern insulator [15]. It is a tight binding model for the honeycomb lattice with additional next to nearest neighbor hopping for which an external staggered vector potential is added [8]. The vector potential is constructed in such a way that the total magnetic flux through the unit cell of the lattice is zero, however it gives rise to an accumulated phase in the hopping amplitude for next to nearest neighboring lattice sites. The experimental realization of the Haldane model has been achieved using both cold atoms [50] and superconducting circuits [67], but the largest advantage of the model is that it is a relatively simple model for a system with intrinsic topological properties. The model is given as

$$H_{\mathrm{f}} = \sum_{\langle i,j \rangle} t_1 c_i^\dagger c_j + \sum_{\langle\langle i,j \rangle\rangle} \sum t_2 \mathrm{e}^{i\phi_{ij}} c_i^\dagger c_j + \lambda_S \sum_{A,B} (n_A - n_B), \tag{4.12}$$

where a lattice asymmetry called the "Semenoff mass" λ_S is added [68]. By comparison, the Kane-Mele model in eq. (3.7) is two copies of the spinless Haldane model with $\lambda_S = 0$.

A finite λ_S reduces the symmetry of the system, and is useful for describing other two-dimensional lattices for which the two sublattices are inequivalent [69], as for instance Boron Nitride (BN) [68, 70]. For Graphene, $\lambda_S = 0$. The accumulated phase for the next to nearest neighbor hopping is given by the

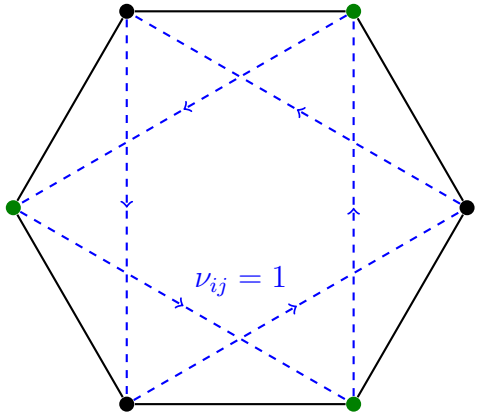

Figure 4.3: Paths in the unit cell for which $\nu_{ij} = 1$. The black and green atoms reside on the A and B sublattice, respectively. Along the solid lines, no phase in the hopping amplitude is accumulated.

line integral of the vector potential [8]

$$\phi_{ij} = \frac{e}{\hbar} \int_{\mathbf{r}_i}^{\mathbf{r}_j} \mathrm{d}\mathbf{r}\, \mathbf{A}(\mathbf{r}), \tag{4.13}$$

dependent on the path between atoms. I choose a vector potential resulting in $\phi_{ij} = \nu_{ij}\phi$, where $\nu_{ij} = 1 = -\nu_{ji}$ along the paths shown in fig. 4.3. This is consistent with the definition [65]

$$\nu_{ij}(\bar{\boldsymbol{\delta}} = \boldsymbol{\delta}_i + \boldsymbol{\delta}_j) = \mathrm{sign}\left((\boldsymbol{\delta}_i \times \boldsymbol{\delta}_j)_z\right), \tag{4.14}$$

where $\boldsymbol{\delta}_i$ and $\boldsymbol{\delta}_j$ are the two constituent vectors of the next to nearest neighbor vector $\bar{\boldsymbol{\delta}}$. For nearest neighbor hopping, no phase is accumulated, and the tight binding model in the previous section can be reused. Using the creation operators $c_A^\dagger, c_B^\dagger$ on the A and B sub-lattices and temporarily suppressing the spin index, the Hamiltonian may be written

$$\begin{aligned} H_\mathrm{f} = {} & t_1 \sum_{i,\boldsymbol{\delta}} \left(c_{i,A}^\dagger c_{i+\delta,B} + h.c. \right) \\ & + t_2 \sum_{\substack{i\in A \\ j\in B}} \sum_{\bar{\boldsymbol{\delta}}} \left(\mathrm{e}^{i\phi\nu(\bar{\boldsymbol{\delta}})} c_{i,A}^\dagger c_{i+\bar{\boldsymbol{\delta}},A} + \mathrm{e}^{i\phi\nu(\bar{\boldsymbol{\delta}})} c_{j,B}^\dagger c_{j+\delta,B} \right) \\ & + M \sum_{\substack{i\in A \\ j\in B}} \left(c_{i,A}^\dagger c_{i,A} - c_{j,B}^\dagger c_{j,B} \right), \end{aligned} \tag{4.15}$$

where $\boldsymbol{\delta}$ and $\overline{\boldsymbol{\delta}}$ are vectors connecting the three nearest and six next-to-nearest neighbors from the chosen origin, accordingly. I now reintroduce the Fourier transformed operators in eq. (4.7). The first term is simply the tight binding model, resulting in eq. (4.8). The second term in eq. (4.15) is written as

$$t_2 \sum_{\boldsymbol{k}} \left(\gamma_2(\boldsymbol{k}, \phi) c^\dagger_{\boldsymbol{k},A} c_{\boldsymbol{k},A} + \gamma_2(\boldsymbol{k}, -\phi) c^\dagger_{\boldsymbol{k},B} c_{\boldsymbol{k},B} \right), \tag{4.16}$$

where

$$\gamma_2(\boldsymbol{k}, \phi) = 2 \left(\cos\left(\sqrt{3} k_y - \phi \right) + 2 \cos\left(\frac{3}{2} k_x \right) \cos\left(\frac{\sqrt{3}}{2} k_y + \phi \right) \right). \tag{4.17}$$

The last term of eq. (4.15) is simple, and can immediately be written as

$$M \sum_{\boldsymbol{k}} \left(c^\dagger_{\boldsymbol{k},A} c_{\boldsymbol{k},A} - c^\dagger_{\boldsymbol{k},B} c_{\boldsymbol{k},B} \right). \tag{4.18}$$

The Haldane model in quasi-momentum space thus states

$$\begin{aligned} H_{\mathrm{f}} &= t_1 \sum_{\boldsymbol{k},\sigma} \gamma_1(\boldsymbol{k}) c^\dagger_{\boldsymbol{k},\sigma,A} c_{\boldsymbol{k},\sigma,B} + h.c. \\ &+ t_2 \sum_{\boldsymbol{k},\sigma} \left(\gamma_2(\boldsymbol{k}, \phi) c^\dagger_{\boldsymbol{k},\sigma,A} c_{\boldsymbol{k},\sigma,A} + \gamma_2(\boldsymbol{k}, -\phi) c^\dagger_{\boldsymbol{k},\sigma,B} c_{\boldsymbol{k},\sigma,B} \right) \\ &+ M \sum_{\boldsymbol{k},\sigma,\sigma} \left(c^\dagger_{\boldsymbol{k},\sigma,A} c_{\boldsymbol{k},\sigma,A} - c^\dagger_{\boldsymbol{k},\sigma,B} c_{\boldsymbol{k},\sigma,B} \right), \end{aligned} \tag{4.19}$$

which in the basis $\psi_{\boldsymbol{k},\sigma}$ given in eq. (4.10) can be written on matrix form as

$$H_{\mathrm{f}} = \sum_{\boldsymbol{k},\sigma} \psi^\dagger_{\boldsymbol{k},\sigma} h(\boldsymbol{k}) \psi_{\boldsymbol{k}\sigma}. \tag{4.20}$$

The matrix $h(\boldsymbol{k})$ is given by

$$h(\boldsymbol{k}) = \begin{pmatrix} t_2 \gamma_2^+(\boldsymbol{k}) + \lambda_S & t_1 \gamma_1(\boldsymbol{k}) \\ t_1 \gamma_1^*(\boldsymbol{k}) & t_2 \gamma_2^-(\boldsymbol{k}) - \lambda_S \end{pmatrix}, \tag{4.21}$$

writing $\gamma_2^\pm(\boldsymbol{k}) = \gamma_2(\boldsymbol{k}, \pm\phi)$. This matrix can be written in terms of a pseudospin field as in eq. (3.3) by

$$h(\boldsymbol{k}) = E_{\boldsymbol{k}} I + \mathbf{d}_{\boldsymbol{k}} \cdot \boldsymbol{\sigma} \tag{4.22}$$

with $\boldsymbol{\sigma} = (\sigma^x, \sigma^y, \sigma^z)$ as the Pauli matrices,

$$E_{\boldsymbol{k}} = \frac{t_2}{2} (\gamma_2^+(\boldsymbol{k}) + \gamma_2^-(\boldsymbol{k})) \tag{4.23}$$

and

$$d_{\boldsymbol{k}}^{x} = t_1 \,\mathrm{Re}\{\gamma_1(\boldsymbol{k})\} \tag{4.24a}$$

$$d_{\boldsymbol{k}}^{y} = -t_1 \,\mathrm{Im}\{\gamma_1(\boldsymbol{k})\} \tag{4.24b}$$

$$d_{\boldsymbol{k}}^{z} = \frac{t_2}{2}\left(\gamma_2(\boldsymbol{k},\phi) - \gamma_2(\boldsymbol{k},-\phi)\right) + \lambda_S. \tag{4.24c}$$

The energy eigenvalues of $h(\boldsymbol{k})$ is

$$\varepsilon_{\pm}(\boldsymbol{k}) = E_{\boldsymbol{k}} \pm |\mathbf{d}_{\boldsymbol{k}}| \tag{4.25a}$$

$$= \frac{1}{2}\left(t_2\gamma_2^{+}(\boldsymbol{k}) + t_2\gamma_2^{-}(\boldsymbol{k}) \pm \sqrt{\left(t_2\gamma_2^{+}(\boldsymbol{k}) - t_2\gamma_2^{-}(\boldsymbol{k}) + 2\lambda_S\right)^2 + 4t_1^2|\gamma_1(\boldsymbol{k})|^2}\right). \tag{4.25b}$$

At the high symmetry points, both the hopping phase ϕ_{ij} and the Semenoff mass λ_S has the effect of opening a gap at the high symmetry points $\mathbf{K}$ and $\mathbf{K}'$, where $\gamma_1(\mathbf{K}) = 0$. This can be seen from eq. (4.25), and the energies at these points are

$$\varepsilon_{\pm}(\mathbf{K}) = \begin{cases} -6t_2 \sin\left(\frac{\pi}{6} - \phi\right) + \lambda_S \\ -6t_2 \sin\left(\frac{\pi}{6} + \phi\right) - \lambda_S. \end{cases} \tag{4.26}$$

In fig. 4.4, the dispersion is plotted over critical lines in the Brillouin zone, and the onset of $t_2 \neq 0$ gives rise to a gap in the spectrum at $\mathbf{K}$. The equation for this gap is the difference

$$\Delta \equiv \varepsilon_{+}(\mathbf{K}) - \varepsilon_{-}(\mathbf{K}) = 6\sqrt{3}t_2 \sin\phi + 2\lambda_S, \tag{4.27}$$

which is zero for

$$-\lambda_S = 3\sqrt{3}t_2 \sin\phi. \tag{4.28}$$

This equation implies that there exist a continuous path in parameter space for which the gap is zero, and hence also continuous regions for which the gap is finite. This path in parameter space does in fact separate topologically distinct phases with different Chern numbers in the QH Effect [8]. The minus sign in front of the Semenoff mass λ_S in eq. (4.28) is due to the chosen orientation of ν_{ij} in fig. 4.3.

Since the Kane-Mele is effectively two copies of the Haldane model with an added lattice asymmetry term,

$$\lambda_S \sum_{A,B} \sum_{\sigma} (n_{A,\sigma} - n_{B,\sigma}), \tag{4.29}$$

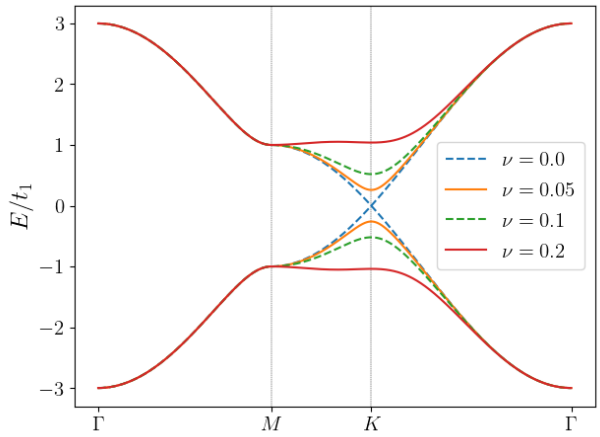

r

Figure 4.4: A gap is opened at the high symmetry point $\boldsymbol{K}$ by the next to nearest hopping amplitude $t_2 = \nu t_1$ for $\lambda_S = 0$ and $\phi = \frac{\pi}{2}$.

it is interesting to note that the gap of a single spin-channel can be closed without necessarily closing the other, thus causing the model to be a spin-polarized insulator at the high symmetry point **K**.

The fermion theory of the bulk is now presented. The Haldane Hamiltonian will serve as a model for the system, with intrinsic topological properties resulting in localized edge states, as will be explicitly shown when an armchair ribbon is considered.

4.1.2 Phonon Dynamics

Phonons are quantized lattice vibrations in a solid [71]. These quasiparticles are collective excitations of ionic displacements in a solid and are essential for our understanding of material properties at the quantum level. The coupling between phonons and the fermionic fields in a solid is not unexpected; the electrons reside in orbitals mostly localized at the lattice sites. This means that an ionic lattice displacement would change the overlap integral between two electron states at different lattice sites, thereby altering the hopping amplitude. As an example of its importance, electron phonon interaction can give rise to special states of matter, such as the superconducting state, which is most easily explained through the Bardeen-Cooper-Schrieffer (BCS) theory of superconductivity [14]. Here, electron-phonon interaction mediates an effective attractive force between different electrons, leading to the condensation

of Cooper pairs that reduces the free energy.

The phonon dynamics of a hexagonal lattice may be obtained in several ways. Allowing for next-to-nearest couplings in the dynamical matrix Φ, I write the Hamiltonian in the harmonic approximation as

$$H_{\text{ph}} = \sum_i \frac{\mathbf{P}_i^2}{2M_i} + \frac{1}{2}\sum_{\langle\langle i,j\rangle\rangle} \mathbf{u}_i^\dagger \Phi^{D_i D_j}(\boldsymbol{\delta}_{ij})\mathbf{u}_j, \tag{4.30}$$

following Thingstad et al. [69], Falkovsky [72]. The first term is the kinetic energy of the ensemble, and the second term represents the potential energy resulting in small deviations from the equilibrium sites. $D_i \in \{A, B\}$ is the labeling of sublattice for lattice site i. The derivation of the phonon normal modes holds for lattices with inequivalent sublattices, but I will only consider parameters for graphene when explicitly used. The first step of diagonalizing the Hamiltonian is by introducing the effective mass $\tilde{M} = \sqrt{M_A M_B}$ and the relative mass $\mu_D = \frac{M_D}{\tilde{M}}$. Introducing

$$\mathbf{u}_i^D = \frac{1}{\sqrt{N_D}}\sum_{\mathbf{q}} \mathrm{e}^{i\mathbf{q}\cdot\mathbf{r}_i}\mathbf{u}_{\mathbf{q}}^D \tag{4.31a}$$

$$\mathbf{P}_i^D = \frac{1}{\sqrt{N_D}}\sum_{\mathbf{q}} \mathrm{e}^{i\mathbf{q}\cdot\mathbf{r}_i}\mathbf{P}_{\mathbf{q}}^D, \tag{4.31b}$$

the Hamiltonian in eq. (4.30) can be rewritten as

$$\begin{aligned} H_{\text{ph}} &= \sum_i \frac{\mathbf{P}_i^2}{2M_i} \\ &\quad + \frac{1}{2}\sum_D \sum_{i\in D}\left(\sum_{\boldsymbol{\delta}_D} (\mathbf{u}_i^D)^\dagger \Phi^{DD'}(\boldsymbol{\delta}_D)\mathbf{u}_{i+\boldsymbol{\delta}_D}^{D'} + \sum_{\bar{\boldsymbol{\delta}}} (\mathbf{u}_i^D)^\dagger \Phi^{DD}(\bar{\boldsymbol{\delta}})\mathbf{u}_{i+\bar{\boldsymbol{\delta}}}^D\right) \\ &= \sum_{\mathbf{q}} \frac{\tilde{\mathbf{P}}_{\mathbf{q}}^\dagger \cdot \tilde{\mathbf{P}}_{\mathbf{q}}}{2\tilde{M}} + \frac{1}{2}\sum_{\mathbf{q}} \tilde{\mathbf{u}}_{\mathbf{q}}^\dagger \mathcal{D}(\mathbf{q})\tilde{\mathbf{u}}_{\mathbf{q}}, \end{aligned} \tag{4.32}$$

where $\boldsymbol{\delta}_D$ are any of the three nearest neighboring vectors connecting lattice D to D', and $\bar{\boldsymbol{\delta}}$ the next to nearest vectors. The rescaled momenta and lattice deviations are given by

$$\tilde{\mathbf{P}}_{\mathbf{q}} = \left(\frac{1}{\sqrt{\mu_A}}\mathbf{P}_{\mathbf{q}}^A, \frac{1}{\sqrt{\mu_B}}\mathbf{P}_{\mathbf{q}}^B\right)^T \tag{4.33a}$$

$$\tilde{\mathbf{u}}_{\mathbf{q}} = \left(\sqrt{\mu_A}\mathbf{u}_{\mathbf{q}}^A, \sqrt{\mu_B}\mathbf{u}_{\mathbf{q}}^B\right)^T \tag{4.33b}$$

and the dynamic coupling matrix is

$$\mathcal{D}(\mathbf{q}) = \begin{pmatrix} \frac{1}{\mu_A}\sum_{\bar{\boldsymbol{\delta}}} \mathrm{e}^{-\mathbf{q}\cdot\bar{\boldsymbol{\delta}}}\Phi^{AA} & \sum_{\boldsymbol{\delta}} \mathrm{e}^{-i\mathbf{q}\cdot\boldsymbol{\delta}}\Phi^{AB} \\ \sum_{\boldsymbol{\delta}} \mathrm{e}^{i\mathbf{q}\cdot\boldsymbol{\delta}}\Phi^{BA} & \frac{1}{\mu_B}\sum_{\bar{\boldsymbol{\delta}}} \mathrm{e}^{-\mathbf{q}\cdot\bar{\boldsymbol{\delta}}}\Phi^{BB} \end{pmatrix}. \tag{4.34}$$

Due to the symmetry $z \to -z$, and as will be clear when the fermion-interactions are considered, the out-of plane modes do not couple to the in-plane modes, and the Hamiltonian may be split into separate degrees of freedom. This has the implication that the z-component of the lattice deviations may be altogether disregarded [72] in this approximation. Therefore, the matrices $\Phi^{DD'}$ in eq. (4.34) may be considered as 2×2-matrices describing the coupling strengths of the in-plane modes. By considering the symmetries in the system, several constraints are imposed on the coupling constants, reducing the number of independent parameters. For a thorough discussion of the symmetry constraints of the system, I refer to Thingstad et al. [69] which gives the force constants in a chiral basis. The eigenvalues $\lambda_\nu(\mathbf{q})$ of $\mathcal{D}(\mathbf{q})$ are related to the phonon spectrum from the relation $\lambda_\nu(\mathbf{q}) = \omega^2_{\mathbf{q},\nu}\tilde{M}$, and the normal modes are found from the corresponding eigenvectors. All necessary ingredients for the introduction of canonical creation and annihilation operators for the phonon modes are present. By diagonalizing the phonon Hamiltonian, the basis $v^\nu_{\mathbf{q}}$ is defined through

$$\tilde{\mathbf{u}}^D = \sum_\nu \mathbf{e}^D_\nu(\mathbf{q}) v^\nu_{\mathbf{q}}, \tag{4.35}$$

where $\mathbf{e}^D_\nu(\mathbf{q})$ are the columns in the matrix that diagonalizes the potential energy $\mathcal{D}(\mathbf{q})$ and ν is an index representing the different phonon branches of the system. Since the phonon Hamiltonian is, by definition, diagonal in the $v^\nu_{\mathbf{q}}$-basis, canonical creation and annihilation operators $b^\dagger_{\mathbf{q},\nu}, b_{\mathbf{q},\nu}$ may be introduced, and H_{ph} may be written on the familiar form

$$H_{\mathrm{ph}} = \sum_{\mathbf{q},\nu} \hbar\omega_{\mathbf{q},\nu}\left(b^\dagger_{\mathbf{q},\nu} b_{\mathbf{q},\nu} + \frac{1}{2}\right). \tag{4.36}$$

In terms of these new bosonic operators, the phonon modes are given by

$$v^\nu_{\mathbf{q}} = \sqrt{\frac{\hbar}{2\tilde{M}\omega_{\mathbf{q},\nu}}}\left(b^\dagger_{-\mathbf{q},\nu} + b_{\mathbf{q},\nu}\right). \tag{4.37}$$

These are the normal modes of the bulk phonons. The dispersions $\omega_{q,\nu}$, whose analytic form can be found in [72], is plotted in fig. 4.5. The acoustic and optical out of-plane modes are included, but will not be relevant for further calculations.

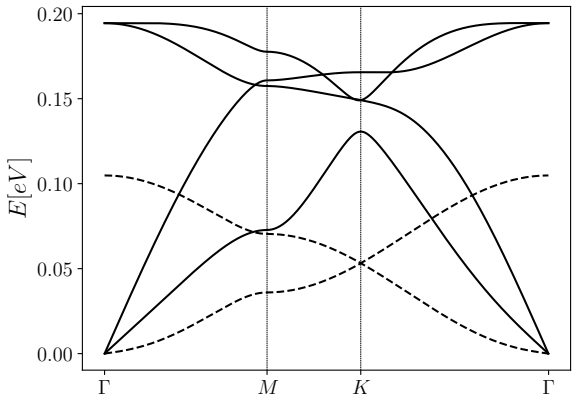

Figure 4.5: Phonon spectrum of Graphene with next to nearest interaction in the ionic displacements for critical lines in the Brillouin zone. The solid lines are the four in-plane modes, and the dashed lines are th out of-plane modes which do not couple to the fermions in this system. The parameters in the dynamic matrix Φ is taken from ref. [69].

4.1.3 Electron-Phonon Coupling

In this section the coupling between lattice fermions and phonons will be presented. Using a similar approach as Thingstad et al. [69], where the overlap integral determining the hopping amplitude between neighboring orbitals is affected due to ionic lattice deviations in the direction of the lattice vectors. The mirror symmetry $z \to -z$ implies that out-of plane phonon modes do not couple to the relevant p_z orbitals of graphene. For systems breaking this symmetry, for instance Rashba spin-orbit coupled systems or in the presence of a magnetic field perpendicular to the lattice, out of plane modes also have to be considered.

I will expand the overlap integral for nearest neighbors only, and the next-to-nearest hopping term of the Haldane model in eq. (4.19) will remain unchanged. For the first term, I expand the hopping parameter as

$$\begin{aligned} t_{ij} &\to t(\boldsymbol{\delta}) + (\mathbf{u}_j - \mathbf{u}_i) \cdot \boldsymbol{\nabla}_{\boldsymbol{\delta}}(t(\boldsymbol{\delta})) \\ &\simeq t(\boldsymbol{\delta}) + \frac{lt(\boldsymbol{\delta})}{a^2}(\mathbf{u}_j - \mathbf{u}_i) \cdot \boldsymbol{\delta} \end{aligned} \tag{4.38}$$

where $l \equiv \frac{\mathrm{d}\ln(t)}{\mathrm{d}\ln a}$ and $a = |\boldsymbol{\delta}|$ is the equilibrium distance between the ions. $\mathbf{u}$

is the local lattice deviation, and $\boldsymbol{\nabla}_{\boldsymbol{\delta}}$ is the gradient in the direction of the neighboring lattice site. The first term of eq. (4.38) results in the normal tight-binding term of eq. (4.19), but the second term introduces the coupling between the lattice and fermions through the Hamiltonian

$$H_{\text{f-ph}} = \sum_{i\in A}\sum_{\boldsymbol{\delta}} \frac{l_1 t_1}{a^2}\boldsymbol{\delta}\cdot\left(\mathbf{u}^B_{i+\boldsymbol{\delta}} - \mathbf{u}^A_i\right) c^\dagger_{i,A} c_{i+\boldsymbol{\delta},B} + h.c. \tag{4.39}$$

I now Fourier transform eq. (4.39) by inserting the momentum representation in eq. (4.31a), obtaining

$$\begin{aligned}
\sum_{i\in A}\sum_{\boldsymbol{\delta}} \boldsymbol{\delta}\cdot\left(\mathbf{u}^B_{i+\boldsymbol{\delta}} - \mathbf{u}^A_i\right) c^\dagger_{i,A} c_{i+\boldsymbol{\delta},B} &= \sum_{i\in A}\sum_{\boldsymbol{\delta}} \frac{\boldsymbol{\delta}\cdot}{\sqrt{N_B N_A}} \sum_{\boldsymbol{k}_1\boldsymbol{k}_2,\mathbf{q}} \\
&\times \left(\frac{e^{i(\mathbf{q}+\boldsymbol{k}_2)\cdot\boldsymbol{\delta}}}{\sqrt{N_B}} e^{i(\mathbf{q}-\boldsymbol{k}_1+\boldsymbol{k}_2)\cdot\mathbf{r}_i}\mathbf{u}^B_{\mathbf{q}} - \frac{e^{i\boldsymbol{k}_2\cdot\boldsymbol{\delta}}}{\sqrt{N_A}} e^{i(\mathbf{q}-\boldsymbol{k}_1+\boldsymbol{k}_2)\cdot\mathbf{r}_i}\mathbf{u}^A_{\mathbf{q}}\right) c^\dagger_{\boldsymbol{k}_1,A} c_{\boldsymbol{k}_2,B} \\
&= \sum_{\boldsymbol{\delta}} \frac{N_A\boldsymbol{\delta}\cdot}{\sqrt{N_B N_A}} \sum_{\boldsymbol{k}_1\boldsymbol{k}_2,\mathbf{q}} \left(\frac{e^{i(\mathbf{q}+\boldsymbol{k}_2)\cdot\boldsymbol{\delta}}}{\sqrt{N_B}}\delta_{\boldsymbol{k}_1,\mathbf{q}+\boldsymbol{k}_2}\mathbf{u}^B_{\mathbf{q}} - \frac{e^{i\boldsymbol{k}_2\cdot\boldsymbol{\delta}}}{\sqrt{N_A}}\delta_{\boldsymbol{k}_1,\mathbf{q}+\boldsymbol{k}_2}\mathbf{u}^A_{\mathbf{q}}\right) c^\dagger_{\boldsymbol{k}_1,A} c_{\boldsymbol{k}_2,B} \\
&= \sum_{\boldsymbol{\delta}} \frac{N_A\boldsymbol{\delta}\cdot}{\sqrt{N_B N_A}} \sum_{\boldsymbol{k},\mathbf{q}} \left(\frac{e^{i(\boldsymbol{k}+\mathbf{q})\cdot\boldsymbol{\delta}}}{\sqrt{N_B}}\mathbf{u}^B_{\mathbf{q}} - \frac{e^{i\boldsymbol{k}\cdot\boldsymbol{\delta}}}{\sqrt{N_A}}\mathbf{u}^A_{\mathbf{q}}\right) c^\dagger_{\boldsymbol{k}+\mathbf{q},A} c_{\mathbf{k},B} \\
&\overset{N_A=N_B}{=} \frac{1}{\sqrt{N_A}} \sum_{\boldsymbol{k},\mathbf{q}}\sum_{\boldsymbol{\delta}} e^{i\boldsymbol{k}\cdot\boldsymbol{\delta}}\boldsymbol{\delta}\cdot\left(e^{i\mathbf{q}\cdot\boldsymbol{\delta}}\mathbf{u}^B_{\mathbf{q}} - \mathbf{u}^A_{\mathbf{q}}\right) c^\dagger_{\boldsymbol{k}+\mathbf{q},A} c_{\mathbf{k},B}.
\end{aligned} \tag{4.40}$$

Inserting this and eq. (4.37), the electron-phonon Hamiltonian in eq. (4.39) is written

$$H_{\text{f-ph}} = \sum_{\boldsymbol{k},\mathbf{q}}\sum_{\nu} g^\nu_{\boldsymbol{k},\mathbf{q}} (b^\dagger_{-\mathbf{q},\nu} + b_{\mathbf{q},\nu}) c^\dagger_{\boldsymbol{k}+\mathbf{q},A} c_{\mathbf{q},B} \tag{4.41}$$

with coupling matrix

$$g^\nu_{\boldsymbol{k},\mathbf{q}} = \frac{l_1 t_1}{a^2\sqrt{N_A}}\sqrt{\frac{\hbar}{2\tilde{M}\omega_{\mathbf{q},\nu}}}\sum_{\boldsymbol{\delta}} e^{i\boldsymbol{k}\cdot\boldsymbol{\delta}}\boldsymbol{\delta}\cdot(e^{i\mathbf{q}\cdot\boldsymbol{\delta}}\mathbf{e}^B_\nu - \mathbf{e}^A_\nu). \tag{4.42}$$

In ref. [69], the bulk fermions is diagonalized, and eq. (4.42) involves additional band indices. In this work, the form of this coupling matrix will be used as a basis for the electron-phonon coupling at the edges of an armchair nanoribbon.

4.2 Armchair Nanoribbon

In this section I will calculate the free fermion and phonon Hamiltonian on an armchair nanoribbon of infinite length and finite width which is determined

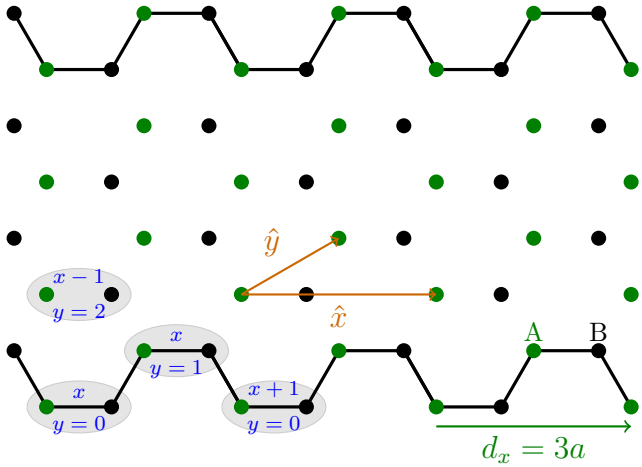

Figure 4.6: Geometry of an armchair ribbon. The unit vectors start and end at unit cells, where each cell contains two atoms on different sublattices, both described by the same coordinates (x, y). The armchair edges are marked in black lines. The lattice extends in the x-direction indefinitely.

by the number N_y of Carbon atoms. I will compute the matrix representation of the free fermion and phonon Hamiltonian, and I will show that the Haldane model in eq. (4.12) gives rise to localized edge states on an armchair ribbon. The phonon eigenstates on the armchair ribbon will be projected onto the upper edge, and are to be used in the coupling matrix in eq. (4.42) for the numerical study of Green's function corrections to localized fermions.

For the characterization of edge modes on a ribbon, a finite system approach is necessary. The honeycomb ribbon will be taken with periodic boundary condition in the x-direction, and open in the y-direction. I will adopt the unit cell labeling from Thingstad et al. [12] for the armchair ribbons. This geometry is one of two ways of constructing a nanoribbon from a hexagonal lattice, the other being one with "zigzag" edges [66] whose phonon eigenstates are much less localized at the edges than in the armchair geometry [12]. The armchair edge geometry is therefore expected to be of greater importance when phonons are considered. The system is shown in fig. 4.6 for a width $N_y = 8$, where the labeling of unit cells is shown. By imposing periodic boundary conditions in the x-direction, the values of k_x only assume discrete values

$$k_x = \frac{2\pi n}{N_x d_x}, \quad n \in \mathbb{Z}, \tag{4.43}$$

where $d_x = 3a$ is the distance between unit cells of the lattice in x-direction.

The first Brillouin zone is thus the interval $k_x a \in [-\frac{\pi}{3}, \frac{\pi}{3}]$.

In the following calculations, a partial Fourier transform is introduced. For a general position dependent operator $O_{x,y,\mu}$ with additional quantum number μ, the partial Fourier transform in the x-direction is defined by

$$O_{x,y,\mu} = \frac{1}{\sqrt{N_x}} \sum_k \mathrm{e}^{ikx} O_{k,y,\mu}, \tag{4.44}$$

where N_x is the number of lattice sites in the x-direction.

For later convenience, I define the quantities

$$\theta_k \equiv \mathrm{e}^{-ikd_x} \tag{4.45}$$

and

$$t_k \equiv 1 + \mathrm{e}^{-ikd_x}. \tag{4.46}$$

These will show up in the matrix representations of both fermion and phonon Hamiltonians.

4.2.1 Topological Armchair Fermions

The Hamiltonian describing topological fermions is the Haldane model, given in eq. (4.12). I introduce the partial Fourier transformed operators $c^\dagger_{k,y,A}, c^\dagger_{k,y,B}$ for creation operators on A- and B-sites, and use the labeling of unit cells as illustrated in fig. 4.6. The goal is to represent the Hamiltonian as $H = \sum_k \psi^\dagger_k H_k \psi_k$, where H_k is the sum of matrix representations of each term in eq. (4.12).

Since the honeycomb lattice consists of two atoms in each unit cell, I define the $2N_y$-dimensional basis

$$\psi_k = (c_{k,1,A}, c_{k,1,B}, c_{k,2,A}, \ldots, c_{k,N_y,B})^T. \tag{4.47}$$

I do not consider spin in this calculation, since the Haldane model is spinless, hence the inclusion only appears as a doubling of the basis and all energy levels become doubly degenerate. If spin dependent terms such as a magnetization or spin-orbit coupling is present, the basis have to be expanded to be $4N_y$-dimensional.

Tight Binding Hamiltonian

I first consider the tight-binding term of the Hamiltonian. By inserting the partial Fourier transform of eq. (4.44) and the unit cell labeling in fig. 4.6, the

term is

$$\begin{aligned} t_1 \sum_{\langle i,j \rangle} c_i^\dagger c_j &= t_1 \sum_{\langle i,j \rangle} c_{i,A}^\dagger c_{j,B} + h.c. \\ &= t_1 \sum_{x,y} \frac{1}{N_x} \sum_{k_1,k_2} \mathrm{e}^{-ik_1 x} c_{k_1,y,A}^\dagger \mathrm{e}^{ik_2 x} \mathrm{e}^{ik_2 a} \\ &\qquad \times \left(\mathrm{e}^{-ik_2 d_x} b_{k_2,y+1} + c_{k_2,y-1,B} + c_{k_2,y,B} \right) + h.c. \\ &= t_1 \sum_{y=1}^{N_y} \sum_{k_x} c_{k,y,A}^\dagger \left(c_{k,y-1,B} + c_{k,y,B} + \mathrm{e}^{-ikd_x} c_{k,y+1,B} \right) + h.c. \end{aligned} \tag{4.48}$$

Here, I have made a gauge transformation [65] on the B-sublattice given by

$$c_{k,y,B} \to c_{k,y,B} \mathrm{e}^{-ika}. \tag{4.49}$$

In the basis given in eq. (4.47), the first term of the Hamiltonian is thus written as $\psi_k^\dagger M_1 \psi_k$, with

$$M_1 = t_1 \begin{pmatrix} & 1 & & \theta_k & & & \\ 1 & & 1 & & & & \\ & 1 & & 1 & & \theta_k & \\ \theta_k^* & & 1 & & 1 & & \\ & & & 1 & & 1 & \\ & & \theta_k^* & & 1 & & \\ & & & & & & \ddots \end{pmatrix}, \tag{4.50}$$

where θ_k is given in eq. (4.45).

Haldane term

For the second term of eq. (4.12), which includes the phase factor $\mathrm{e}^{i\pm\phi}$, I temporarily ignore the B-sublattice and drop the lattice index A when writing out the operators. Proceeding similarly as for the tight binding term, the

Haldane hopping term is

$$\begin{aligned}
\sum_{\langle\langle i,j\rangle\rangle} \mathrm{e}^{i\nu_{ij}\phi} c_i^\dagger c_j &= \sum_{x,y,\bar{\boldsymbol{\delta}}} \mathrm{e}^{i\nu(\bar{\boldsymbol{\delta}})\phi} \frac{1}{N_x} \sum_{k_1,k_2} \mathrm{e}^{-i(k_1-k_2)x} \mathrm{e}^{ik_2\bar{\boldsymbol{\delta}}_x} c^\dagger_{k_1,y} c_{k_{2,y+\bar{\boldsymbol{\delta}}_y}} \\
&= \sum_{j=1}^{N_y} \sum_k \Big[\mathrm{e}^{i\phi} \left(c^\dagger_{k,j} c_{k,j+1} + \mathrm{e}^{ikd_x} c^\dagger_{k,j} c_{k,j-2} + \mathrm{e}^{-ikd_x} c^\dagger_{k,j} c_{k,j+1} \right) \\
&\qquad + \mathrm{e}^{-i\phi} \left(c^\dagger_{k,j} c_{k,j-1} + \mathrm{e}^{-ikd_x} c^\dagger_{k,j} c_{k,j+2} + \mathrm{e}^{ikd_x} c^\dagger_{k,j} c_{k,j-1} \right) \Big] \\
&= \sum_{j=1}^{N_y} \sum_k \Big[\mathrm{e}^{i\phi} \left(t_k c^\dagger_{k,j} c_{k,j+1} + \mathrm{e}^{ikd_x} c^\dagger_{k,j} c_{k,j-2} \right) \\
&\qquad + \mathrm{e}^{-i\phi} \left(t_k^* c^\dagger_{k,j} c_{k,j-1} + \mathrm{e}^{-ikd_x} c^\dagger_{k,j} c_{k,j+2} \right) \Big] \\
&= \sum_{j=1}^{N_y} \sum_k \mathrm{e}^{i\phi} \left(t_k c^\dagger_{k,j} c_{k,j+1} + \mathrm{e}^{ikd_x} c^\dagger_{k,j} c_{k,j-2} \right) + h.c. \qquad (4.51)
\end{aligned}$$

For the B-sublattice, the only difference from eq. (4.51) is a relative minus sign in front of the hopping phase ϕ. This is due to the definition in eq. (4.14), where the sign is opposite for the A and B-sublattices. Represented in the basis ineq. (4.47), the matrix representation of the second term of the Haldane model thus takes the form $\psi_k^\dagger M_2 \psi_k$, with

$$M_2 = t_2 \begin{pmatrix}
0 & 0 & \mathrm{e}^{i\phi} t_k & 0 & \mathrm{e}^{-i\phi}\theta_k & 0 & \\
0 & 0 & 0 & \mathrm{e}^{-i\phi} t_k & 0 & \mathrm{e}^{i\phi}\theta_k & \cdots \\
\mathrm{e}^{-i\phi} t_k^* & 0 & 0 & 0 & \mathrm{e}^{i\phi} t_k & 0 & \\
0 & \mathrm{e}^{i\phi} t_k^* & 0 & 0 & 0 & \mathrm{e}^{-i\phi} t_k & \\
\mathrm{e}^{i\phi}\theta_k^* & 0 & \mathrm{e}^{-i\phi} t_k^* & 0 & 0 & 0 & \\
0 & \mathrm{e}^{-i\phi}\theta_k^* & 0 & \mathrm{e}^{i\phi} t_k^* & 0 & 0 & \\
 & \vdots & & & & & \ddots
\end{pmatrix}. \qquad (4.52)$$

Sublattice mass term

The last term of the model in eq. (4.12) consider the lattice asymmetry, including a mass term associated with the A-and B-sublattice fermions. Finding the matrix representations is straightforward, and only contributes with an alternating diagonal with strength λ_S. The term can thus be written $\psi_k^\dagger M_3 \psi_k$

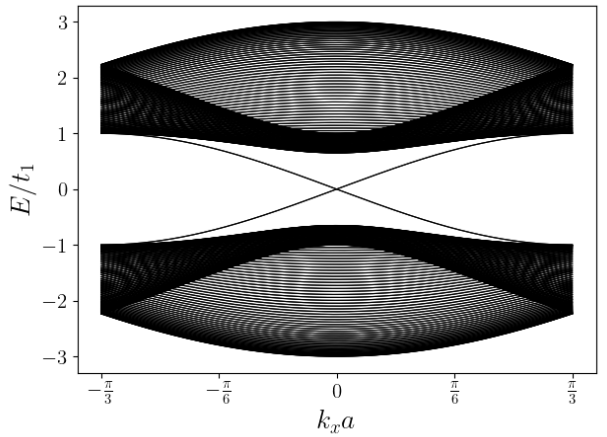

Figure 4.7: The electronic band structure of the Haldane model on an armchair ribbon with $t_2 = -0.125t_1$. The width of the sample is here $N_y = 100$, and the next-to-nearest neighbor hopping phase is set to $\phi = \pi/2$. The Semenoff mass is set to 0.

with

$$M_3 = \lambda_S \begin{pmatrix} 1 & & & \\ & -1 & & \\ & & 1 & \\ & & & \ddots \end{pmatrix} \tag{4.53}$$

For the armchair nanoribbon, the Haldane model including a lattice asymmetry parameter λ_S is thus

$$H = \sum_k \psi_k^\dagger H_k \psi_k, \tag{4.54}$$

with

$$H_k = M_1 + M_2 + M_3. \tag{4.55}$$

The matrix representation of the Hamiltonian may now be diagonalized to extract eigenvalues and eigenstates of the system. The dispersion over the one-dimensional Brillouin zone is shown in fig. 4.7 for a system of width $N_y = 100$. Apart from two crossing bands, the system is insulating with a band gap $\sim 2t_1$. By setting the chemical potential in the bulk gap, the Fermi velocity v_F can be estimated from the approximately linear gapless states in fig. 4.7 as

$$v_F \simeq 4\text{eV}\frac{a}{\hbar} \simeq 863\text{km/s}. \tag{4.56}$$

In appendix A.1 I compute the corresponding matrix representation for a Rashba spin-orbit coupling term which is not considered further in this thesis.

4.2.2 Localized Edge States

I now show that the two gapless states in the bulk gap of fig. 4.7 are localized at the edges. In fig. 4.8 I have plotted the localization of these states as a function of k_x and the position along the width of the lattice y, where the states are normalized by

$$\sum_y |\psi_i(k_x, y)| \equiv 1. \tag{4.57}$$

The first thing to notice is that the states is exponentially damped towards the interior for k_x not to close to the Brillouin zone edge. Moreover, the states are localized at opposite edges, such that a localized state on one edge propagate the opposite direction of the other.

The gapless states in the bulk gap in fig. 4.7 is thus localized at the edges and propagates in opposite directions for the upper and lower edge. For the spinful Kane-Mele model of a topological insulator given in eq. (3.7), there exist two degenerate states (Kramers pairs) on the same edge propagating in the opposite direction with opposite spin[10]. Due to the localization of these states, the fermionic theory most suitable for their description is one-dimensional. In the spinless Haldane model, these reside on opposite edges.

4.2.3 Phonons

In this section I compute the phonon spectrum of the armchair nanoribbon. The force constants are taken from [72], summarized in [69]. These are constants approximated by matching the resulting analytic phonon spectrum with the experimentally observed data. The full phonon Hamiltonian is given in eq. (4.30). This is expanded as

$$H_{\text{ph}} = \sum_D \sum_{i \in D} \frac{\mathbf{P}_i^2}{2M} + \frac{1}{2} \sum_D \sum_{\langle\langle i,j \rangle\rangle} \sum_{\mu,\nu} u_i^{\mu, D_i} \Phi_{\mu\nu}^i(\boldsymbol{\delta}_{ij}) u_j^{\nu, D_j}, \tag{4.58}$$

where all information about the force constants are given in the dynamical matrix $\Phi(\boldsymbol{\delta}_{ij})$. The vector $\boldsymbol{\delta}$ here refer to all neighboring vectors labeled in fig. 4.9, and the indices μ, ν are Cartesian coordinates representing the direction of lattice displacement. Given the translational invariance of Φ, it is only dependent on the neighboring vectors between lattice sites, not the position in the lattice itself. A partial Fourier transform of eq. (4.58) along the x-axis

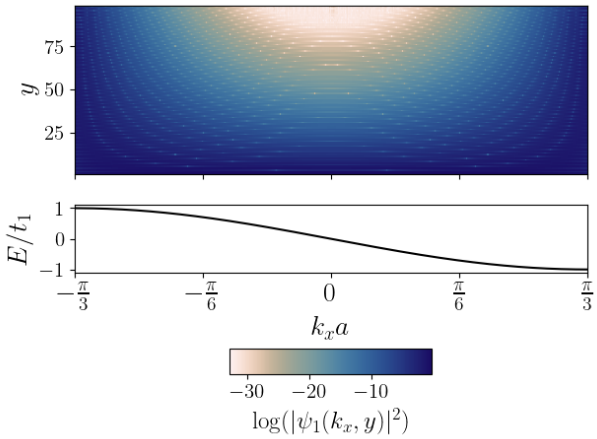

(a) Localized state at the lower edge.

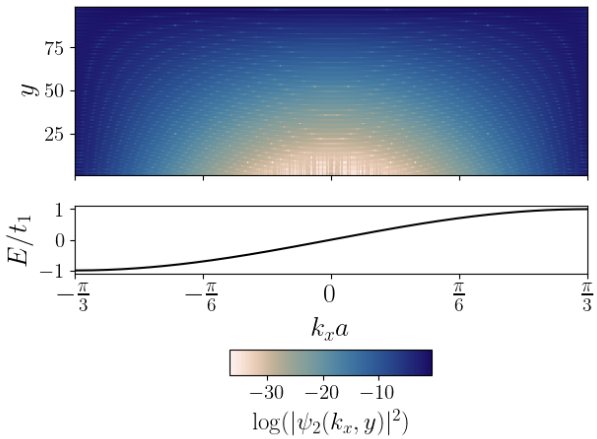

(b) Localized state at the upper edge

Figure 4.8: Localization of electronic states in the bulk gap of the same system as in fig. 4.7. The states show an exponential decay of fermion density for a large slice of the Brillouin zone.

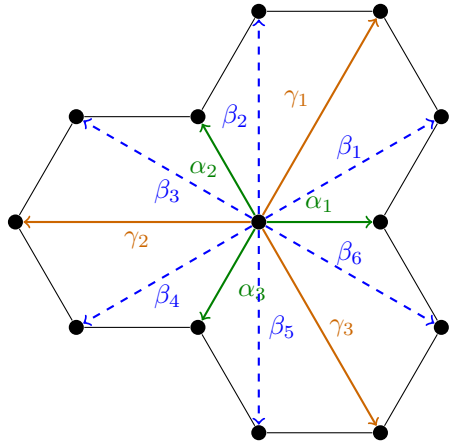

Figure 4.9: Neighboring vectors on the honeycomb lattice including up to third-nearest neighbors.

can now be carried out. With

$$u^{\mu,D}_{x,y} = \frac{1}{\sqrt{N_x}} \sum_q \mathrm{e}^{iqx} u^{\mu,D}_{q,y}, \tag{4.59}$$

and a similar transformation for the momenta, I have

$$\begin{aligned}
\sum_D \sum_{\langle\langle i,j \rangle\rangle} u^{\mu,D_i}_i \Phi^i_{\mu\nu}(\boldsymbol{\delta}_{ij}) u^{\nu,D_j}_j &= \sum_D \sum_{\langle\langle i,j \rangle\rangle} \frac{1}{N_x} \sum_{q_1,q_2} \mathrm{e}^{iq_1x_i} u^{\mu,D_i}_{q_1,y_i} \Phi^i_{\mu\nu}(\boldsymbol{\delta}_{ij}) \mathrm{e}^{iq_2x_j} u^{\nu,D_j}_{q_2,y_j} \\
&= \sum_D \sum_i \sum_{\boldsymbol{\delta}} \frac{1}{N_x} \sum_{q_1,q_2} \mathrm{e}^{i(q_1+q_2)x_i} \mathrm{e}^{iq_2\delta_x} u^{\mu,D_i}_{q_1,y_i} \Phi^i_{\mu\nu}(\boldsymbol{\delta}) u^{\nu,D_{\boldsymbol{\delta}}}_{q_2,y_i+\delta_y} \\
&= \sum_D \sum_y \sum_{\boldsymbol{\delta}} \sum_q \mathrm{e}^{iq\delta_x} u^{\mu,D_i}_{q,y} \Phi^D_{\mu\nu}(\boldsymbol{\delta}) u^{\nu,D_{\boldsymbol{\delta}}}_{q,y+\delta_y},
\end{aligned}$$

where $D_{\boldsymbol{\delta}}$ denote the sublattice A or B, depending on at which of these $\boldsymbol{\delta}$ ends. The total phonon Hamiltonian in eq. (4.58) is now

$$H_{\mathrm{ph}} = \sum_q \sum_D \sum_y \frac{\mathbf{P}^D_{-q,y} \mathbf{P}^D_{q,y}}{2M} + \frac{1}{2} \sum_q \sum_D \sum_y \sum_{\mu,\nu} \sum_{\boldsymbol{\delta}} \mathrm{e}^{iq\delta_x} u^{\mu,D}_{-q,y} \Phi_{\mu\nu}(\boldsymbol{\delta}) u^{\nu,D_{\boldsymbol{\delta}}}_{q,y+\delta_y}. \tag{4.60}$$

I now consider the armchair nanoribbon geometry, for which the first Brillouin zone is reduced because of a $d_x = 3a$ periodicity in the x-direction.

Within the labeling convention of fig. 4.6, the vectors in fig. 4.9 satisfy

$$\boldsymbol{\alpha}_1 = (0,0) \qquad \boldsymbol{\beta}_1 = (0,1) = -\boldsymbol{\beta}_4 \tag{4.61a}$$
$$\boldsymbol{\alpha}_2 = (-1,1) \qquad \boldsymbol{\beta}_2 = (-1,2) = -\boldsymbol{\beta}_5 \tag{4.61b}$$
$$\boldsymbol{\alpha}_3 = (0,-1) \qquad \boldsymbol{\beta}_3 = (-1,1) = -\boldsymbol{\beta}_6, \tag{4.61c}$$

where the first components is in units of d_x, and the second component is a number to represent its index position in the y-direction. For the neighboring vectors starting at an atom at another sublattice, a relative minus sign is added. The vectors α_i and γ_i connect ions on different sublattices, while β_i connects ions on equivalent sites. Focusing on the second term in eq. (4.60), I split the sum over neighbors in these three terms, one for each of α_i, β_i. The potential energy with nearest and next to nearest neighbors couplings is

$$\begin{aligned}
&\frac{1}{2}\sum_q \sum_D \sum_y \sum_{\mu,\nu} \sum_{\boldsymbol{\delta}} \mathrm{e}^{iq\delta_x} u^{\mu,D}_{-q,y} \Phi_{\mu\nu}(\boldsymbol{\delta}) u^{\nu,D_{\boldsymbol{\delta}}}_{q,y+\delta_y} \\
&= \frac{1}{2}\sum_q \sum_D \sum_y \sum_{\mu,\nu} u^{\mu,D}_{-q,y} \left(\sum_{\boldsymbol{\alpha}} \Phi^D_{\mu\nu}(\boldsymbol{\alpha}) \mathrm{e}^{iq\alpha_x} u^{\nu,D'}_{q,y+\alpha_y} + \sum_{\boldsymbol{\beta}} \Phi^D_{\mu\nu}(\boldsymbol{\beta}) \mathrm{e}^{iq\beta_x} u^{\nu,D}_{q,y+\beta_y} \right) \\
&= \frac{1}{2}\sum_q \sum_y \sum_{\mu,\nu} M^{\mu\nu}_{q,y},
\end{aligned} \tag{4.62}$$

where

$$\begin{aligned}
M^{\mu\nu}_{q,y} = \Big\{ & u^{\mu,A}_{-q,y} \Big(\Phi^0_{\mu\nu} u^{\nu,A}_{q,y} + \Big[\Phi^{\alpha_1}_{\mu\nu} u^{\nu,B}_{q,y} + \Phi^{\alpha_2}_{\mu\nu} \mathrm{e}^{-iqd} u^{\nu,B}_{q,y+1} + \Phi^{\alpha_3}_{\mu\nu} u^{\nu,B}_{q,y-1} \Big] \\
& + \Big[\left(\Phi^{\beta_1}_{\mu\nu} + \Phi^{\beta_3}_{\mu\nu} \mathrm{e}^{-iqd} \right) u^{\nu,A}_{q,y+1} + \Phi^{\beta_2}_{\mu\nu} \mathrm{e}^{-iqd} u^{\nu,A}_{q,y+2} \\
& \qquad + \left(\Phi^{\beta_4}_{\mu\nu} + \Phi^{\beta_6}_{\mu\nu} \mathrm{e}^{iqd} \right) u^{\nu,A}_{q,y-1} + \Phi^{\beta_5}_{\mu\nu} \mathrm{e}^{iqd} u^{\nu,A}_{q,y-2} \Big] \Big) \\
& + u^{\mu,B}_{-q,y} \Big(\Phi^0_{\mu\nu} u^{\nu,B}_{q,y} + \Big[\Phi^{-\alpha_1}_{\mu\nu} u^{\nu,A}_{q,y} + \Phi^{-\alpha_2}_{\mu\nu} \mathrm{e}^{iqd} u^{\nu,A}_{q,y-1} + \Phi^{-\alpha_3}_{\mu\nu} u^{\nu,A}_{q,y+1} \Big] \\
& + \Big[\left(\Phi^{\beta_1}_{\mu\nu} + \Phi^{\beta_3}_{\mu\nu} \mathrm{e}^{-iqd} \right) u^{\nu,B}_{q,y+1} + \Phi^{\beta_2}_{\mu\nu} \mathrm{e}^{-iqd} u^{\nu,B}_{q,y+2} \\
& \qquad + \left(\Phi^{\beta_4}_{\mu\nu} + \Phi^{\beta_6}_{\mu\nu} \mathrm{e}^{iqd} \right) u^{\nu,B}_{q,y-1} + \Phi^{\beta_5}_{\mu\nu} \mathrm{e}^{iqd} u^{\nu,B}_{q,y-2} \Big] \Big) \Big\} .
\end{aligned} \tag{4.63}$$

Here, I have used the notation $\Phi^D_{\mu\nu}(\boldsymbol{\delta}) \to \Phi^{\boldsymbol{\delta}}_{\mu\nu}$, as the coupling matrix do not depend on the sublattice except for the edges.

The on site coupling constants $\Phi^0_{\mu\nu}$ are found through the stability condition

$$\sum_{\boldsymbol{\delta}} \Phi^{\boldsymbol{\delta}}_{\mu\nu} = 0, \tag{4.64}$$

where the sum goes over nearest neighbors, including the zero-vector.

For Graphene, the parameters should not differ for the two different sublattices, which reduces the number of free parameters in the dynamical matrix. Adopting the notation from Thingstad et al. [69], Falkovsky [72], I introduce the chiral basis $\xi, \eta = x \pm iy$, which one can utilize to further reduce the number of free parameters. The coupling constants of the system are

$$\begin{aligned} \alpha &\equiv \Phi^D_{\xi\eta}(\boldsymbol{\alpha}_1) \qquad \beta \equiv \Phi^D_{\xi\xi}(\boldsymbol{\alpha}_1) = (\Phi^D_{\eta\eta}(\boldsymbol{\alpha}_1))^* \\ \gamma &\equiv \Phi^D_{\xi\eta}(\boldsymbol{\beta}_1) \qquad \delta \equiv \Phi^D_{\xi\xi}(\boldsymbol{\beta}_1) = (\Phi^D_{\eta\eta}(\boldsymbol{\beta}_1))^*, \end{aligned} \tag{4.65}$$

where the vectors $\boldsymbol{\alpha}_i, \boldsymbol{\beta}_i$ is shown in fig. 4.9. The constants for other neighboring vectors can be determined by using the symmetric properties of the system. The neighboring vectors are related by consecutive rotations of $2\pi/3$ radians in the complex plane. In the chiral basis, the couplings transform according to

$$\begin{aligned} \Phi^D_{\xi\xi}(R_3\boldsymbol{\alpha}_i) &= \Phi^D_{\xi\xi}(\boldsymbol{\alpha}_i)\mathrm{e}^{\frac{i2\pi}{3}} \qquad \Phi^D_{\eta\eta}(R_3\boldsymbol{\alpha}_i) = \Phi^D_{\eta\eta}(\boldsymbol{\alpha}_i)\mathrm{e}^{-\frac{i2\pi}{3}} \\ \Phi^D_{\xi\eta}(R_3\boldsymbol{\alpha}_i) &= \Phi^D_{\xi\eta}(\boldsymbol{\alpha}_i) \qquad \Phi^D_{\eta\xi}(R_3\boldsymbol{\alpha}_i) = \Phi^D_{\eta\xi}(\boldsymbol{\alpha}_i), \end{aligned} \tag{4.66}$$

where R_3 are three-fold rotations. These operators constitute the elements of the C_3 symmetry group. Using the relations in eq. (4.66) with the stability condition in eq. (4.64), I can compute $\Phi^0_{\mu\nu}$ for the bulk and edges for both sublattices. To make it clear, I will denote the different constants as $\Phi^{D,\text{bulk/upper edge (UE)/lower edge (LE)}}_{\mu\nu}$, where again $D \in (A, B)$ denotes the specific sublattice and (μ, ν) are chiral components. The lower edge corresponds to the $y = 0$-term in the Hamiltonian, while the upper edge corresponds to $y = N_y - 1$.

For an atom on sublattice A that do not reside on the edge, the equations are

$$\begin{aligned} &\Phi^{A,\text{bulk}}_{\xi\xi} + (\beta + 2\delta)(1 + \mathrm{e}^{\frac{i2\pi}{3}} + \mathrm{e}^{-\frac{i2\pi}{3}}) = 0 \implies \Phi^{A,\text{bulk}}_{\xi\xi} = 0 \\ &\Phi^{A,\text{bulk}}_{\eta\eta} + (\beta + 2\delta)(1 + \mathrm{e}^{-\frac{i2\pi}{3}} + \mathrm{e}^{\frac{i2\pi}{3}}) = 0 \implies \Phi^{A,\text{bulk}}_{\eta\eta} = 0 \\ &\Phi^{A,\text{bulk}}_{\xi\eta} + 3\alpha + 6\gamma = 0 \implies \Phi^{A,\text{bulk}}_{\xi\eta} = -3(\alpha + 2\gamma) \\ &\Phi^{A,\text{bulk}}_{\eta\xi} + 3\alpha + 6\gamma = 0 \implies \Phi^{A,\text{bulk}}_{\eta\xi} = -3(\alpha + 2\gamma). \end{aligned} \tag{4.67}$$

These couplings for atoms on sublattice B are equal in the bulk, $\Phi^{B,\text{bulk}}_{\mu\nu} = \Phi^{A,\text{bulk}}_{\mu\nu}$. For the edges, the stability condition in eq. (4.64) results in

$$\begin{aligned}
\Phi^{A,\text{LE}}_{\xi\xi} &= -\beta(1+\mathrm{e}^{\frac{i2\pi}{3}}) & \Phi^{B,\text{LE}}_{\xi\xi} &= -\beta(1+\mathrm{e}^{-\frac{i2\pi}{3}}) \\
\Phi^{A,\text{LE}}_{\eta\eta} &= -\beta(1+\mathrm{e}^{-\frac{i2\pi}{3}}) & \Phi^{B,\text{LE}}_{\eta\eta} &= -\beta(1+\mathrm{e}^{\frac{i2\pi}{3}}) \\
\Phi^{A,\text{UE}}_{\xi\xi} &= -\beta(1+\mathrm{e}^{-\frac{i2\pi}{3}}) & \Phi^{B,\text{UE}}_{\xi\xi} &= -\beta(1+\mathrm{e}^{\frac{i2\pi}{3}}) \\
\Phi^{A,\text{UE}}_{\eta\eta} &= -\beta(1+\mathrm{e}^{\frac{i2\pi}{3}}) & \Phi^{B,\text{UE}}_{\eta\eta} &= -\beta(1+\mathrm{e}^{-\frac{i2\pi}{3}}) \\
\Phi^{A,\text{LE}}_{\xi\eta} &= \Phi^{A,\text{LE}}_{\eta\xi} = -2\alpha - 3\gamma & \Phi^{B,\text{LE}}_{\xi\eta} &= \Phi^{B,\text{LE}}_{\eta\xi} = -2\alpha - 3\gamma \\
\Phi^{A,\text{UE}}_{\xi\eta} &= \Phi^{A,\text{UE}}_{\eta\xi} = -2\alpha - 3\gamma & \Phi^{B,\text{UE}}_{\xi\eta} &= \Phi^{B,\text{UE}}_{\eta\xi} = -2\alpha - 3\gamma.
\end{aligned} \tag{4.68}$$

Cartesian basis

The coupling constants $\Phi^{D}_{\mu\nu}(\boldsymbol{\delta})$ in the Cartesian basis are related through those given in the chiral basis by the transformation

$$\begin{aligned}
\Phi^{D}_{xx}(\boldsymbol{\delta}) &= \Phi^{D}_{\xi\xi}(\boldsymbol{\delta}) + \Phi^{D}_{\xi\eta}(\boldsymbol{\delta}) + \Phi^{D}_{\eta\xi}(\boldsymbol{\delta}) + \Phi^{D}_{\eta\eta}(\boldsymbol{\delta}) \\
\Phi^{D}_{xy}(\boldsymbol{\delta}) &= i\left(\Phi^{D}_{\xi\xi}(\boldsymbol{\delta}) - \Phi^{D}_{\xi\eta}(\boldsymbol{\delta}) + \Phi^{D}_{\eta\xi}(\boldsymbol{\delta}) - \Phi^{D}_{\eta\eta}(\boldsymbol{\delta})\right) \\
\Phi^{D}_{yx}(\boldsymbol{\delta}) &= i\left(\Phi^{D}_{\xi\xi}(\boldsymbol{\delta}) + \Phi^{D}_{\xi\eta}(\boldsymbol{\delta}) - \Phi^{D}_{\eta\xi}(\boldsymbol{\delta}) - \Phi^{D}_{\eta\eta}(\boldsymbol{\delta})\right) \\
\Phi^{D}_{yy}(\boldsymbol{\delta}) &= -\Phi^{D}_{\xi\xi}(\boldsymbol{\delta}) + \Phi^{D}_{\xi\eta}(\boldsymbol{\delta}) + \Phi^{D}_{\eta\xi}(\boldsymbol{\delta}) - \Phi^{D}_{\eta\eta}(\boldsymbol{\delta}).
\end{aligned} \tag{4.69}$$

Using eqs. (4.65), (4.66) and (4.69), the coupling constants are

$$\begin{aligned}
&\Phi_{xx}(\boldsymbol{\alpha}_1) = 2(\alpha+\beta) && \Phi_{xy}(\boldsymbol{\alpha}_1) = \Phi_{yx}(\boldsymbol{\alpha}_1) = 0 && \Phi_{yy}(\boldsymbol{\alpha}_1) = 2(\alpha-\beta) \\
&\Phi_{xx}(\boldsymbol{\alpha}_2) = 2\alpha-\beta && \Phi_{xy}(\boldsymbol{\alpha}_2) = \Phi_{yx}(\boldsymbol{\alpha}_2) = -\sqrt{3}\beta && \Phi_{yy}(\boldsymbol{\alpha}_2) = 2\alpha+\beta \\
&\Phi_{xx}(\boldsymbol{\alpha}_3) = 2\alpha-\beta && \Phi_{xy}(\boldsymbol{\alpha}_3) = \Phi_{yx}(\boldsymbol{\alpha}_3) = +\sqrt{3}\beta && \Phi_{yy}(\boldsymbol{\alpha}_3) = 2\alpha+\beta
\end{aligned} \tag{4.70}$$

for the nearest neighboring vectors. The stability condition in eq. (4.64) gives the remaining ones, resulting in

$$\begin{aligned}
\Phi^{D,\text{Bulk}}_{\mu\nu} &= -6\alpha\delta_{\mu\nu} & \Phi^{D,\text{LE/UE}}_{xx} &= -4\alpha-\beta & \Phi^{D,\text{LE/UE}}_{yy} &= -4\alpha+\beta \\
\Phi^{A,\text{LE}}_{xy} &= \Phi^{A,\text{LE}}_{yx} & &= \Phi^{B,\text{UE}}_{xy} = \Phi^{B,\text{UE}}_{yx} & &= \sqrt{3}\beta \\
\Phi^{B,\text{LE}}_{xy} &= \Phi^{B,\text{LE}}_{yx} & &= \Phi^{A,\text{UE}}_{xy} = \Phi^{A,\text{UE}}_{yx} & &= -\sqrt{3}\beta.
\end{aligned} \tag{4.71}$$

By introducing the $4N_y$-dimensional basis

$$\mathbf{u}_q = (u^A_{x,0}, u^B_{x,0}, u^A_{y,0}, u^B_{y,0}, \ldots, u^A_{x,N_y-1}, u^B_{x,N_y-1}, u^A_{y,N_y-1}, u^B_{y,N_y-1})^T \tag{4.72}$$

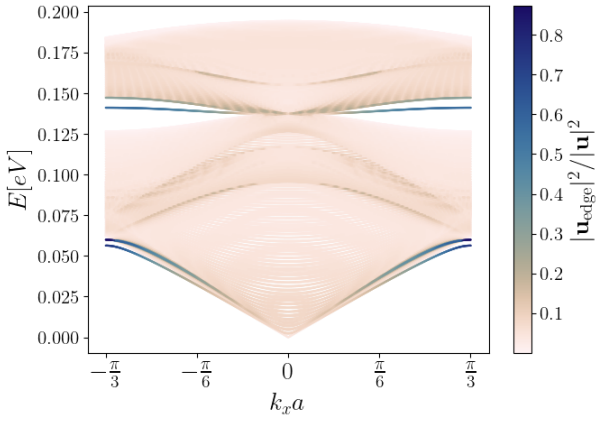

Figure 4.10: Phonon spectrum of graphene armchair ribbon with $N_y = 100$. The phonon eigenstate is denoted by $\mathbf{u}$, and $\mathbf{u}_{\text{edge}}$ the projection onto the outermost lattice sites on the nanoribbon.

and the corresponding canonical momentum, the phonon Hamiltonian in eq. (4.58) can be written on matrix form

$$H = \frac{1}{2M}\sum_q \mathbf{P}_q^\dagger \mathbf{P}_q + \frac{1}{2}\sum_q \mathbf{u}_q^\dagger M_q \mathbf{u}_q. \tag{4.73}$$

The factor θ_q is given in eq. (4.45). The stability condition ensures that the sum of each row and column in M_q is 0 at $q = 0$. In numerical calculations, I have restricted the analysis to only include nearest neighbor interaction. This is because the analysis gives rise to imaginary eigenvalues with the inclusion of next-to-nearest neighbors, suggesting that a more thorough symmetry analysis in the finite system should be studied for correct implementation. I henceforth disregard the next to nearest interaction by setting $\delta = \gamma = 0$ in eq. (4.65), and match the resulting energy spectrum with the optical frequency $\omega_\Gamma \simeq 0.2$eV at the Γ-point [69]. The nearest neighbor Hamiltonian should nevertheless give a qualitatively correct description of the phonon dynamics on the nanoribbon. In the computed spectrum in fig. 4.10, I have taken a system of width $N_y = 100$ and marked the projection of eigenstates onto the edges of the system. It is apparent that there are, in addition to bulk modes, localized states on the edges of the graphene nanoribbon. These are, as opposed to the fermions in fig. 4.8, more localized at the edges closer to the Brillouin zone boundary.

4.2.4 Electron-Phonon Coupling on Armchair Edges

As has now been shown, the edges of the graphene nanoribbon host highly localized, effectively one-dimensional states. I will replace the fermionic theory of the edges by a one-dimensional description, whose dispersion is assumed to be linear. The coupling between phonons and fermions on the edges are therefore also replaced by coupling independent of the fermion momentum k, but where the bulk parameters in [69] is inserted in eq. (4.42). The summation over neighboring lattice vectors is replaced by the convention depicted in fig. 4.9, and the lattice deviations are found by projecting the eigenstates onto one of the edges. The resulting coupling is therefore expected to be strongest for the most localized phonon states shown in fig. 4.10. In chapter 6, I use the phonon spectrum and obtained coupling constants to numerically compute the corrections to the fermionic Green's functions caused by these interactions. First, the theory of one-dimensional fermions must be developed.

"So in this paper we must be content only to present considerations of a rather mathematical nature without entering into real physical problems."

— Sin-Itiro Tomonaga, *1950*

Chapter 5. Bosonization and Luttinger Liquids

Bosonization and Luttinger Liquids

In this chapter, I will first present a qualitative discussion of interacting fermions in one dimension and some of its key properties. By deriving a bosonization identity, I will then present the mathematical framework that will be utilized in the computation of correlation functions. This derivation will be done through "constructive bosonization" of the fermionic fields and involves a reorganization of the total Fock space in terms of individual Hilbert spaces consisting of a fixed number of particles. This reorganization relies upon the non-existence of single particle excitations that would change the total number of particles in a general quantum state, as is the case in one dimension.

5.1 Fermions in One Dimension

In one dimension the Fermi surface reduces to distinct points. This drastically reduces the scattering possibilities compared to that of higher dimensions, whose Fermi surface typically is continuous and simply connected. By this argument alone, it should be no surprise that an interacting fermion theory reduced to one dimension should exhibit features not present in higher-dimensional systems [22, 41].

5.1.1 Breakdown of Fermi Liquid Theory

The kinematics in one dimension is highly restricted due to the reduced available phase space. By considering a array of spinless fermions, the Pauli exclusion principle forbids a single fermion to "move" past another, lest it too "moves". This causes forward scattering of a single electron to be singular. Thus, one-particle scattering is not allowed, whilst collective ones are of significant importance. This is weakly analogous to a traffic jam, where individual vehicles cannot pass each other and only moves at as a collective unit [23]. The consequences of these physical insights also occur when applying Fermi liquid theory. In one dimension, the particle-hole bubble diagram is known to have an infrared divergence called the Peierls divergence [21]. This means that the regular many-body approach to perturbation theory based on the Landau quasiparticle picture breaks down, and a replacement for Fermi liquid theory is necessary if one wants to solve an interacting system. Luttinger showed [26] that any interaction destroys the discontinuity in the occupation number at the Fermi level for $T = 0$, in contrast to the nonzero quasiparticle residue in Fermi liquid theory. As briefly discussed in chapter 2, Landau's theory of interacting electrons is based on the idea that one can adiabatically transform

the non-interacting system into that of the interacting with a one-to-one correspondence between the two ensembles of states. However, a key property of interacting one-dimensional systems is the separation of spin- and charge-degrees of freedom in collective particle-hole excitations, of which there is no way to smoothly transform a non-interacting system of single particle excitations into [41].

These exotic states of matter in which collective particle excitations called "holons" and "spinons" are long-lived excitations, and phenomena like spin-charge separation occur if these excitations propagate with different velocities. Analogous to Landaus Fermi liquid, a theory of interacting fermions based the free Fermi gas, Haldane [20] coined the term "Luttinger liquid" for the description of interacting fermions in one dimension, based on the exactly soluble Tomonaga-Luttinger model [25, 26], and presented a recipe for adding interactions to the problem.

One of the key properties of Luttinger liquids is the power-law dependence of correlation functions. In stark contrast to Fermi liquids, these exponents are interaction-dependent and thus *non-universal* [20, 22]. Although the system of interacting fermions on the graphene nanoribbon is a two-dimensional system, the long-distance physics of the edge states can be treated as a one-dimensional system, and the theory serves as a good model. As shown in fig. 4.8, these states are localized at the edges with an exponentially decaying probability density, allowing for a one-dimensional picture.

5.1.2 The Tomonaga-Luttinger model

Tomonaga presented a mathematical framework for solving many-fermionic systems in terms of the Fourier components of the density waves in his seminal 1950 paper [25]. By first considering an ideal Fermi gas whose particle-hole excitations only occur near the Fermi level, and then adding inter-particle forces whose interaction length is not too short, and whose strength not to large, Tomonaga was able to show that the density fields could be represented in terms of Bose-field under these restricting conditions. These limitations on the scattering possibilities proved fruitful, and set the stone for further investigations. The methods Tomonaga presented in this paper was at an early stage adopted to the theories of electron-phonon coupling in one dimension and its role in superconductivity [28, 29].

In 1963, Luttinger proposed an exactly soluble model of a many-fermion system with linear dispersion, and showed that any interactions in one dimension completely destroys the quasiparticle discontinuity in the momentum distribution. This is a first indication that Fermi liquid theory is insufficient in one dimension. The Tomonaga and Luttinger models was compared and found

to be equivalent as long as the particle-hole excitations are sufficiently close to the Fermi level [27]. The Luttinger model is described by the non-interacting Hamiltonian

$$H_L = -iv_F \int_{-\frac{L}{2}}^{\frac{L}{2}} \mathrm{d}x\, \boldsymbol{\psi}^\dagger \sigma_z \partial_x \boldsymbol{\psi}, \tag{5.1}$$

where $\boldsymbol{\psi} = \begin{pmatrix} \psi_R & \psi_L \end{pmatrix}^T$ is a two-component spinor representing the right/left-moving fermions. Inserting the Fourier transform representation

$$\boldsymbol{\psi}(x) = \frac{1}{\sqrt{L}} \sum_n \mathrm{e}^{i\frac{2\pi n}{L}x} \boldsymbol{c}_n \tag{5.2}$$

yields the momentum resolved kinetic energy

$$H_L = \frac{2\pi v_F}{L} \sum_n n \boldsymbol{c}_n^\dagger \sigma_z \boldsymbol{c}_n, \tag{5.3}$$

where the sum runs over all integers. This Hamiltonian represent massless Dirac-fermions, as the dispersion is linear in momentum. Since the sum runs over all n, the energy is not bounded from below, and all physical quantities has to be compared to a properly defined vacuum state, which will be described in the subsequent bosonic reconstruction of the theory.

5.1.3 Realization in Topological Insulators

Tomonaga originally presented his work with the note that he had not been successful in the generalization to three dimensions, and that the theory should only be understood as a purely mathematical work [25]. Luttinger also pointed out that his model was quite unrealistic of two reasons; one being a one-dimensional system, and the other that the fermions are massless [26]. In modern physics, these views have been altered, and multiple systems have been shown to exhibit Luttinger liquid behavior [23], as for instance in Carbon nanotubes [73] and organic conductors [74].

In chapter 3, I described helical edge states that arises in time reversal invariant systems. These are best described as helical Luttinger liquids, and have been observed at the edges of InAs/GaSb [75] and Bi/SiC [16] QSH insulators.

5.2 Constructive Bosonization of a 1D Fermionic Theory

In this section I will derive the bosonization identities used to compute the fermionic Green's functions. A fermionic theory is a model describing the

physical properties of fermions, i.e. electrons. In the second quantized formalism discussed in section 2.1, this is described by a set of single-particle creation and annihilation operators satisfying the canonical anticommutation relations for fermions given in eq. (2.5).

The term "bosonization" refers to the transformation of a system of interacting fermions into a system of possibly non-interacting bosons. The idea of bosonization is that one can represent the fermionic creation and annihilation operators $(c_\mu^\dagger, c_\mu)$ in terms of new bosonic operators a_μ. This works if one can reorganize the total Fock space $\mathcal{F}$ spanned by $\{c_{k\mu}\}$ as a direct sum over Hilbert spaces with *fixed* particle numbers [76]. The fundamental excitations within these individual subspaces are particle-hole-excitations obeying the bosonic commutation relations in eq. (2.6).

Single bosonic operators cannot possibly change the total number of fermions of a given species in the system as fermionic operators do. Thus, a purely bosonic representation is not possible. This obstacle can nevertheless be avoided by the inclusion of so called Klein factors $F_\mu^\dagger, F_\mu$ whose only effect is to raise or lower the occupancy of the single particle state μ. By definition, the Klein factors commute with boson operators a_μ that is yet to be introduced. Although the creation and/or destruction of single particle states is possible to incorporate through the Klein factors, their presence will not be of great importance, as all physical quantities that I will compute include exactly one $F_\mu^\dagger$ and one F_μ for each fermion species, and the exclusion of these does not affect the resulting Green's functions. These factors ensure the correct (anti)-commutations between fermions of different species, and also connects the different sectors of $\mathcal{F}$ with different fermion particle numbers.

There are multiple ways of bosonizing a fermionic theory, either by integrating out fermionic degrees of freedom in the partition function by introducing auxiliary bosonic field(s) formulated in the framework of path integrals, or by mapping the theory as an exact operator identity through "constructive" bosonization in second quantization. I will use the latter and follow the lines of von Delft and Schoeller [76].

For the proofs of completeness and explicit representation of Klein Factors I refer to the derivation of Haldane [20], which is recapitulated in Appendix B of Giamarchi [22]. Completeness is shown by comparing the partition function in both fermion and boson language, and finding that they are indeed equal.

5.2.1 Fermionic theory

The starting point of the bosonization procedure is a theory of fermionic fields $\psi_\mu(x)$ describing the many-particle state. Here, μ is taken to be any set of quantum numbers relevant for the problem. A real space description of the

fermionic fields may be defined through

$$\psi_\mu(x) = \frac{1}{\sqrt{L}} \sum_k \mathrm{e}^{-ikx} c_{k\mu}, \tag{5.4}$$

where $c_{k,\mu}$ satisfy the anticommutation relations in eq. (2.5), and the normalization is chosen such that the density has unit norm [1]. The inverse of eq. (5.4) is

$$c_{k\mu} = \frac{1}{\sqrt{L}} \int_{-\frac{L}{2}}^{\frac{L}{2}} \mathrm{d}x\, \mathrm{e}^{ikx} \psi_\mu(x), \tag{5.5}$$

where L is the length of the lattice. Keeping L finite, the wavenumber assumes only discrete values

$$k = \frac{2\pi}{L}(n_k - \frac{1}{2}\delta_b), \tag{5.6}$$

where the role of δ_b become apparent when performing the k-summation in eq. (5.4), obtaining

$$\psi_\mu(x + L/2) = \mathrm{e}^{i\pi\delta_b} \psi_\mu(x - L/2). \tag{5.7}$$

This means that δ_b sets the periodicity of the fields. In real space, $\psi_\mu(x)$ obey

$$\begin{aligned}
\{\psi_\mu(x), \psi^\dagger_{\mu'}(x')\} &= \frac{1}{L} \sum_{k,k'} \mathrm{e}^{-ikx} \mathrm{e}^{ik'x'} \{c_{k\mu}, c^\dagger_{k'\mu'}\} \\
&= \delta_{\mu\mu'} \frac{1}{L} \sum_n \mathrm{e}^{-i(\frac{2\pi}{L}(n-\frac{1}{2}\delta_b))(x-x')} \\
&= \delta_{\mu\mu'} \frac{1}{L} \sum_n 2\pi\delta\left(\frac{2\pi}{L}(x-x') - 2\pi n\right) \mathrm{e}^{i\frac{\pi}{L}(x-x')\delta_b} \\
&= \delta_{\mu\mu'} \sum_n \delta(x - x' - nL) \mathrm{e}^{i\pi n\delta_b},
\end{aligned}$$

which for restricted $x, x' \in [-L/2, L/2]$ gives the standard anticommutation for a normalized fermion field

$$\{\psi_\mu(x), \psi^\dagger_\mu(x')\} = \delta_{\mu\mu'}\delta(x - x'). \tag{5.8}$$

Similarly, the fields obey

$$\{\psi_\mu(x), \psi_{\mu'}(x')\} = 0. \tag{5.9}$$

From here δ_b will be taken to be 0, thereby fixing the periodicity of the electron field.

[1] Compared to von Delft and Schoeller [76], who chooses to normalize the fields such that the correlation functions are normalized to 1, the difference is a factor $\sqrt{2\pi}$ in the fermionic fields.

5.2.2 Fock Space and Definition of Vacuum

I will in this subsection go through the organization of the Fock space needed to construct a bosonic theory. The definitions follow that of von Delft and Schoeller [76], except for a minor difference in the definition of boson operators. As already pointed out presenting the Tomonaga-Luttinger model, one has to compute physical quantities with respect to the vacuum (Fermi sea). In these one dimensional systems whose fundamental excitations are particle-hole excitations, the natural definition of the vacuum would be a state for which there are zero particle-hole excitations. However, an infinite amount of such states exists, and this definition does not suffice. The vacuum state is defined by the properties

$$c_{k\mu} \left|\mathbf{0}_0\right\rangle \equiv 0 \qquad k(n_k) > 0 \tag{5.10a}$$

$$c^\dagger_{k\mu} \left|\mathbf{0}_0\right\rangle \equiv 0 \qquad k(n_k) \leq 0, \tag{5.10b}$$

which ensures that for all species μ, the state with $n_k = 0$ is always the highest filled energy level. Moreover, the lowest unoccupied level is by definition the state with $n_k = 1$.

Observable quantities are measured relative to their vacuum expectation values. Since an infinite number of occupied states is assumed, introducing fermion normal ordering of operators is needed, which for linear combinations of destruction or creation operators is equivalent to a subtraction of the vacuum expectation value [22]. In a normal ordered operator product, the creation operators for $k > 0$ are put to the left of destruction operators with $k > 0$, and opposite for $k \leq 0$. The normal ordering is thus defined through

$$\overset{*}{*} O_1 O_2 O_3 \ldots \overset{*}{*} = O_1 O_2 O_3 \cdots - \left\langle \mathbf{0}_0 \right| O_1 O_2 O_3 \ldots \left| \mathbf{0}_0 \right\rangle, \tag{5.11}$$

with $O_i \in \{c^\dagger_\mu, c_\mu\}$ being a fermionic creation or annihilation operator. Both the vacuum and normal ordering is now defined, but a general $\boldsymbol{N}$-particle state is yet to be described in terms of the fermion operators.

The number of fermions of a given species μ relative to the vacuum is eigenvalues of the number operator

$$\hat{N}_\mu \equiv \sum_{n_k} \overset{*}{*} c^\dagger_{n_k\mu} c_{n_k\mu} \overset{*}{*}, \tag{5.12}$$

where the integer n_k is used to denote the wavenumber in eq. (5.6).

Consider m different fermion species, such that $\boldsymbol{N} = (N_1, \ldots, N_m) \in \mathbb{Z}^m$ describes a system where there is N_μ fermions of type μ. N_μ can take negative values since the occupancy is measured relative to zero. A general $\boldsymbol{N}$-particle state is denoted $\left|\boldsymbol{N}\right\rangle$ and is a state-vector whose eigenvalues of $\hat{N}_\mu$ is N_μ for all

species. Such a state can have an arbitrary number of particle-hole excitations. The set of states $\{|\boldsymbol{N}\rangle\}$ span the $\boldsymbol{N}$-particle Hilbert space $\mathcal{H}_{\boldsymbol{N}}$. If there are no single-particle excitations in the problem, the total Fock space may be written as a direct sum

$$\mathcal{F} = \bigoplus_{\boldsymbol{N}} \mathcal{H}_{\boldsymbol{N}}, \tag{5.13}$$

where all relevant interactions in the problem are boson-like (particle-hole), and happen within each subspace $\mathcal{H}_{\boldsymbol{N}}$. The $\boldsymbol{N}$-particle ground state contain no particle-hole excitations, and is constructed from the vacuum as

$$|\boldsymbol{N}_0\rangle = \prod_{\mu=1}^{m} (C_\mu)^{N_\mu} |\boldsymbol{0}_0\rangle , \tag{5.14}$$

where the ordering of creation and annihilation operators is specified trough

$$(C_\mu)^{N_\mu} = \begin{cases} c^\dagger_{N_\mu,\mu} c^\dagger_{N_\mu-1,\mu} \dots c^\dagger_{1,\mu}, & N_\mu > 0 \\ 1 & N_\mu = 0 \\ c_{N_\mu+1,\mu} c_{N_\mu+2,\mu} \dots c_{0,\mu} & N_\mu < 0. \end{cases} \tag{5.15}$$

The interpretation of the $\boldsymbol{N}$-particle ground state in eq. (5.14) is evident; for each species μ of fermions in the already infinitely filled Fermi sea, each $C_\mu^{N_\mu}$ creates or destroys μ-flavored single particle excitations until the number of occupied states relative to the vacuum is N_μ. Naturally, this general state can be constructed through linear combination of fermionic operators

$$|\boldsymbol{N}\rangle = \tilde{f}(\{c^\dagger_{k,\mu}\}, \{c_{k,\mu}\}) \, |\boldsymbol{N}_0\rangle . \tag{5.16}$$

One can show that these states can also be written in terms of only bosonic creation operators

$$|\boldsymbol{N}\rangle = f(\{a^\dagger_{q,\mu}\}) \, |\boldsymbol{N}_0\rangle . \tag{5.17}$$

The goal of the bosonization procedure is to find the representation of the fermionic field in terms of these bosons. That a mapping from eq. (5.16) to eq. (5.17) exists is a non-trivial statement, but the proof of completeness in the boson representation can be carried out by computing the grand canonical partition function using both the fermion and boson representation, and finding that they are equal [20].

In the fermion representation, the state $|\boldsymbol{N}\rangle$ is created by a linear combination of single particle and single hole excitations of the $\boldsymbol{N}$-particle ground state $|\boldsymbol{N}_0\rangle$. In the bosonic representation, the exact same state is created by a sum of combined particle-hole excitations. Clearly, creating an $\boldsymbol{N}$-particle state from the vacuum cannot be achieved purely through bosonic operators, since these preserve the total particle number. This is where Klein factors F_μ contribute, which are unitary operators satisfying $F^\dagger_\mu F_\mu = 1$.

5.2.3 Boson Operators

In this section I will define the boson operators that constitute the fundamental excitations in one-dimensional fermion theories. These operators span the entire Fock space, in the sense that any $\boldsymbol{N}$-particle state can be constructed as linear combination of particle-hole excitations of the $\boldsymbol{N}$-particle ground state $|\boldsymbol{N}_0\rangle$ as in eq. (5.17). Starting with the normal ordered density operator

$$:\rho_\mu(x): = :\psi_\mu^\dagger(x)\psi_\mu(x):, \tag{5.18}$$

the goal is to show that these fundamental excitations can be written in terms of operators with bosonic commutation relations. By inserting eq. (5.4), the density can be written

$$\begin{aligned} :\rho_\mu(x): &= \frac{1}{L}\sum_{k,k'} \mathrm{e}^{ikx}\mathrm{e}^{-ik'x} :c_{k,\mu}^\dagger c_{k',\mu}: \\ &= \frac{1}{L}\sum_{k,q} \mathrm{e}^{-iqx} :c_{k+q,\mu}^\dagger c_{k,\mu}: \\ &= \frac{1}{L}\sum_{q} \mathrm{e}^{-iqx} :\rho_\mu(q):, \end{aligned} \tag{5.19}$$

where the normal ordered Fourier components of the density is defined by

$$:\rho_\mu(q): = \begin{cases} \sum_k c_{k+q,\mu}^\dagger c_{k,\mu} & q \neq 0 \\ \hat{N}_\mu & q = 0. \end{cases} \tag{5.20}$$

The commutation relations for this density wave is reminiscent of bosons, up to a normalization constant. Therefore, I define the operators

$$a_{q,\mu}^\dagger \equiv \left(\frac{2\pi}{L|q|}\right)^{\frac{1}{2}} \sum_k c_{k+q,\mu}^\dagger c_{k,\mu} \qquad \text{for } q > 0 \tag{5.21a}$$

$$a_{q,\mu} \equiv \left(\frac{2\pi}{L|q|}\right)^{\frac{1}{2}} \sum_k c_{k-q,\mu}^\dagger c_{k,\mu} \qquad \text{for } q > 0, \tag{5.21b}$$

which will be very important in the following calculations. In eq. (5.21), the factor $\sum_k c_{k+q,\mu}^\dagger c_{k,\mu}$ is essentially the Fourier components of the fermion density, as seen from eqs. (5.19) and (5.20), and the factor in front is a normalization constant ensuring correct commutation relations, which will be shown. The dispersion of the system is not yet taken into account, and when considering the Tomonaga-Luttinger model with two separate branches of fermions of

each type (left and right moving) the definition of the $a_{q,\mu}$-operators is slightly modified to simultaneously incorporate both branches. An important thing to notice is that in an $\boldsymbol{N}$-particle ground state $|\boldsymbol{N}_0\rangle$, which is a state with no particle-hole excitations, the action of $a_{q,\mu}$ is

$$a_{q,\mu}\,|\boldsymbol{N}_0\rangle = 0. \tag{5.22}$$

This is because there are no available states to create when acting with $c^\dagger_{k-q}$ on $c_k\,|\boldsymbol{N}_0\rangle$ since $q > 0$. This also makes it clear why the bosonic destruction operator is not included in eq. (5.17). Similarly, by taking the adjoint of eq. (5.22),

$$\langle \boldsymbol{N}_0|\, a^\dagger_{q,\mu} = 0. \tag{5.23}$$

It will now be shown that these operators indeed satisfy bosonic properties. The commutation for annihilation operators of different species is

$$\begin{aligned}
[a_{q,\mu}, a_{q',\mu'}] &= \frac{2\pi}{L\sqrt{|q||q'|}} \sum_{k,k'} [c^\dagger_{k-q,\mu} c_{k,\mu}, c^\dagger_{k'-q',\mu} c_{k',\mu}] \\
&= \frac{2\pi}{L\sqrt{|q||q'|}} \sum_{k,k'} \delta_{\mu\mu'} \left(c^\dagger_{k-q,\mu} c_{k',\mu'} \delta_{k,k'-q'} - c^\dagger_{k'-q',\mu'} c_{k,\mu} \delta_{k-q,k'} \right) \\
&= 0,
\end{aligned} \tag{5.24}$$

where the two last terms cancel after performing one of the k-summations. A similar calculation yield $[a^\dagger_{q,\mu}, a^\dagger_{q',\mu'}] = 0$. For $[a_{q\mu}, a^\dagger_{q',\mu'}]$, the calculation is a bit more involved as

$$\begin{aligned}
[a_{q,\mu}, a^\dagger_{q',\mu'}] &= \frac{2\pi}{L\sqrt{|q||q'|}} \sum_{k,k'} [c^\dagger_{k-q,\mu} c_{k,\mu}, c^\dagger_{k'+q',\mu} c_{k',\mu}] \\
&= \frac{2\pi}{L\sqrt{|q||q'|}} \sum_{k,k'} \delta_{\mu\mu'} \left(c^\dagger_{k-q,\mu} c_{k',\mu} \delta_{k,k'+q'} - c^\dagger_{k'+q',\mu'} c_{k,\mu} \delta_{k-q,k'} \right) \\
&= \frac{2\pi}{L\sqrt{|q||q'|}} \sum_{k} \delta_{\mu\mu'} \left(c^\dagger_{k-q,\mu} c_{k-q',\mu} - c^\dagger_{k-q+q',\mu'} c_{k,\mu} \right).
\end{aligned}$$

For $q \neq q'$, these last terms are normal ordered and can be calculated directly, giving 0. For $q = q'$, they are not, and a variable change in the momentum index is not well behaved as it involves a subtraction of infinite quantities. That they are not normal ordered for all k can be seen for example by considering the case when $q > k > 0$ such that normal ordering of $c^\dagger_{k-q} c_{k-q}$ would be different from $c^\dagger_k c_k$. By considering the ground state expectation values through the

fermionic normal ordering [77], the commutator is [1]

$$\begin{aligned}
[a_{q\mu}, a^\dagger_{q',\mu'}] &= \frac{2\pi}{L|q|}\delta_{\mu\mu'}\delta_{qq'}\sum_k \left(c^\dagger_{k-q}c_{k-q} - c^\dagger_k c_k\right) \\
&= \frac{\delta_{\mu\mu'}\delta_{qq'}}{n_q}\sum_{k=-\infty}^{\infty}\Big(\overset{*}{*}\, c^\dagger_{k-q}c_{k-q}\,\overset{*}{*} - \overset{*}{*}\, c^\dagger_k c_k\,\overset{*}{*} \\
&\qquad - \langle \mathbf{0}_0|c^\dagger_k c_k|\mathbf{0}_0\rangle + \langle \mathbf{0}_0|c^\dagger_{k-q}c_{k-q}|\mathbf{0}_0\rangle\Big) \\
&= \frac{\delta_{\mu\mu'}\delta_{qq'}}{n_q}\left(\sum_{k=-\infty}^{q} 1 - \sum_{k=-\infty}^{0} 1\right) \\
&= \delta_{\mu\mu'}\delta_{qq'},
\end{aligned} \tag{5.25}$$

where the properties in eq. (5.10) have been used in addition to a safe relabeling of momentum indices in the normal ordered operators.

5.2.4 Bosonization Identity

The task of representing an arbitrary state $|\boldsymbol{N}\rangle$ as in eqs. (5.16) and (5.17) still remain. The goal now is to represent $\psi(x)$ through the bosons defined in eq. (5.21).

To see how $a_{q,\mu}$ relates to the electron field $\psi_\mu(x)$, the commutator is computed as

$$\begin{aligned}
[a_{q,\mu}, \psi_{\mu'}(x)] &= \frac{1}{\sqrt{n_q}}\frac{1}{\sqrt{L}}\sum_{k,k'} \mathrm{e}^{-ik'x}\underbrace{[c^\dagger_{k+q,\mu}c_{k,\mu}, c_{k',\mu'}]}_{=-\delta_{k',k+q}\delta_{\mu\mu'}c_k} \\
&= -\frac{1}{\sqrt{n_q}}\frac{1}{\sqrt{L}}\sum_k \mathrm{e}^{-i(k+q)x}c_k \\
&= -\frac{\delta_{\mu\mu'}}{\sqrt{n_q}}\mathrm{e}^{-iqx}\psi_\mu(x) \equiv \delta_{\mu\mu'}\alpha_q(x)\psi_\mu(x),
\end{aligned} \tag{5.26}$$

where eqs. (5.4) and (5.21) have been inserted and

$$\alpha_q(x) \equiv -\frac{1}{\sqrt{n_q}}\mathrm{e}^{-iqx} \tag{5.27}$$

is defined. Likewise,

$$[a^\dagger_{q,\mu}, \psi_{\mu'}(x)] = \delta_{\mu\mu'}\alpha^*_q(x)\psi_\mu(x). \tag{5.28}$$

[1] The muted quantum number is μ for all appearing operators.

I now act with this commutator on the state $|\boldsymbol{N}_0\rangle$, and use eqs. (5.22) and (5.26) to obtain

$$\begin{aligned}[a_{q,\mu}, \psi_\mu(x)]\,|\boldsymbol{N}_0\rangle &= (a_{q,\mu}\psi_\mu(x) - \psi_\mu(x)a_{q,\mu})\,|\boldsymbol{N}_0\rangle \\ &= a_{q,\mu}\psi_\mu(x)\,|\boldsymbol{N}_0\rangle = \alpha_q(x)\psi_\mu(x)\,|\boldsymbol{N}_0\rangle\,, \end{aligned} \tag{5.29}$$

which shows that the state $\psi_\mu(x)\,|\boldsymbol{N}_0\rangle$ is an eigenstate of the annihilation operator $a_{q,\mu}$ with eigenvalue $\alpha_q(x)$. Consequently, $\psi_\mu(x)\,|\boldsymbol{N}_0\rangle$ is a coherent boson state as this is the defining property, as described in chapter 2. By including the Klein factor F_μ and a yet to be determined phase operator $\hat{\lambda}_\mu$, the coherent state representation is found by inserting eq. (2.16), obtaining

$$\psi_\mu(x)\,|\boldsymbol{N}_0\rangle = \exp\left(\sum_{q>0}\alpha_q(x)a^\dagger_{q\mu}\right)F_\mu\hat{\lambda}_\mu\,|\boldsymbol{N_0}\rangle \tag{5.30a}$$

$$\equiv \mathrm{e}^{-i\phi^\dagger_\mu(x)}F_\mu\hat{\lambda}_\mu\,|\boldsymbol{N}_0\rangle\,, \tag{5.30b}$$

where the fields

$$\phi^\dagger_\mu(x) \equiv -i\sum_{q>0}\left(\frac{2\pi}{L|q|}\right)^{\frac{1}{2}}\mathrm{e}^{-\xi\frac{|q|}{2}}\mathrm{e}^{-iqx}a^\dagger_{q,\mu} \tag{5.31a}$$

$$\phi_\mu(x) \equiv i\sum_{q>0}\left(\frac{2\pi}{L|q|}\right)^{\frac{1}{2}}\mathrm{e}^{-\xi\frac{|q|}{2}}\mathrm{e}^{iqx}a_{q,\mu} \tag{5.31b}$$

are introduced. The "effective bandwidth" ξ is a parameter that regularizes the ultraviolet divergence in the q-integral, and is usually taken to be 0 at the end of calculations [22]. The fields satisfy

$$[a_{q,\mu}, \phi_{\mu'}] = [a^\dagger_{q,\mu}, \phi^\dagger_{\mu'}] = 0 \tag{5.32}$$

and

$$\begin{aligned}[a^\dagger_{q,\mu}, i\phi_{\mu'}(x)] &= -\sum_{q'>0}\frac{1}{\sqrt{n_{q'}}}\mathrm{e}^{-\xi\frac{|q'|}{2}}\mathrm{e}^{iq'x}\underbrace{[a^\dagger_{q,\mu}, a_{q',\mu'}]}_{-\delta_{\mu\mu'}\delta_{qq'}} \\ &= -\delta_{\mu\mu'}\alpha^*_q(x)\mathrm{e}^{-\xi\frac{|q|}{2}}\,, \end{aligned} \tag{5.33}$$

where the definition of $\alpha_q(x)$ in eq. (5.27) has been inserted. Some physical insight in these fields can be obtained by noticing that the normal ordered

fermion density may be written in terms of ϕ_μ and $\phi_\mu^\dagger$ (with $\xi \to 0$) as

$$
\begin{aligned}
{}^*_*\,\rho_\mu(x)\,{}^*_*
&= {}^*_*\,\psi_\mu^\dagger(x)\psi_\mu(x)\,{}^*_* = \frac{1}{L}\sum_q \mathrm{e}^{-iqx}\sum_k {}^*_*\,c_{k+q,\mu}^\dagger c_{k,\mu}\,{}^*_* \\
&= \frac{1}{L}\left(\sum_{q>0}\mathrm{e}^{-iqx}\left(\frac{L|q|}{2\pi}\right)^{\frac{1}{2}} a_{q,\mu}^\dagger + \sum_{q<0}\mathrm{e}^{-iqx}\left(\frac{L|q|}{2\pi}\right)^{\frac{1}{2}} a_{q,\mu} + \hat{N}_\mu\right) \\
&= \frac{1}{L}\sum_{q>0}\sqrt{n_q}\left(\mathrm{e}^{-iqx}a_{q,\mu}^\dagger + \mathrm{e}^{iqx}a_{q,\mu}\right) + \frac{\hat{N}_\mu}{L} \\
&= \frac{1}{2\pi}\nabla\left(\phi_\mu(x) + \phi_\mu^\dagger(x)\right) + \frac{\hat{N}_\mu}{L} \equiv \frac{1}{2\pi}\nabla\Phi_\mu + \frac{\hat{N}_\mu}{L}.
\end{aligned}
\tag{5.34}
$$

From this, it is clear that the electron density is the average density $\rho_{0,\mu} = N_\mu/L$ plus a displacement field $\Phi_\mu(x)$ dependent on particle-hole excitations. If this displacement field is very slowly varying, the fermion density is simply the number of particles divided by the volume of the system.

The action of the phase operator $\hat{\lambda}_\mu$ in eq. (5.30) can be derived by considering what the expectation value of the particle number conserving operator $F_\mu^\dagger\psi_\mu(x)$ is in the ground state. By inserting eqs. (5.23) and (5.30) and using that $[F_\mu^\dagger, a_{q,\mu'}^\dagger] = 0$, the average is

$$
\begin{aligned}
\langle \boldsymbol{N}_0|F_\mu^\dagger\psi_\mu(x)|\boldsymbol{N}_0\rangle &= \langle \boldsymbol{N}_0|F_\mu^\dagger \exp\left(\sum_{q>0}\alpha_q(x)a_{q\mu}^\dagger\right)F_\mu\hat{\lambda}_\mu|\boldsymbol{N}_0\rangle \\
&= \langle \boldsymbol{N}_0|\big(1 + \sum_{q>0}\alpha_q(x)a_{q,\mu}^\dagger + \dots\big)\hat{\lambda}_\mu|\boldsymbol{N}_0\rangle \\
&= \langle \boldsymbol{N}_0|\hat{\lambda}_\mu|\boldsymbol{N}_0\rangle\,.
\end{aligned}
\tag{5.35}
$$

Using the representation in eq. (5.4) instead gives

$$
\begin{aligned}
\langle \boldsymbol{N}_0|F_\mu^\dagger\psi_\mu(x)|\boldsymbol{N}_0\rangle &= \frac{1}{\sqrt{L}}\sum_{n_k}\mathrm{e}^{-i\frac{2\pi}{L}n_k x}\underbrace{\langle \boldsymbol{N}_0|F_\mu^\dagger c_{k,\mu}|\boldsymbol{N}_0\rangle}_{\delta_{n_k,N_\mu}} \\
&= \frac{1}{\sqrt{L}}\mathrm{e}^{-i\frac{2\pi}{L}N_\mu x},
\end{aligned}
\tag{5.36}
$$

which implies

$$
\hat{\lambda}_\mu = \frac{1}{\sqrt{L}}\mathrm{e}^{-i\frac{2\pi}{L}\hat{N}_\mu x}. \tag{5.37}
$$

Now, the only thing remaining is to consider what the action of $\psi_\mu(x)$ on a general state $|\boldsymbol{N}\rangle$ is. As in eq. (5.17), $|\boldsymbol{N}\rangle$ is written as a linear combination

of particle-hole excitations on top of the $\boldsymbol{N}$-particle ground state $|\boldsymbol{N}_0\rangle$. The action of the bosonic annihilation operator on the ground state need not be considered in this linear combination, since it destroys the ground state as in eq. (5.22). The action of ψ_μ is thus

$$\psi_{\mu'}(x)\,|\boldsymbol{N}\rangle = \psi_{\mu'}(x) f(\{a^\dagger_{q,\mu}\})\,|\boldsymbol{N}_0\rangle\,. \tag{5.38}$$

Now commute $\psi_{\mu'}(x)$ past all $a^\dagger_{q,\mu}$ operators using eq. (5.26), giving

$$\begin{aligned}\psi_{\mu'}(x)\,|\boldsymbol{N}\rangle &= f(\{a^\dagger_{q,\mu} - \delta_{\mu\mu'}\alpha^*_q(x)\})\psi_{\mu'}(x)\,|\boldsymbol{N}_0\rangle \\ &= f(\{a^\dagger_{q,\mu} - \delta_{\mu\mu'}\alpha^*_q(x)\})\mathrm{e}^{-i\phi^\dagger_{\mu'}(x)} F_{\mu'}\hat{\lambda}_{\mu'}\,|\boldsymbol{N}_0\rangle\,.\end{aligned} \tag{5.39}$$

The operator $f(\{a^\dagger_{q,\mu} - \delta_{\mu\mu'}\alpha^*_q(x)\})$ is expressed through the Hilbert space operator identity in eq. (A.2.5), with the commutation relation in eq. (5.33). I obtain

$$\begin{aligned}f(\{a^\dagger_{q,\mu} - \delta_{\mu\mu'}\alpha^*_q(x)\}) &= f(\{a^\dagger_{q,\mu} + [a^\dagger_{q,\mu}, i\phi_{\mu'}(x)]\,\}) \\ &= \mathrm{e}^{-i\phi_{\mu'}(x)} f(\{a^\dagger_{q,\mu}\})\mathrm{e}^{i\phi_{\mu'}(x)}.\end{aligned} \tag{5.40}$$

By using eq. (5.32), all operators $\phi^\dagger_{\mu'}, F_{\mu'}$ and $\hat{\lambda}_{\mu'}$ can be commuted to the left, giving

$$\psi_{\mu'}(x)\,|\boldsymbol{N}\rangle = F_{\mu'}\hat{\lambda}_{\mu'}\mathrm{e}^{-i\phi^\dagger_{\mu'}(x)}\mathrm{e}^{-i\phi_{\mu'}(x)} f(\{a^\dagger_{q,\mu}\})\mathrm{e}^{i\phi_{\mu'}(x)}\,|\boldsymbol{N}_0\rangle\,. \tag{5.41}$$

As already mentioned, the $\boldsymbol{N}$-particle ground state contains no particle-hole excitations, such that

$$\begin{aligned}f(\{a^\dagger_{q,\mu}\})\exp(i\phi_{\mu'}(x))\,|\boldsymbol{N}_0\rangle &= f(\{a^\dagger_{q,\mu}\})(1+\mathcal{O}(a_{q,\mu'}))\,|\boldsymbol{N}_0\rangle \\ &= f(\{a^\dagger_{q,\mu}\})\,|\boldsymbol{N}_0\rangle \\ &= |\boldsymbol{N}\rangle\,,\end{aligned} \tag{5.42}$$

where eq. (5.22) has been used. Hence, the action of $\psi_{\mu'}(x)$ on a general state is clear, and the bosonized form of the fermionic field is

$$\psi_\mu(x) = F_\mu \frac{1}{\sqrt{L}}\mathrm{e}^{-i\frac{2\pi}{L}\hat{N}_\mu x}\mathrm{e}^{-i\phi^\dagger_\mu(x)}\mathrm{e}^{-i\phi_\mu(x)}, \tag{5.43}$$

where eq. (5.37) has been inserted. The ϕ_μ-fields are defined in eq. (5.31).

Equation (5.43) is the bosonization identity of fermionic fields in one dimension. The electron field operator can thus be represented as a Klein factor modulated by a phase factor which is similar to the normal ordered fermion density in eq. (5.34), i.e.

$$\psi_\mu(x) \sim F_\mu \mathrm{e}^{-2\pi i^*_* \rho_\mu(x)^*_*}. \tag{5.44}$$

5.3 Bosonization of the Luttinger Model

Thus far, no particular fermion dispersion has been considered. By considering the low-energy limit of a quantum spin hall insulator which hosts effective one-dimensional states at the edges, the dispersion may be linearized in the vicinity of the Fermi momentum to reduce the free fermion theory to the Tomonaga-Luttinger model for finite k_F. This model discerns between left and right moving fermions. I will denote these two branches with the quantum number $r \in \{\mathrm{L}, \mathrm{R}\}$, and define the quantity

$$\eta_r = \begin{cases} 1 & r = \mathrm{R} \\ -1 & r = \mathrm{L} \end{cases}. \tag{5.45}$$

The Hamiltonian in eq. (5.1) may be written

$$H = -iv_F \sum_{\sigma,r} \eta_r \int_{-\frac{L}{2}}^{\frac{L}{2}} \mathrm{d}x\, \psi^\dagger_{\sigma,r}(x)\partial_x \psi_{\sigma,r}(x), \tag{5.46}$$

which is transformed to

$$H = \sum_{k,\sigma} \sum_{r=(R,L)} v_F(\eta_r k - k_F) c^\dagger_{k,\sigma,r} c_{k,\sigma,r} \tag{5.47}$$

after inserting eq. (5.4) where the momentum summation is performed relative to the Fermi momentum for both branches, i.e. $k \to \eta_r k - k_F$.

The sum over k in (5.47) ranges over all momenta, with an infinitely filled Dirac sea below the Fermi momentum. This is the Tomonaga-Luttinger model, and will serve as the basis for the calculations of spectral properties in the one dimensional system on the edges of a quantum spin hall insulator.

In the solutions of the Tomonaga-Luttinger model [25, 26], the cutoff factor ξ is introduced to ensure convergence in the momentum integrals as in eq. (5.31), and taken to be zero at the end of the calculations. However, this cutoff is a good parameter to define the bandwidth, or range of validity of the model including interactions [22]. Since the linear dispersion is a good approximation of the localized edge states of a QSH nanoribbon only for a narrow slice in the Brillouin zone, I keep ξ finite throughout. The density fluctuations are linear combinations of all particle-hole excitations, which in the plane-wave basis is given in eq. (5.20), and for the current model states

$$\rho^\dagger_r(q) = \sum_k c^\dagger_{k+q,r} c_{k,r}, \quad q \neq 0, \tag{5.48}$$

satisfying $\rho^\dagger(q) = \rho(-q)$ [1]. For $q = 0$, ρ_r is simply the number operator of a given species. The commutation relation for the densities is [22]

$$[\rho_r^\dagger(q), \rho_{r'}^\dagger(-q')] = -\delta_{r,r'}\delta_{q,q'}\frac{\eta_r q L}{2\pi}, \tag{5.49}$$

where a subtraction of two infinities in the normal ordered densities has been made as in eq. (5.25). The commutation in eq. (5.49) is reminiscent of the normal bosonic commutation relations. As in eq. (5.21), one may now introduce

$$\begin{aligned} a_{q,\mu}^\dagger &= \left(\frac{2\pi}{L|q|}\right)^{\frac{1}{2}} \sum_r \Theta(\eta_r q)\rho_{r,\mu}^\dagger(q) \\ a_{q,\mu} &= \left(\frac{2\pi}{L|q|}\right)^{\frac{1}{2}} \sum_r \Theta(\eta_r q)\rho_{r,\mu}(q), \end{aligned} \tag{5.50}$$

that satisfies such commutation relations. Θ is the Heaviside step function, and the additional quantum number μ has been added for the possibility of adding spin to the problem, and the total density wave is for a branch r is $\rho^\dagger(q) = \sum_{r,\mu}\rho_{r,\mu}^\dagger(q)$. Consider now the commutator between the Hamiltonian (eq. (5.47)) and a_q;

$$\begin{aligned} [H, a_q] &= \left(\frac{2\pi}{L|q|}\right)^{\frac{1}{2}} \sum_{k_1,r_1}\sum_{k_2,r_2} v_F(\eta_{r_1}k_1 - k_F)\Theta(\eta_{r_2}q)\underbrace{[c_{k_1,r_1}^\dagger c_{k_1,r_1}, c_{k_2-q,r_2}^\dagger c_{k_2,r_2}]}_{\substack{=\delta_{r_1,r_2}[\delta_{k_1,k_2}c_{k_2-q,r}^\dagger c_{k_1,r} \\ -\delta_{k_2-q,k_1}c_{k_1,r}^\dagger c_{k_2,r}]}} \\ &= \left(\frac{2\pi}{L|q|}\right)^{\frac{1}{2}} \sum_{k,r}\Big(v_F(\eta_r(k-q) - k_F)\Theta(\eta_r q)c_{k-q,r}^\dagger c_{k,r} \\ &\qquad - v_F(\eta_r k - k_F)\Theta(\eta_r q)c_{k-q,r}^\dagger c_{k,r}\Big) \\ &= -qv_F\left(\frac{2\pi}{L|q|}\right)^{\frac{1}{2}} \sum_{k,r}\eta_r\Theta(\eta_r q)c_{k-q,r}^\dagger c_k \\ &= -v_F|q|a_q. \end{aligned}$$

This result suggests that the dynamics of the system may be represented in terms of these bosonic operators with a Hamiltonian of the form

$$\tilde{H} = \sum_q \tilde{\varepsilon}_q a_q^\dagger a_q, \tag{5.51}$$

[1] The notation of daggers on the fermion density is opposite to that in the previous section to express $a^\dagger \sim \rho^\dagger$, $a \sim \rho$.

since this is compatible with the commutation relation $[\tilde{H}, a_{q'}] = -\tilde{\varepsilon}_{q'} a_{q'}$, so the free fermion spectrum is preserved with the kinetic energy term $\tilde{\varepsilon}_q = v_F|q| = \varepsilon_q$. When writing the Hamiltonian of the form of eq. (5.51), the modes for $q = 0$ is neglected, since the operator $a_{q=0}$ is undefined. For this static limit, terms proportional to the number of bosons N_r of different species appear as a shift in the energy. These terms do not modify the dynamics of the system, but rather serves as an altering of the zero point energy which I will neglect.

Since the Hamiltonian is diagonal in the boson operators a_q, the time evolution of these operators can be computed through eq. (2.25). The fermionic fields in the system is now expressed by the bosonization identity in eq. (5.43). Measured from the Fermi level $\mu = v_F k_F$, the fermionic fields is thus given as

$$\psi_r(x) = \mathrm{e}^{ik_F(\eta_r x - v_F t)} \tilde{\psi}_r(x,t), \tag{5.52}$$

with

$$\tilde{\psi}_r^\dagger(x,t) = F_r^\dagger \frac{1}{\sqrt{L}} \mathrm{e}^{-i\phi_r^\dagger(x,t)} \mathrm{e}^{-i\phi_r(x,t)}. \tag{5.53}$$

Absorbing the phase factor $\hat{\lambda}_r$ in eq. (5.43), the field $\phi_r(x,t)$ defined in eq. (5.31) takes the form

$$\phi_r(x,t) = \eta_r \frac{\pi}{L} N_r x - i \sum_{q \neq 0} \Theta(\eta_r q) \left(\frac{2\pi}{L|q|} \right)^{\frac{1}{2}} \mathrm{e}^{-\xi \frac{|q|}{2}} \mathrm{e}^{iqx} a_q(t). \tag{5.54}$$

5.3.1 Adding Spin and Interactions

I will now show how spin degrees of freedom separates from the charge, and how spin-dependent interactions may be added to the system. The density bosons in eq. (5.50) is

$$a_{q,\sigma} = \left(\frac{2\pi}{L|q|} \right)^{\frac{1}{2}} \sum_r \Theta(\eta_r q) \rho_{r,\sigma}(q), \tag{5.55}$$

where the density wave $\rho_{r,\sigma}$ is defined through eq. (5.48) as

$$\rho_{r,\sigma}^\dagger(q) = \sum_k c_{k+q,r,\sigma}^\dagger c_{k,r,\sigma}, \quad q \neq 0. \tag{5.56}$$

In the spinful Luttinger model without interactions, the kinetic excitation energy of density waves is

$$\sum_{q \neq 0} \sum_\sigma v_F |q| a_{q,\sigma}^\dagger a_{q,\sigma}. \tag{5.57}$$

The charge and spin components of the electron density may be separated into disjoint degrees of freedom by defining the operators

$$\rho_r(q) \equiv \sum_\sigma \rho_{r,\sigma}(q) \tag{5.58a}$$

$$\sigma_r(q) \equiv \sum_\sigma \sigma \rho_{r,\sigma}(q). \tag{5.58b}$$

I further define the operators

$$a_{q,c} \equiv \left(\frac{\pi}{L|q|}\right)^{\frac{1}{2}} \sum_r \Theta(\eta_r q)\rho_r(q) \tag{5.59a}$$

$$a_{q,s} \equiv \left(\frac{\pi}{L|q|}\right)^{\frac{1}{2}} \sum_r \Theta(\eta_r q)\sigma_r(q) \tag{5.59b}$$

describing charge (c) and spin (s) density wave fluctuations. The operator appearing in the bosonized form of $\psi_{r,\sigma}$ is the boson $a_{q,\sigma}$, which is related to $a_{q,c}$ and $a_{q,s}$ by

$$a_{q,\sigma} = (a_{q,c} + \sigma a_{q,s})/\sqrt{2}. \tag{5.60}$$

In terms of the operators in eq. (5.59), the kinetic energy in eq. (5.57) decouple as

$$\begin{aligned}
\sum_{q,\sigma} v_F|q| a^\dagger_{q,\sigma} a_{q,\sigma} &= \sum_{q,\sigma} \frac{v_F|q|}{2} \left(a^\dagger_{q,c} + \sigma a^\dagger_{q,s}\right)\left(a_{q,c} + \sigma a_{q,s}\right) \\
&= \sum_q \left(v_F|q| a^\dagger_{q,c} a_{q,c} + v_F|q| a^\dagger_{q,s} a_{q,s} + \sum_\sigma \sigma \frac{v_F|q|}{2} (a^\dagger_{q,c} a_{q,s} + a^\dagger_{q,s} a_{q,c}) \right) \\
&= \sum_q \left(v_F|q| a^\dagger_{q,c} a_{q,c} + v_F|q| a^\dagger_{q,s} a_{q,s} \right).
\end{aligned} \tag{5.61}$$

These definitions allow for the exact diagonalization for possibly spin-dependent density-density interactions by taking an interaction on the form [32]

$$\begin{aligned}
\hat{V} &= \frac{1}{2L} \sum_q \sum_{\sigma\sigma'} v_{\sigma\sigma'}(q) \rho^\dagger_q \rho_q \\
&= \frac{1}{2} \sum_q \sum_{\sigma\sigma'} |q| \frac{v_{\sigma\sigma'}(q)}{2\pi} \left(a^\dagger_{q,\sigma} + a_{-q,\sigma}\right)\left(a^\dagger_{-q,\sigma'} + a_{q,\sigma'}\right)
\end{aligned} \tag{5.62}$$

where

$$v_{\sigma\sigma'}(q) = V(q) + \sigma\sigma' U(q) \tag{5.63}$$

are Fourier transformed two-particle interactions. Scattering across branches with $q = 2k_F$ (g_1-terms in "g-ology" models) is not considered in this thesis. In the context of the QSH state, a $2k_F$-scattering requires an intrinsic spin-flipping mechanism which is absent in the electron-phonon coupling. Lattice vibrations might have a renormalizing effect on such scattering terms ($g_{1\perp}$), but this is not further discussed in this thesis.

By inserting eq. (5.60) into the interaction term, the Hamiltonian is decoupled in the charge and spin bosons, resulting in

$$H = \sum_q |q| \left[\left(v_F + \frac{V(q)}{\pi} \right) a^\dagger_{q,c} a_{q,c} + \frac{V(q)}{2\pi} \left(a^\dagger_{q,c} a^\dagger_{-q,c} + a_{q,c} a_{-q,c} + 1 \right) \right.$$
$$\left. + \left(v_F + \frac{U(q)}{\pi} \right) a^\dagger_{q,s} a_{q,s} + \frac{U(q)}{2\pi} \left(a^\dagger_{q,s} a^\dagger_{-q,s} + a_{q,s} a_{-q,s} + 1 \right) \right].$$

This Hamiltonian can be brought to diagonal form by a Bogoliubov transformation. I therefore introduce the charge- and spin- Bogoliubov bosons

$$\varrho_q = u_{q,c} a_{q,c} - v_{q,c} a^\dagger_{-q,c} \tag{5.64a}$$
$$\varsigma_q = u_{q,s} a_{q,s} - v_{q,s} a^\dagger_{-q,s}. \tag{5.64b}$$

Here, $u_{q,\alpha} = \cosh(\theta_{q,\alpha})$ and $v_{q,\alpha} = \sinh(\theta_{q,\alpha})$ are dependent on the specific interaction through $\theta_{q,\alpha}$. The inverse coordinate transformation is given by

$$a_{q,c} = u_{q,c} \varrho_q + v_{q,c} \varrho^\dagger_{-q} \tag{5.65a}$$
$$a_{q,s} = u_{q,s} \varsigma_q + v_{q,s} \varsigma^\dagger_{-q}. \tag{5.65b}$$

By tuning the parameter $\theta_{q,\alpha}$, cross terms involving two creation or annihilation operators can be eliminated, and the Hamiltonian of the problem is

$$H = \sum_q |q| \left(v_c(q) \varrho^\dagger_q \varrho_q + v_s(q) \varsigma^\dagger_q \varsigma_q \right). \tag{5.66}$$

This is achieved if the parameters satisfy

$$\tanh(2\theta_{q,c}) = \frac{-V(q)}{V(q) + \pi v_F} \tag{5.67a}$$
$$\tanh(2\theta_{q,s}) = \frac{-U(q)}{U(q) + \pi v_F}. \tag{5.67b}$$

The spin and charge sector have thus been separated. The renormalized, q-dependent Fermi velocities $v_c(q)$ and $v_c(q)$ for the charge- and spin- channel

is also dependent on the Bogoliubov parameters, and is found to be

$$v_c(q) = \left(v_F + \frac{V_q}{\pi} - \frac{1}{\pi} \frac{V_q^2}{\pi v_F + V_q} \right) \cosh(2\theta_{q,c})$$

$$= v_F \sqrt{1 + \frac{2V_q}{\pi v_F}} \tag{5.68a}$$

$$v_s(q) = v_F \sqrt{1 + \frac{2U_q}{\pi v_F}}. \tag{5.68b}$$

Note that $v_c(q \to 0)$ is in general different from $v_s(q \to 0)$, and the characteristic Fermi velocities of the spin and charge bogolons are distinct. This hints at the separation of spin and charge, a known property special for one dimensional Fermi systems.

5.3.2 The Interacting Green's Function

In this section, I will employ the bosonization techniques to compute the correlation function of a spinless system with density-density interactions at $T = 0$. To compute the spectral properties of the Tomonaga-Luttinger system, the retarded Green's function, G^R, must be evaluated. As described in section 2.2, this function is the probability amplitude that an injected state at a specified time and place is ejected from the system at some later time and place. It is related to the lesser and greater Green's functions given in eq. (2.31), where the greater Green's function $G_r^>(x,t)$ is the expected value of the operators representing a particle that is created at $(0,0)$ and annihilated at (x,t). A similar interpretation can be imputed to the lesser Green's function with holes instead of particles. These are defined in eq. (2.30). Spectral properties of the system is related to the Fourier transformed Green's function $G^R(k,\omega)$ and the relation [32]

$$G_r^>(k_F + q, \omega) = G_r^<(k_F - q, -\omega) \tag{5.69}$$

indicate that it is sufficient to only consider the Fourier transform of $G^>(x,t)$ to obtain the total momentum resolved Green's function.

I now calculate the greater Greens function $G_r^>(x,t)$ for interacting electron densities using the representation of the fermionic fields in eq. (5.43). As shown above, and by Mattis and Lieb [77], the dynamics of the system is governed by the Bogoliubov transformed bosonic operators

$$\beta_q = u_q a_q - v_q a_{-q}^\dagger \tag{5.70}$$

and its hermitian conjugate through the Hamiltonian

$$H = \sum_{q \neq 0} \omega_q \beta_q^\dagger \beta_q. \tag{5.71}$$

The parameters $u_q = \cosh\theta_q$ and $v_q = \sinh\theta_q$ is related to the interaction potential between the electron densities by

$$\tanh(2\theta_q) = -\frac{V_q}{V_q + 2\pi v_F}, \tag{5.72}$$

where V_q is the Fourier transformed two-particle interaction [32]. Comparing this to eq. (5.67), it is clear that the spinless case corresponds to rescaling the potential by a factor 2. For clarity i explicitly refer the a-bosons in terms of the β-bosons

$$a_q = u_q\beta_q + v_q\beta^\dagger_{-q} \tag{5.73a}$$
$$a^\dagger_{-q} = v_q\beta_q + u_q\beta^\dagger_{-q}. \tag{5.73b}$$

The fermionic field is given by the bosonization identity in eq. (5.43), where ϕ_r is expressed in terms of the number operator N_r and the β-bosons as

$$\phi_r(x) = \eta_r\frac{\pi}{L}N_r x - i\sum_{q\neq 0}\Theta(\eta_r q)\left(\frac{2\pi}{L|q|}\right)^{\frac{1}{2}} \mathrm{e}^{-\xi\frac{|q|}{2}}\mathrm{e}^{iqx}(u_q\beta_q + v_q\beta^\dagger_{-q}). \tag{5.74}$$

For the current state of affairs, the time evolution of operators can be imputed to the β-bosons, since the Hamiltonian is diagonal in this basis. As presented in eq. (2.25), this is expressed as

$$\beta_q(t) = \mathrm{e}^{iHt}\beta_q\mathrm{e}^{-iHt}, \tag{5.75}$$

which can be promptly evaluated using the Baker-Hausdorff formula (eq. (A.2.3)) as

$$\beta_q(t) = \beta_q\mathrm{e}^{-i\omega_q t} \tag{5.76a}$$
$$\beta^\dagger_q(t) = \beta^\dagger_q\mathrm{e}^{i\omega_q t}. \tag{5.76b}$$

To compute the correlation function, the commutation relations of the $\phi_r(x,t)$-field must be worked out. Since $\beta_q(t)$ is a boson operator, fields commute as $[\phi_r(x), \phi_{r'}(x')] = [\phi^\dagger_r(x), \phi^\dagger_{r'}(x')] = 0$, but calculating $[\phi_r(x), \phi^\dagger_{r'}(x')]$ requires some work. Including the time-evolved bosons, $a_q(t)$, I first compute

$$\begin{aligned}
&[a_{q_1}(t_1), a^\dagger_{q_2}(t_2)] \\
&= \left(u_{q_1}\beta_{q_1}\mathrm{e}^{-i\omega_{q_1}t_1} + v_{q_1}\beta^\dagger_{-q_1}\mathrm{e}^{i\omega_{q_1}t_1}\right)\left(u_{q_2}\beta^\dagger_{q_2}\mathrm{e}^{i\omega_{q_2}t_2} + v_{q_2}\beta_{-q_2}\mathrm{e}^{-i\omega_{q_2}t_2}\right) \\
&- \left(u_{q_2}\beta^\dagger_{q_2}\mathrm{e}^{i\omega_{q_2}t_2} + v_{q_2}\beta_{-q_2}\mathrm{e}^{-i\omega_{q_2}t_2}\right)\left(u_{q_1}\beta_{q_1}\mathrm{e}^{-i\omega_{q_1}t_1} + v_{q_1}\beta^\dagger_{-q_1}\mathrm{e}^{i\omega_{q_1}t_1}\right) \\
&= \delta_{q_1q_2}\left(u^2_{q_1}\mathrm{e}^{i\omega_{q_1}(t_2-t_1)} - v^2_{q_1}\mathrm{e}^{-i\omega_{q_1}(t_2-t_1)}\right).
\end{aligned} \tag{5.77}$$

Using this result, $[\phi_r(x), \phi^\dagger_{r'}(x')]$ can be evaluated as

$$\begin{aligned}
&[\phi_r(x_1,t_1), \phi^\dagger_{r'}(x_2,t_2)] \\
&\quad = \delta_{r,r'} \sum_{q_1\neq 0}\sum_{q_2\neq 0} \Theta(\eta_r q_1)\Theta(\eta_{r'} q_2) \frac{2\pi}{L\sqrt{|q_1||q_2|}} \\
&\qquad \times \mathrm{e}^{iq_1x_1}\mathrm{e}^{-iq_2x_2}\mathrm{e}^{-\xi\frac{|q_1|+|q_2|}{2}} [a_{q_1}(t_1), a^\dagger_{q_2}(t_2)] \\
&\quad \overset{(5.77)}{=} \delta_{r,r'} \sum_{q\neq 0} \Theta(\eta_r q) \frac{2\pi}{L|q|} \mathrm{e}^{iq(x_1-x_2)}\mathrm{e}^{-\xi|q|} \left(u_q^2 \mathrm{e}^{i\omega_q(t_2-t_1)} - v_q^2 \mathrm{e}^{-i\omega_q(t_2-t_1)} \right).
\end{aligned} \tag{5.78}$$

Notice the special case when $x_1 = x_2$ and $t_1 = t_2$,

$$\begin{aligned}
[\phi_r(x,t), \phi^\dagger_r(x,t)] &= \sum_{q\neq 0} \Theta(\eta_r q) \frac{2\pi}{L|q|} \mathrm{e}^{-\xi|q|} (\cosh^2\theta_q - \sinh^2\theta_q) \\
&= \sum_{n=1}^{\infty} \frac{1}{n} \mathrm{e}^{-\xi\frac{2\pi}{L}n} = \sum_{n=1}^{\infty} \frac{1}{n} \left(\mathrm{e}^{-\xi\frac{2\pi}{L}}\right)^n \\
&= -\ln\left(1 - \mathrm{e}^{-\xi\frac{2\pi}{L}}\right) \qquad (5.79a) \\
&\overset{L\to\infty}{=} -\ln\left(\frac{2\pi\xi}{L}\right). \qquad (5.79b)
\end{aligned}$$

In terms of the time-evolved operators, the correlation function is on the form

$$\langle \psi(x,t)\psi^\dagger(0,0)\rangle = \frac{\mathrm{e}^{ik_F(\eta_r x - v_F t)}}{L} \langle \mathrm{e}^{i\phi^\dagger_r(x,t)} F_r \mathrm{e}^{i\phi_r(x,t)} \mathrm{e}^{-i\phi^\dagger_r(0,0)} F_r^\dagger \mathrm{e}^{-i\phi_r(0,0)} \rangle, \tag{5.80}$$

and to get further I use the Baker-Hausdorff formula in eq. (A.2.2) for the operators in the expectation value. The resulting series is truncated at the first order in the commutator since it is a c-number, as seen in eq. (5.78). The Klein-factor may be commuted past the boson operators, and the product of all Klein-Factors is equal to one if there is as many creation operators and annihilation operators of the same kind in the expectation value [76]. The result is

$$\begin{aligned}
\mathrm{e}^{i\phi^\dagger_r(x,t)}\mathrm{e}^{i\phi_r(x,t)} &= \mathrm{e}^{i(\phi^\dagger_r(x,t)+\phi_r(x,t)) + \frac{1}{2}[i\phi^\dagger_r(x,t), i\phi_r(x,t)]} \\
&= \mathrm{e}^{i(\phi^\dagger_r(x,t)+\phi_r(x,t))} \mathrm{e}^{-\frac{1}{2}\ln\left(1-\mathrm{e}^{-\xi\frac{2\pi}{L}}\right)} \\
&= \mathrm{e}^{i(\phi^\dagger_r(x,t)+\phi_r(x,t))} \left(1 - \mathrm{e}^{-\xi\frac{2\pi}{L}}\right)^{-\frac{1}{2}},
\end{aligned}$$

where eq. (5.79a) has been used. The same holds for the second pair of exponentials in the expectation value,

$$\begin{aligned} \mathrm{e}^{-i\phi_r^\dagger(0,0)}\mathrm{e}^{-i\phi_r(0,0)} &= \mathrm{e}^{-i(\phi_r^\dagger(0,0)+\phi_r(0,0))}\mathrm{e}^{-\frac{1}{2}\ln\left(1-\mathrm{e}^{-\xi\frac{2\pi}{L}}\right)} \\ &= \mathrm{e}^{-i(\phi_r^\dagger(0,0)+\phi_r(0,0))}\left(1-\mathrm{e}^{-\xi\frac{2\pi}{L}}\right)^{-\frac{1}{2}}. \end{aligned}$$

Using eq. (A.2.2) again, skipping the index r, and using the notation $\phi_0 = \phi_r(0,0), \phi = \phi_r(x,t)$, I need to compute

$$\begin{aligned} \mathrm{e}^{i(\phi^\dagger+\phi)}\mathrm{e}^{-i(\phi_0^\dagger+\phi_0)} &= \mathrm{e}^{i[(\phi^\dagger-\phi_0^\dagger)+(\phi-\phi_0)]+\frac{1}{2}[\phi^\dagger+\phi,\phi_0^\dagger+\phi_0]} \\ &= \mathrm{e}^{i[(\phi^\dagger-\phi_0^\dagger)+(\phi-\phi_0)]}\mathrm{e}^{\frac{1}{2}\left([\phi^\dagger,\phi_0]+[\phi,\phi_0^\dagger]\right)}. \end{aligned} \tag{5.81}$$

Using the definition in eq. (5.74) and taking $\exp\left(2i\eta_r\frac{\pi}{L}N_r x\right) \simeq 1$ as $L\to\infty$ leads to

$$\begin{aligned} i[(\phi^\dagger-\phi_0^\dagger)+(\phi-\phi_0)] &\equiv X \qquad (5.82)\\ &\simeq \sum_{q\neq 0}\Theta(\eta_r q)\left(\frac{2\pi}{L|q|}\right)^{\frac{1}{2}} \\ &\quad\times\left\{u_q\beta_q^\dagger\left(1-\mathrm{e}^{-i(qx-\omega_q t)}\right)+v_q\beta_{-q}\left(1-\mathrm{e}^{-i(qx+\omega_q t)}\right)\right. \\ &\quad\left.+\,u_q\beta_q\left(\mathrm{e}^{i(qx-\omega_q t)}-1\right)+v_q\beta_{-q}^\dagger\left(\mathrm{e}^{i(qx+\omega_q t)}-1\right)\right\}. \end{aligned}$$

The other relevant quantity in the exponential is

$$\begin{aligned} [\phi^\dagger,\phi_0]+[\phi,\phi_0^\dagger] &= [\phi,\phi_0^\dagger]-[\phi_0,\phi^\dagger] \equiv Y. \qquad (5.83)\\ &= \sum_{q\neq 0}\Theta(\eta_r q)\frac{2\pi}{L|q|}\mathrm{e}^{-\xi|q|}\left(u_q^2\left(\mathrm{e}^{i(qx-\omega_q t)}-\mathrm{e}^{-i(qx-\omega_q t)}\right)\right. \\ &\quad\left.-\,v_q^2\left(\mathrm{e}^{i(qx+\omega_q t)}-\mathrm{e}^{-i(qx+\omega_q t)}\right)\right) \\ &= 2i\sum_{q\neq 0}\Theta(\eta_r q)\frac{2\pi}{L|q|}\mathrm{e}^{-\xi|q|}\left(u_q^2\sin(qx-\omega_q t)-v_q^2\sin(qx+\omega_q t)\right) \end{aligned}$$

So far, only scalars have been factorized out of the expectation value. To proceed, I need to evaluate $\langle \mathrm{e}^X\rangle$, where X is given in eq. (5.82). Since this is an operator linear in the β-operators, for which the Hamiltonian is diagonal, the expectation value can be computed using the identity in eq. (A.2.6). At thermal equilibrium, the expectation value is $\langle\beta_{q_1}^\dagger\beta_{q_2}\rangle = \delta_{q_1,q_2}n_B(\omega_{q_1})$, where n_B is the Bose distribution given in eq. (2.26). Using these relations, one

sees that not all terms survive in $\langle X^2 \rangle$; only those with one creation and one annihilation operator contributes. Moreover, terms where the q's have opposite sign will be zero due to the Heaviside step functions $\Theta(\eta_r q)\Theta(\eta_r(-q)) = 0$.

$$\begin{aligned}
\langle X^2 \rangle = \frac{2\pi}{L} \sum_{q_1 \neq 0} \sum_{q_2 \neq 0} \Theta(\eta_r q_1)\Theta(\eta_r q_2) \frac{1}{\sqrt{|q_1||q_2|}} \mathrm{e}^{-\xi \frac{|q_1|}{2}} \mathrm{e}^{-\xi \frac{|q_2|}{2}} \\
\times \Big\{ u_{q_1} u_{q_2} \left(1 - \mathrm{e}^{-i(q_1 x - \omega_{q_1} t)}\right) \left(\mathrm{e}^{i(q_2 x - \omega_{q_2} t)} - 1\right) \langle \beta^\dagger_{q_1} \beta_{q_2} \rangle \\
+ v_{q_1} v_{q_2} \left(1 - \mathrm{e}^{-i(q_1 x + \omega_{q_1} t)}\right) \left(\mathrm{e}^{i(q_2 x + \omega_{q_2} t)} - 1\right) \langle \beta_{-q_1} \beta^\dagger_{-q_2} \rangle \\
+ u_{q_1} u_{q_2} \left(\mathrm{e}^{i(q_1 x - \omega_{q_1} t)} - 1\right) \left(1 - \mathrm{e}^{-i(q_2 x - \omega_{q_2} t)}\right) \langle \beta_{q_1} \beta^\dagger_{q_2} \rangle \\
+ v_{q_1} v_{q_2} \left(\mathrm{e}^{i(q_1 x + \omega_{q_1} t)} - 1\right) \left(1 - \mathrm{e}^{-i(q_2 x + \omega_{q_2} t)}\right) \langle \beta^\dagger_{-q_1} \beta_{-q_2} \rangle \Big\} \\
= \frac{2\pi}{L} \sum_{q \neq 0} \Theta(\eta_r q) \frac{2(1 + 2n_B(\omega_q))}{|q|} \mathrm{e}^{-\xi|q|} \\
\times \left(u_q^2(\cos(qx - \omega_q t) - 1) + v_q^2(\cos(qx + \omega_q t) - 1)\right).
\end{aligned}$$

The greater Green's function in eq. (5.80) may now be written as

$$iG_r^> = \langle \psi(x,t)\psi^\dagger(0,0) \rangle = \frac{\mathrm{e}^{ik_F(\eta_r x - v_F t)}}{L} \left(1 - \mathrm{e}^{-\xi \frac{2\pi}{L}}\right)^{-1} \mathrm{e}^{\frac{1}{2}Y} \mathrm{e}^{\frac{1}{2}\langle X^2 \rangle}. \quad (5.84)$$

Having $\omega_q > 0$ for all $q \neq 0$, the number of occupied states at each q tends to zero as $T \to 0$. In this limit, $n_B(\omega_q) = 0$, and the quantity in the exponential is

$$\begin{aligned}
\frac{1}{2}\left(Y + \langle X^2 \rangle\right) = \frac{1}{2} \sum_{q \neq 0} \Theta(\eta_r q) \frac{2\pi}{L|q|} \mathrm{e}^{-\xi|q|} \\
\times \left(u_q^2 \left(2\mathrm{e}^{i(qx - \omega_q t)} - 2\right) + v_q^2 \left(2\mathrm{e}^{-i(qx + \omega_q t)} - 2\right)\right) \\
= \frac{1}{2} \sum_{q \neq 0} \Theta(\eta_r q) \frac{2\pi}{L|q|} \mathrm{e}^{-\xi|q|} 2 \left(2v_q^2 \left(\cos(qx)\mathrm{e}^{-i\omega_q t} - 1\right) + \mathrm{e}^{-i\omega_q t}\mathrm{e}^{iqx} - 1\right) \\
= \sum_{q \neq 0} \Theta(\eta_r q) \frac{2\pi}{L|q|} \mathrm{e}^{-\xi|q|} \left(\mathrm{e}^{iqx}\mathrm{e}^{-i\omega_q t} + 2v_q^2 \left(\cos(qx)\mathrm{e}^{-i\omega_q t} - 1\right)\right) \\
+ \ln\left(1 - \mathrm{e}^{-\xi \frac{2\pi}{L}}\right), \quad (5.85)
\end{aligned}$$

where both the relation in eq. (5.79a) and $u_q^2 - v_q^2 = 1$ has been used. By

inserting this into eq. (5.84), the greater Green's function is at $T = 0$

$$iG_r^>(x,t)\mathrm{e}^{i\mu t} = \frac{\mathrm{e}^{ik_F\eta_r x}}{L} \times \exp\left(\sum_{q\neq 0}\Theta(\eta_r q)\frac{2\pi}{L|q|}\mathrm{e}^{-\xi|q|}\left(\mathrm{e}^{iqx}\mathrm{e}^{-i\omega_q t} + 2v_q^2\left(\cos(qx)\mathrm{e}^{-i\omega_q t} - 1\right)\right)\right), \tag{5.86}$$

which is the exact same result for the greater Green's function as found by Meden and Schönhammer [32]. Further analytic work can be made by replacing v_q^2 by a exponential cutoff $v_q^2 \simeq \nu \mathrm{e}^{-\Lambda|q|}$, and the summation in the exponent of eq. (5.86) can be solved exactly. This approximation does however not correspond to any physically realizable interaction [35]. In the "g-ology" models of density-density interactions, this replacement suppress certain peaks in the spectral function [36].

Chapter 6.
Phonon Corrections

Phonon Corrections

In this chapter, phonon corrections to the two-point correlation function will be computed using a non-perturbative approach at zero temperature. The phonons interact with the one-dimensional fermionic states through a coupling strength g_q independent of the fermionic quasimomentum k. This assumed k-independence of the electron-phonon interaction in a narrow window close to the Fermi momentum allows for an exact diagonalization of the theory, which is generally not possible in higher-dimensional coupled electron-phonon systems.

The corrections to the fermionic Green's function is found through the bosonization scheme presented in chapter 5. For armchair edges off graphene, these calculations are therefore relevant only if the bosonization procedure gives a qualitatively good description of localized edge states with helicity as a good quantum number.

The interaction with phonons then appears as the Fourier components of the density coupled to bosonic excitations with momentum exchange q. The recipe for the calculations follow the same lines as that for the bare electron-electron density interaction in section 5.3.2, and I will first go through preliminary definitions and general calculations common to all types of interactions.

For each system, I write down the Hamiltonian of the system in terms of phonons b_q and density bosons a_q (or its Bogoliubov transformed equivalent β_q if two-particle interactions are present) for the kinetic energy of particle-hole excitations. I then diagonalize the Hamiltonian $H = H_{\text{el}} + H_{\text{ph}} + H_{\text{el-ph}}$ and find the representation of $a_q(t)$ in terms of the diagonal basis. I then insert this representation into $\phi(x)$ given by eq. (5.54) and proceed to compute the greater Green's function $G_r^>(x,t)$ in real space, which is given in eq. (2.30) and takes the form

$$iG_r^>(x,t) = \frac{\mathrm{e}^{ik_F(\eta_r x - v_F t)}}{L} \langle \mathrm{e}^{i\phi_r^\dagger(x,t)} \mathrm{e}^{i\phi_r(x,t)} \mathrm{e}^{-i\phi_r^\dagger(0,0)} \mathrm{e}^{-i\phi_r(0,0)} \rangle \,. \tag{6.1}$$

This is evaluated in the large L limit and at zero temperature. In this equation, all energies are measured relative to the chemical potential $\mu = v_F k_F$. Before proceeding, I introduce the shorthand notation $\phi_0 \equiv \phi_r(0,0)$ and $\phi \equiv \phi_r(x,t)$ with the index r left tacit for the context. Now eq. (A.2.2) is used to join quantities in the exponential of eq. (6.1), which results in

$$iG_r^>(x,t) = \frac{\mathrm{e}^{ik_F(\eta_r x - v_F t)}}{L} \langle \mathrm{e}^{i(\phi^\dagger + \phi) - \frac{1}{2}[\phi^\dagger, \phi]} \mathrm{e}^{-i(\phi_0^\dagger + \phi_0) - \frac{1}{2}[\phi_0^\dagger, \phi_0]} \rangle \,. \tag{6.2}$$

This form is possible due to the fact that $[\phi^\dagger, \phi']$ will turn out to be a scalar quantity, and higher order commutators are zero, hence terminating the series representation in eq. (A.2.2). Moreover, in addition to being scalar, $[\phi^\dagger, \phi] =$

$[\phi_0^\dagger, \phi_0]$ is constant for equal coordinates, and can be added and factored out of the expectation value. At this point, the Green's function has the form

$$\begin{aligned} iG_r^>(x,t) &= \frac{e^{ik_F(\eta_r x - v_F t)}}{L} \left\langle e^{i(\phi^\dagger + \phi)} e^{-i(\phi_0^\dagger + \phi_0)} \right\rangle e^{[\phi_0, \phi_0^\dagger]} \\ &= \frac{e^{ik_F(\eta_r x - v_F t)}}{L} \left\langle e^{i(\phi^\dagger + \phi) - i(\phi_0^\dagger + \phi_0)} \right\rangle e^{\frac{1}{2}\left([\phi, \phi_0^\dagger] - [\phi_0, \phi^\dagger]\right)} e^{[\phi_0, \phi_0^\dagger]} \\ &\equiv \frac{e^{ik_F(\eta_r x - v_F t)}}{L} \left\langle e^X \right\rangle e^{\frac{1}{2}Y} e^{[\phi_0, \phi_0^\dagger]}, \end{aligned} \tag{6.3}$$

where I defined the quantities X and Y as

$$X \equiv i(\phi^\dagger + \phi) - i(\phi_0^\dagger + \phi_0) \tag{6.4a}$$

$$Y \equiv [\phi, \phi_0^\dagger] - [\phi_0, \phi^\dagger]\,. \tag{6.4b}$$

As is clear from these expressions, the commutation relations of ϕ must be calculated for each system. In these computations, I utilize the shorthand notation

$$\overline{\sum_q} (\,\cdot\,) \equiv \sum_{q \neq 0} \Theta(\eta_r q) \left(\frac{2\pi}{L|q|} \right)^{\frac{1}{2}} e^{-\xi \frac{|q|}{2}} (\,\cdot\,) \tag{6.5}$$

appearing in $\phi_r(x)$. It is understood that quantities appearing in $(\,\cdot\,)$ is to be summed over, rather than being a multiplicative factor of the entire sum. Including the time evolution of a_q and taking the large L-limit, the fields appearing in the exponent of ψ in eq. (5.43) is given by

$$\phi_r(x,t) \overset{L\to\infty}{\simeq} -i \overline{\sum_q} e^{iqx} a_q(t) \tag{6.6a}$$

$$\phi_r^\dagger(x,t) \overset{L\to\infty}{\simeq} i \overline{\sum_q} e^{-iqx} a_q^\dagger(t). \tag{6.6b}$$

The remaining expectation value in eq. (6.3) can be assessed using eq. (A.2.6), as the operator X will be linear in boson operators for which the Hamiltonian is diagonal. This expectation value can be computed either at zero or non-zero temperature. The general form of the resulting Green's function will thus be

$$iG_r^>(x,t) = \frac{e^{ik_F(\eta_r x - v_F t)}}{L} e^Z, \tag{6.7}$$

where

$$Z \equiv \frac{1}{2} \langle X^2 \rangle + \frac{1}{2} Y + [\phi_0, \phi_0^\dagger]\,. \tag{6.8}$$

The definitions of X, Y is given in eq. (6.4). Hence, all physics in the system is captured in the function $Z(x,t)$ which in turn is constructed by boson operators representing an infinite linear combination of particle-hole excitations.

For the spinful case, the interactions with phonons does not couple to spin degrees of freedom. The result of this is that the spin and charge sector of the electron density decouples even without spin dependent interactions. Denoting $G(g)$ as the Green's function whose electron-phonon coupling is g, the Green's function for the spinful case (without density-density interactions) appears as

$$G(x,t) \sim \Big(G(g=0)G(\sqrt{2}g)\Big)^{\frac{1}{2}}, \tag{6.9}$$

where the factor $\sqrt{2}$ is due to the normalization of the density-operator. If spin-dependent density-density interactions are present, the characteristic velocities in the two G's in eq. (6.9) are in general different, and the system displays a separation of spin and charge currents. I now use the definitions and general recipe above to compute the explicit form of the greater Green's function.

6.1 Diagonalization of the Electron - Phonon Hamiltonian

The coupled fermion phonon system in one dimension is a problem that has been studied earlier, both in general terms [28, 29] and by utilizing variants of the previously discussed bosonization techniques [30, 31]. I will show that the bosonization of the fermionic fields allow for hybridization between the quantized lattice vibrations and electron densities using canonical ladder operators, transforming the Hamiltonian into a system of uncoupled harmonic oscillators below a momentum cutoff for the electron-phonon coupling. The Hamiltonian describing electron-phonon interactions is written on the general form

$$\begin{aligned} H = &\sum_{k,\sigma} \varepsilon_k c^\dagger_{k,\sigma} c_{k,\sigma} + \sum_{q,\nu} \omega_{q,\nu} b^\dagger_{q,\nu} b_{q,\nu} \\ &+ \sum_{k,\sigma} \sum_{q,\nu} g^\nu_q c^\dagger_{k+q,\sigma} c_{k,\sigma} \frac{1}{\sqrt{2\omega_{q,\nu}}} \left(b_{q,\nu} + b^\dagger_{-q,\nu}\right). \end{aligned} \tag{6.10}$$

As Tomonaga studied in his seminal paper [25] by linearizing the electronic excitation spectrum close to the Fermi momentum k_F as

$$\varepsilon_k = v_F(\eta_r k - k_F). \tag{6.11}$$

The kinetic energy of the fermions relevant for the dynamics of the interacting system may be written in terms of the a-operators in eq. (5.50) as [30]

$$\sum_{|q|<q_c,\sigma} \varepsilon_q a^\dagger_{q,\sigma} a_{q,\sigma} + \text{constant}, \tag{6.12}$$

where the constant term of the full electron Hamiltonian will be neglected . This Hamiltonian describes a set of particle-hole excitations with bosonic nature. The spin quantum number can be replaced by the introduction of spin and charge -densities as shown in section 5.3.1, but the theory described in the following section allows for the inclusion of any quantum number, and I will keep the spin as an auxiliary parameter demonstrating the diagonalization procedure.

The system of interest is one in which density waves with momentum q excites quantized lattice vibrations at the edges of an armchair ribbon. The transformation from a fermionic to a bosonic frame of reference is only exact when the system consists of an infinite Dirac sea, but serves as a good approximation in the long distance limit.

The electron-phonon coupling $g_q = g_{-q} = g^*_q$ is restricted to be non-zero for $|q| < q_c$, where q_c is negligible compared to the Fermi momentum k_F. The dynamics of the Tomonaga-model is restricted to low energy excitations for small $|q| = |\eta_r k - k_F| \ll q_c$ and the cutoff in the electron-phonon coupling will not be of great importance to these low energetically excited states. In the following, the cutoff on q is not explicitly written.

The diagonalization of eq. (6.10) is done in the following steps. First, I reorganize the total Fock space as in chapter 5 and represent the fermion dynamics through eq. (6.12). By canonical quantization, the bosonic operators for both the fermionic density-bosons and different phonon branches can be represented in terms of generalized coordinates. By applying an orthogonal transformation to the resulting dynamical matrix, the Hamiltonian is transformed to uncoupled harmonic oscillators in new canonical coordinates whose normal modes and corresponding energy spectrum can be found. The method described here is applicable to any number of phonon branches, and specific expressions for energy eigenvalues depend on the system under investigation.

Note that the diagonalization procedure could be executed by inserting the boson operator representation of ρ_q and keeping the $b_{q,\nu}$-operators in the interaction term of eq. (6.10). In this case, the interaction term will be on the form

$$\left(a_{q,\sigma} + a^\dagger_{-q,\sigma}\right)\left(b^\dagger_{q,\nu} + b_{-q,\nu}\right), \tag{6.13}$$

which can not be diagonalized naively, but can be solved with a Bogoliubov-Valatin transformation [78]. Even for the spinless case with only one single

phonon branch present, an at least 4-dimensional basis is needed to compute eigenmodes and energies. Although equivalent, the approach described in this section is less cumbersome than the Bogoliubov-Valatin transform for the specific interaction.

6.1.1 Diagonalization and Canonical Quantization

In the quantum harmonic oscillator, ladder operators $a^\dagger$ and a is introduced as linear combinations of the position x and momentum p satisfying canonical commutation relations [79]. The bosonic excitations $a_{q,\alpha}$ are in terms of generalized coordinate and conjugate momenta introduced as

$$\begin{aligned} a^\dagger_{q,\alpha} &= \sqrt{\frac{\varepsilon_q}{2}} Q_{-q,\alpha} - \frac{i}{\sqrt{2\varepsilon_q}} P_{-q,\alpha} \\ a_{q,\alpha} &= \sqrt{\frac{\varepsilon_q}{2}} Q_{q,\alpha} + \frac{i}{\sqrt{2\varepsilon_q}} P_{q,\alpha}, \end{aligned} \tag{6.14}$$

where α is some quantum number (or collection thereof) and ε_q is the energy necessary to excite one boson $a_{q,\alpha}$. Thus, starting from bosonic ladder operators, the coordinate Q and its conjugate momenta P can be written in terms of creation and destruction operators as

$$Q_{q,\alpha} = \frac{1}{\sqrt{2\varepsilon_q}} \left(a_{q,\alpha} + a^\dagger_{-q,\alpha} \right) \tag{6.15a}$$

$$P_{q,\alpha} = -i\sqrt{\frac{\varepsilon_q}{2}} (a_{q,\alpha} - a^\dagger_{-q,\alpha}). \tag{6.15b}$$

To prove that (Q, P) constitute quantum mechanical coordinate and conjugate momenta, the Dirac bracket must satisfy [80]

$$[Q_{q,\alpha}, P^\dagger_{q',\alpha'}] = i\delta_{qq'}\delta_{\alpha\alpha'}, \tag{6.16}$$

Using the shorthand notation $\tilde{a} = a_{q',\alpha'}$ and that $P^\dagger_q = P_{-q}$ from the constraint that P_q is real, this is calculated as

$$\begin{aligned} [Q, \tilde{P}^\dagger] &= \frac{i}{2}\sqrt{\frac{\varepsilon_{q'}}{\varepsilon_q}} \left((a + a^\dagger)(\tilde{a}^\dagger - \tilde{a}) - (\tilde{a}^\dagger - \tilde{a})(a + a^\dagger) \right) \\ &= \frac{i}{2}\sqrt{\frac{\varepsilon_{q'}}{\varepsilon_q}} \left(-a\tilde{a} - a^\dagger\tilde{a} + a\tilde{a}^\dagger + a^\dagger\tilde{a}^\dagger + \tilde{a}a + \tilde{a}a^\dagger - \tilde{a}^\dagger a - \tilde{a}^\dagger a^\dagger \right) \\ &= \frac{i}{2}\sqrt{\frac{\varepsilon_{q'}}{\varepsilon_q}} (-a^\dagger\tilde{a} + a\tilde{a}^\dagger + (\delta_{qq'}\delta_{\alpha\alpha'} + a^\dagger\tilde{a}) + (\delta_{qq'}\delta_{\alpha\alpha'} - a\tilde{a}^\dagger)) \\ &= \frac{i}{2}\sqrt{\frac{\varepsilon_{q'}}{\varepsilon_q}} 2\delta_{qq'}\delta_{\alpha\alpha'} = i\delta_{qq'}\delta_{\alpha\alpha'} \end{aligned}$$

assuming that the operators satisfies $[a_{q,\alpha}, a^\dagger_{q',\alpha'}] = \delta_{qq'}\delta_{\alpha\alpha'}$.

In the present problem, both the phonon Hamiltonian and the kinetic term in eq. (6.12) include terms on the form $a^\dagger_{q,\alpha}a_{q,\alpha}$, which is

$$\begin{aligned} a^\dagger_{q,\alpha}a_{q,\alpha} &= \left(\sqrt{\frac{\varepsilon_q}{2}}Q_{-q,\alpha} - \frac{i}{\sqrt{2\varepsilon_q}}P_{-q,\alpha}\right)\left(\sqrt{\frac{\varepsilon_q}{2}}Q_{q,\alpha} + \frac{i}{\sqrt{2\varepsilon_q}}P_{q,\alpha}\right) \\ &= \frac{\varepsilon_q}{2}Q_{-q,\alpha}Q_{q,\alpha} + \frac{1}{2\varepsilon_q}P_{-q,\alpha}P_{q,\alpha} + \frac{i}{2}\left(Q_{-q,\alpha}P_{q,\alpha} - P_{-q,\alpha}Q_{q,\alpha}\right). \end{aligned}$$

Using eq. (6.16), and shifting the q-summation for the last term leads to

$$\varepsilon_q a^\dagger_{q,\alpha}a_{q,\alpha} = \frac{1}{2}\left(P_{-q,\alpha}P_{q,\alpha} + \varepsilon_q^2 Q_{-q,\alpha}Q_{q,\alpha} - \varepsilon_q\right), \tag{6.17}$$

which is a harmonic oscillator Hamiltonian. The last term can be disregarded when studying the dynamics of the system, and serves only as a shift in the zero-point energy.

I can now write the free parts of eq. (6.10) solely in terms of canonical coordinates. For bosons representing fermion densities, I use the notation $(P_{q,\sigma}, Q_{q,\sigma})$. The kinetic energy in eq. (6.12) is written

$$H_{\rm f} = \frac{1}{2}\sum_{q,\sigma}\left(P_{-q,\sigma}P_{q,\sigma} + \varepsilon_q^2 Q_{-q,\sigma}Q_{q,\sigma}\right). \tag{6.18}$$

Correspondingly, the quantized phonon spectrum is described in terms of the coordinates $(u_{q,\nu}, p_{q,\nu})$ for the phonon mode ν as

$$H_{\rm ph} = \frac{1}{2}\sum_{q,\nu}\left(p_{-q,\nu}p_{q,\nu} + \omega^2_{q,\nu}u_{-q,\nu}u_{q,\nu}\right). \tag{6.19}$$

The coordinate $u_{q,\nu}$ describes collective lattice deviations from equilibrium position in the crystal with wavelength $2\pi/q$, and $p_{q,\nu}$ is the momentum of these oscillations.

The k-summation is factored out in eq. (6.10) and replaced by ρ_{-q} using eq. (5.48). The factor in the coupling term linear in phonon operators can be evaluated by inserting eq. (6.14), and states

$$b_{q,\nu} + b^\dagger_{-q,\nu} = 2\sqrt{\frac{\omega_{q,\nu}}{2}}u_{q,\nu}. \tag{6.20}$$

Inserting these in the coupling term of eq. (6.10), I find

$$\sum_{k,\sigma}\sum_{q,\nu} g^\nu_q c^\dagger_{k+q,\sigma}c_{k,\sigma}\frac{1}{\sqrt{2\omega_{q,\nu}}}\left(b_{q,\nu} + b^\dagger_{-q,\nu}\right) = \sum_{q,\nu,\sigma} g^\nu_q \rho_{-q,\sigma}u_{q,\nu}. \tag{6.21}$$

I now insert eq. (5.50) to get ρ_{-q} in terms of $a_{q,\sigma}$, and eq. (6.14) to express these in terms of canonical coordinates. I obtain

$$\begin{aligned}\sum_{q,\nu,\sigma} g_q^\nu \rho_{-q,\sigma} u_{q,\nu} &= \sum_{q,\nu,\sigma} g_q^\nu \left(\frac{L|q|}{2\pi}\right)^{\frac{1}{2}} \left(a_{q,\sigma}^\dagger u_{q,\nu} + a_{-q,\sigma} u_{q,\nu}\right) \\ &\equiv \sum_{q,\nu,\sigma} G_q^\nu \sqrt{\frac{\varepsilon_q}{2}} \left[\left(Q_{-q,\sigma} - \frac{i}{\varepsilon_q} P_{-q,\sigma}\right) u_{q,\nu} + \left(Q_{q,\sigma} + \frac{i}{\varepsilon_q} P_{q,\sigma}\right) u_{-q,\nu}\right] \\ &= \sum_{q,\nu,\sigma} G_q^\nu \sqrt{\frac{\varepsilon_q}{2}} \left(Q_{q,\sigma}^\dagger u_{q,\nu} + u_{q,\nu}^\dagger Q_{q,\sigma}\right),\end{aligned}$$

where the terms containing $P_{q,\sigma}$ has been canceled in the q-summation and the quantity

$$G_q^\nu \equiv g_q^\nu \left(\frac{L|q|}{2\pi}\right)^{\frac{1}{2}} \tag{6.22}$$

is defined. The full Hamiltonian is now

$$\begin{aligned}H = \frac{1}{2} \sum_q \Bigg(&\sum_\sigma \left(P_{q,\sigma}^\dagger P_{q,\sigma} + \varepsilon_q^2 Q_{q,\sigma}^\dagger Q_{q,\sigma}\right) + \sum_\nu \left(p_{q,\nu}^\dagger p_{q,\nu} + \omega_{q,\nu}^2 u_{q,\nu}^\dagger u_{q,\nu}\right) \\ &+ \sum_{\nu,\sigma} 2 G_q^\nu \sqrt{\frac{\varepsilon_q}{2}} \left(Q_{q,\sigma}^\dagger u_{q,\nu} + u_{q,\nu}^\dagger Q_{q,\sigma}\right)\Bigg),\end{aligned} \tag{6.23}$$

which is to be diagonalized. Letting the system consist of n independent boson modes, I define the basis

$$\Pi_q \equiv (P_{q,\uparrow}, P_{q,\downarrow}, p_{q,\nu_1}, \ldots, p_{q,\nu_n})^T \tag{6.24a}$$

$$\Phi_q \equiv (Q_{q,\uparrow}, Q_{q,\downarrow}, u_{q,\nu_1}, \ldots, u_{q,\nu_n})^T \tag{6.24b}$$

for which the Hamiltonian in eq. (6.23) is expressed as

$$H = \frac{1}{2} \sum_q \left(\Pi_q^\dagger \Pi_q + \Phi_q^\dagger M_q \Phi_q\right). \tag{6.25}$$

The coupling matrix M_q determines the degree of hybridization between electron density waves and phonons, and the normal modes of the system is found by an orthogonal transformation that diagonalize M_q through

$$M_q = S_q S_q^{-1} M_q S_q S_q^{-1} \equiv S_q D_q S_q^{-1}. \tag{6.26}$$

The matrix D_q is a diagonal matrix whose entries are the squared energy eigenvalues.

$$D_q = \begin{pmatrix} \lambda_{q,1}^2 & & \\ & \lambda_{q,2}^2 & \\ & & \ddots \end{pmatrix} \tag{6.27}$$

The Hamiltonian is now written as uncoupled harmonic oscillators

$$H = \frac{1}{2}\sum_q \left(\tilde{\Pi}_q^\dagger \tilde{\Pi}_q + \tilde{\Phi}_q^\dagger D_q \tilde{\Phi}_q\right), \tag{6.28}$$

where the new coordinates and conjugate momenta are defined through

$$\tilde{\Pi}_q = S_q^{-1}\Pi_q \qquad \tilde{\Pi}_q^\dagger = \Pi_q^\dagger S_q \tag{6.29a}$$

$$\tilde{\Phi}_q = S_q^{-1}\Phi_q \qquad \tilde{\Phi}_q^\dagger = \Phi_q^\dagger S_q. \tag{6.29b}$$

The combined electron phonon Hamiltonian is thus transformed into non-interacting Bose gases with dispersion given by the energies $\lambda_{q,j}$ in D_q.

6.1.2 Recovering Density-Bosons

For the calculations of fermionic Green's functions through the bosonization scheme in chapter 5, the explicit representation of density-bosons $a_{q,\sigma}$ and their evolution in time is required. These can be found by canonical quantization of the harmonic oscillator in eq. (6.28), resulting in a diagonal theory quadratic in new boson operators whose time evolution in the Heisenberg picture is simple. Firstly, the Dirac bracket of the new operators is

$$\begin{aligned}
[\tilde{\Phi}_{q,k}, \tilde{\Pi}_{q',n}^\dagger] &= [S_{kl}^{-1}\Phi_{q,l}, \Pi_{q',m}^\dagger S_{mn}] \\
&= S_{kl}^{-1} S_{mn} \underbrace{[\Phi_{q,l}, \Pi_{q',m}^\dagger]}_{=i\delta_{qq'}\delta_{lm}} \\
&= S_{kl}^{-1} S_{ln} i\delta_{qq'} \\
&= i\delta_{kn}\delta_{qq'},
\end{aligned}$$

where I use the notation $A_{q,k}$ for the k'th component of a general vector A_q. Since the commutation is on normal form, I can define new boson operators $B_{q,i}$ through eq. (6.14), which is written out as

$$B_{q,i} = \sqrt{\frac{\lambda_{q,i}}{2}}\tilde{\Phi}_{q,i} + \frac{i}{\sqrt{2\lambda_{q,i}}}\tilde{\Pi}_{q,i} \tag{6.30a}$$

$$B_{q,i}^\dagger = \sqrt{\frac{\lambda_{q,i}}{2}}\tilde{\Phi}_{-q,i} - \frac{i}{\sqrt{2\lambda_{q,i}}}\tilde{\Pi}_{-q,i}. \tag{6.30b}$$

These operators satisfy the normal bosonic commutation relation

$$[B_{q,i}, B^\dagger_{q',j}] = \delta_{qq'}\delta_{ij}. \tag{6.31}$$

The Hamiltonian is now written on diagonal form as

$$H = \sum_{q,i} \lambda_{q,i} B^\dagger_{q,i} B_{q,i} + \text{constant}, \tag{6.32}$$

and the time-evolution of the $B_{q,i}$-operators in the Heisenberg picture is simply

$$B_{q,i}(t) = B_{q,i} \mathrm{e}^{-i\lambda_{q,i}t} \tag{6.33a}$$
$$B^\dagger_{q,i}(t) = B^\dagger_{q,i} \mathrm{e}^{i\lambda_{q,i}t}. \tag{6.33b}$$

The task now is to find the representation of the original density-bosons $a_{q,\sigma}(t)$ in terms of $B_{q,i}(t)$. Inverting eq. (6.30), I find

$$\tilde{\Phi}_{q,i} = \frac{1}{\sqrt{2\lambda_{q,i}}}\left(B_{q,i} + B^\dagger_{-q,i}\right) \qquad \tilde{\Phi}^\dagger_{q,i} = \frac{1}{\sqrt{2\lambda_{q,i}}}\left(B^\dagger_{q,i} + B_{-q,i}\right) \tag{6.34a}$$
$$\tilde{\Pi}_{q,i} = -i\sqrt{\frac{\lambda_{q,i}}{2}}\left(B_{q,i} - B^\dagger_{-q,i}\right) \qquad \tilde{\Pi}^\dagger_{q,i} = i\sqrt{\frac{\lambda_{q,i}}{2}}\left(B^\dagger_{q,i} - B_{-q,i}\right), \tag{6.34b}$$

and inserting this into the definitions in eq. (6.29), I find the representations

$$\Phi_{q,i} = S_{ij}\tilde{\Phi}_{q,j} = S_{ij}\frac{1}{\sqrt{2\lambda_{q,j}}}\left(B_{q,j} + B^\dagger_{-q,j}\right) \tag{6.35a}$$
$$\Phi^\dagger_{q,i} = \tilde{\Phi}^\dagger_{q,j}S^{-1}_{ji} = S^{-1}_{ji}\frac{1}{\sqrt{2\lambda_{q,j}}}\left(B^\dagger_{q,j} + B_{-q,j}\right) \tag{6.35b}$$
$$\Pi_{q,i} = S_{ij}\tilde{\Pi}_{q,j} = -iS_{ij}\sqrt{\frac{\lambda_{q,j}}{2}}\left(B_{q,j} - B^\dagger_{-q,j}\right) \tag{6.35c}$$
$$\Pi^\dagger_{q,i} = \tilde{\Pi}^\dagger_{q,j}S^{-1}_{ji} = iS^{-1}_{ji}\sqrt{\frac{\lambda_{q,j}}{2}}\left(B^\dagger_{q,j} - B_{-q,j}\right) \tag{6.35d}$$

with implicit summation over j. To obtain the boson operators corresponding to the coordinate and conjugate momenta $\Phi_{q,i}, \Pi_{q,i}$, I insert eq. (6.15) and

find

$$\begin{aligned}
a_{q,i} &= \sqrt{\frac{\varepsilon_{q,i}}{2}}\Phi_{q,i} + \frac{i}{\sqrt{2\varepsilon_{q,i}}}\Pi_{q,i} \\
&= \sqrt{\frac{\varepsilon_{q,i}}{2}}\left(S_{ij}\frac{1}{\sqrt{2\lambda_{q,j}}}\left(B_{q,j} + B^\dagger_{-q,j}\right)\right) \\
&\quad + \frac{i}{\sqrt{2\varepsilon_{q,i}}}\left(-iS_{ij}\sqrt{\frac{\lambda_{q,j}}{2}}\left(B_{q,j} - B^\dagger_{-q,j}\right)\right) \\
&= S_{ij}\left(B_{q,j}\frac{1}{2}\left(\sqrt{\frac{\varepsilon_{q,i}}{\lambda_{q,j}}} + \sqrt{\frac{\lambda_{q,j}}{\varepsilon_{q,i}}}\right) + B^\dagger_{-q,j}\frac{1}{2}\left(\sqrt{\frac{\varepsilon_{q,i}}{\lambda_{q,j}}} - \sqrt{\frac{\lambda_{q,j}}{\varepsilon_{q,i}}}\right)\right) \\
&\equiv S_{ij}\left(\Sigma_{ij}B_{q,j} + \Delta_{ij}B^\dagger_{-q,j}\right), \qquad (6.36)
\end{aligned}$$

where I defined

$$\Sigma_{ij} \equiv \frac{1}{2}\left(\sqrt{\frac{\varepsilon_{q,i}}{\lambda_{q,j}}} + \sqrt{\frac{\lambda_{q,j}}{\varepsilon_{q,i}}}\right) \qquad (6.37a)$$

$$\Delta_{ij} \equiv \frac{1}{2}\left(\sqrt{\frac{\varepsilon_{q,i}}{\lambda_{q,j}}} - \sqrt{\frac{\lambda_{q,j}}{\varepsilon_{q,i}}}\right). \qquad (6.37b)$$

The dispersion $\varepsilon_{q,i}$ appearing in eq. (6.37) is the unperturbed excitation spectrum of boson mode i. The hermitian conjugate of eq. (6.36) is

$$\begin{aligned}
a^\dagger_{q,i} &= \sqrt{\frac{\varepsilon_{q,i}}{2}}\Phi^\dagger_{q,i} - \frac{i}{\sqrt{2\varepsilon_{q,i}}}\Pi^\dagger_{q,i} \\
&= \sqrt{\frac{\varepsilon_{q,i}}{2}}S^{-1}_{ji}\frac{1}{\sqrt{2\lambda_{q,j}}}\left(B^\dagger_{q,j} + B_{-q,j}\right) \\
&\quad - \frac{i}{\sqrt{2\varepsilon_{q,i}}}iS^{-1}_{ji}\sqrt{\frac{\lambda_{q,j}}{2}}\left(B^\dagger_{q,j} - B_{-q,j}\right) \\
&= S^{-1}_{ji}\left(B^\dagger_{q,j}\frac{1}{2}\left(\sqrt{\frac{\varepsilon_{q,i}}{\lambda_{q,j}}} + \sqrt{\frac{\lambda_{q,j}}{\varepsilon_{q,i}}}\right) + B_{-q,j}\frac{1}{2}\left(\sqrt{\frac{\varepsilon_{q,i}}{\lambda_{q,j}}} - \sqrt{\frac{\lambda_{q,j}}{\varepsilon_{q,i}}}\right)\right) \\
&= S^{-1}_{ji}\left(\Sigma_{ij}B^\dagger_{q,j} + \Delta_{ij}B_{-q,j}\right). \qquad (6.38)
\end{aligned}$$

The quantities Σ_{ij} and Δ_{ij} satisfy the identity

$$\Sigma^2_{ij} - \Delta^2_{ij} = 1, \qquad (6.39)$$

which is reminiscent of symplectic Bogoliubov transformations applied to interacting boson Hamiltonians, where this is set as a requirement to ensure proper commutation relations. In this approach, these relations come naturally from the definitions and the form of the interaction. The relation in eq. (6.39) is satisfied by hyperbolic functions $\Sigma_{ij} = \cosh(\theta_{ij})$ and $\Delta_{ij} = \sinh(\theta_{ij})$ with the Bogoliubov mixing parameter

$$\theta_{ij} = \frac{1}{2}\ln\left(\frac{\varepsilon_{q,i}}{\lambda_{q,j}}\right). \tag{6.40}$$

The a-operators are expressed through the sum, rather than the difference of these hyperbolic functions. This sum can in general be very large, even if the difference of its constituents remain equal to 1. For realistic coupling strengths, the mixing angle will be small and $\Delta_{ij}/\Sigma_{ij} \sim \mathcal{O}(g^2)$. I can now compute the commutation relation for the time evolved a-bosons of different species

$$\begin{aligned}
&[a_{q,i}(t), a^\dagger_{q',k}(t')] = \\
&S_{ij}S^{-1}_{lk}[\Sigma_{ij}B_{q,j}\mathrm{e}^{-i\lambda_{q,j}t} + \Delta_{ij}B^\dagger_{-q,j}\mathrm{e}^{i\lambda_{q,j}t}, \Sigma_{kl}B^\dagger_{q',l}\mathrm{e}^{i\lambda_{q',l}t'} + \Delta_{kl}B_{-q',l}\mathrm{e}^{-i\lambda_{q',l}t'}] \\
&= S_{ij}S^{-1}_{lk}\Big(\Sigma_{ij}\Sigma_{kl}\mathrm{e}^{-i\lambda_{q,j}t}\mathrm{e}^{i\lambda_{q',l}t'}[B_{q,j}, B^\dagger_{q',l}] \\
&\quad + \Sigma_{ij}\Delta_{kl}\mathrm{e}^{-i\lambda_{q,j}t}\mathrm{e}^{-i\lambda_{q',l}t'}[B_{q,j}, B_{-q',l}] + \Delta_{ij}\Sigma_{kl}\mathrm{e}^{i\lambda_{q,j}t}\mathrm{e}^{i\lambda_{q',l}t'}[B^\dagger_{-q,j}, B^\dagger_{q',l}] \\
&\qquad + \Delta_{ij}\Delta_{kl}\mathrm{e}^{i\lambda_{q,j}t}\mathrm{e}^{-i\lambda_{q',l}t'}[B^\dagger_{-q,j}, B_{-q',l}]\Big) \\
&= S_{ij}S^{-1}_{lk}\Big(\Sigma_{ij}\Sigma_{kl}\mathrm{e}^{-i\lambda_{q,j}t}\mathrm{e}^{i\lambda_{q',l}t'}\delta_{qq'}\delta_{jl} - \Delta_{ij}\Delta_{kl}\mathrm{e}^{i\lambda_{q,j}t}\mathrm{e}^{-i\lambda_{q',l}t'}\delta_{qq'}\delta_{jl}\Big) \\
&= S_{ij}S^{-1}_{jk}\Big(\Sigma_{ij}\Sigma_{kj}\mathrm{e}^{-i\lambda_{q,j}(t-t')} - \Delta_{ij}\Delta_{kj}\mathrm{e}^{i\lambda_{q,j}(t-t')}\Big)\delta_{qq'}.
\end{aligned} \tag{6.41}$$

Note that at equal times, the commutator satisfy $[a_{q,i}(t), a^\dagger_{q',k}(t)] = \delta_{ik}\delta_{qq'}$. This quantity will be used in the calculations of Green's functions.

6.2 Single Phonon Branch

In this section I will compute phonon corrections to $G^>_r$ caused by a single acoustic phonon branch. In all cases under consideration, the coupling term will remain unchanged, however the constituents of the interaction will have different physical interpretations and alter the form of the resulting Green's functions in different ways.

The phonon Hamiltonian for all cases is written as

$$H_{\mathrm{ph}} = \frac{1}{2}\sum_q \left(p^\dagger_q p_q + \omega^2_q u^\dagger_q u_q\right), \tag{6.42}$$

where $\omega_q = v_s|q|$. To linear order in lattice displacement, the normal coordinate u_q couples to a density wave ρ_{-q} as [30]

$$H_{\text{int}} = \sum_q g_q \rho_{-q} u_q. \tag{6.43}$$

6.2.1 Spinless Fermions Without Density-Interactions

I will first compute the phonon corrections to non-interacting spinless fermions. The dynamics of fermion densities is captured by the Hamiltonian

$$H_{\text{el}} = \sum_q \varepsilon_q a_q^\dagger a_q. \tag{6.44}$$

Following section 6.1.1 with only one phonon mode and spinless a_q-bosons, the theory may be written on the same form as eq. (6.23), with

$$\Phi_q = \Phi_{-q}^\dagger = (Q_q, u_q)^T \tag{6.45a}$$

$$\Pi_q = \Pi_{-q}^\dagger = (P_q, p_q)^T \tag{6.45b}$$

as the basis. The coupling matrix M_q is given by

$$M_q = \begin{pmatrix} \varepsilon_q^2 & \tilde{G}_q \\ \tilde{G}_q & \omega_q^2 \end{pmatrix}, \tag{6.46}$$

where

$$\tilde{G}_q = G_q \sqrt{2\varepsilon_q} = g_q \left(\frac{L|q|}{2\pi}\right)^{\frac{1}{2}} \sqrt{2\varepsilon_q}. \tag{6.47}$$

M_q may be diagonalized as

$$D_q = S_q^{-1} M_q S_q = \begin{pmatrix} \lambda_{q,1}^2 & \\ & \lambda_{q,2.}^2 \end{pmatrix} \tag{6.48}$$

The density-bosons may now be recovered using eqs. (6.36) and (6.38). I will use the notation $a_q = a_{q,1}, \Sigma_{1j} = \Sigma_j, \Delta_{1j} = \Delta_j$, where the index 1 is due to the placement of Q_q and P_q in the basis Φ_q and Π_q respectively. I will in the following also drop the index on the matrices, using the shorthand notation $S_{1j} = S_j, S_{j1}^{-1} = S_j^{-1}$. The fields $\phi_r(x,t)$ in eq. (6.6) is in this system given by

$$\phi_r(x,t) = -i\overline{\sum_q} \mathrm{e}^{iqx} S_j \left(\Sigma_j B_{q,j} \mathrm{e}^{-i\lambda_{q,j}t} + \Delta_j B_{-q,j}^\dagger \mathrm{e}^{i\lambda_{q,j}t}\right) \tag{6.49a}$$

$$\phi_r^\dagger(x,t) = i\overline{\sum_q} \mathrm{e}^{-iqx} S_j^{-1} \left(\Sigma_j B_{q,j}^\dagger \mathrm{e}^{i\lambda_{q,j}t} + \Delta_j B_{-q,j} \mathrm{e}^{-i\lambda_{q,j}t}\right). \tag{6.49b}$$

For the computation of Z in eq. (6.8), the exact form of the commutator for these fields is important. This is evaluated as

$$\begin{aligned}[\phi_r(x,t),\phi^\dagger_{r'}(x',t')] &= \overline{\sum_q}\,\overline{\sum_{q'}} \mathrm{e}^{i(qx-q'x')}[a_q(t),a_{q'}(t')] \\ &= \delta_{rr'}\sum_{q\neq 0}\Theta(\eta_r q)\frac{2\pi}{L|q|}\mathrm{e}^{-\xi|q|}\mathrm{e}^{iq(x-x')}S_jS_j^{-1}\left(\Sigma_j^2\mathrm{e}^{-i\lambda_{q,j}(t-t')}-\Delta_j^2\mathrm{e}^{i\lambda_{q,j}(t-t')}\right).\end{aligned} \tag{6.50}$$

Note the appearance of opposite phases. In the simplest approximation, the effect of this term is to reduce the singularity in the Green's function $G^>_r(x,t)$ at $x=ut$ for a characteristic velocity u, and appear as an algebraic pole at $x=-ut$ with exponent dependent on Δ_j.

Computing Z

I will now compute $Z(x,t)$, the quantity defined in eq. (6.8) which appears in the Green's function in eq. (6.7). The calculation of Z given in eq. (6.8) requires the computation of several quantities. The first of which I will compute is the commutator of ϕ-fields at $x=0$ and $t=0$, found by inserting eq. (6.50) as

$$[\phi_0,\phi_0^\dagger] = \sum_{q\neq 0}\Theta(\eta_r q)\frac{2\pi}{L|q|}\mathrm{e}^{-\xi|q|} \simeq -\ln\left(\frac{2\pi}{L}\xi\right), \tag{6.51}$$

where a large L-approximation is responsible for the rightmost expression. The quantity Y in eq. (6.4b) is computed as

$$\begin{aligned}Y = \sum_{q\neq 0}\Theta(\eta_r q)\frac{2\pi}{L|q|}\mathrm{e}^{-\xi|q|}S_jS_j^{-1}\big[&\mathrm{e}^{iqx}\left(\Sigma_j^2\mathrm{e}^{-i\lambda_{q,j}t}-\Delta_j^2\mathrm{e}^{i\lambda_{q,j}t}\right) \\ &-\mathrm{e}^{-iqx}\left(\Sigma_j^2\mathrm{e}^{i\lambda_{q,j}t}-\Delta_j^2\mathrm{e}^{-i\lambda_{q,j}t}\right)\big].\end{aligned}$$

The last term appearing in Z involves the expectation value of X^2, where X is given in eq. (6.4a) and takes the form

$$\begin{aligned}
X = \overline{\sum_q} \Big(& \mathrm{e}^{-iqx} S_j^{-1} \left(\Sigma_j B_{q,j}^\dagger \mathrm{e}^{i\lambda_{q,j}t} + \Delta_j B_{-q,j} \mathrm{e}^{-i\lambda_{q,j}t} \right) \\
& - S_j^{-1} \left(\Sigma_j B_{q,j}^\dagger + \Delta_j B_{-q,j} \right) + S_j \left(\Sigma_j B_{q,j} + \Delta_j B_{-q,j}^\dagger \right) \\
& - \mathrm{e}^{iqx} S_j \left(\Sigma_j B_{q,j} \mathrm{e}^{-i\lambda_{q,j}t} + \Delta_j B_{-q,j}^\dagger \mathrm{e}^{i\lambda_{q,j}t} \right) \Big) \\
= \overline{\sum_q} \Big(& S_j^{-1} \Sigma_j B_{q,j}^\dagger \left(\mathrm{e}^{-iqx} \mathrm{e}^{i\lambda_{q,j}t} - 1 \right) + S_j^{-1} \Delta_j B_{-q,j} \left(\mathrm{e}^{-iqx} \mathrm{e}^{-i\lambda_{q,j}t} - 1 \right) \\
& + S_j \Sigma_j B_{q,j} \left(1 - \mathrm{e}^{iqx} \mathrm{e}^{-i\lambda_{q,j}t} \right) + S_j \Delta_j B_{-q,j}^\dagger \left(1 - \mathrm{e}^{iqx} \mathrm{e}^{i\lambda_{q,j}t} \right) \Big) \\
\equiv \overline{\sum_q} & \left(C_j^{(1)} B_{q,j}^\dagger + C_j^{(2)} B_{-q,j} + C_j^{(3)} B_{q,j} + C_j^{(4)} B_{-q,j}^\dagger \right), \qquad (6.52)
\end{aligned}$$

where I defined the temporary factors $C_j^{(i)}$. The expectation value $\langle X^2 \rangle$ can now be computed. In this calculation, terms whose expectation value is proportional to $\delta_{q,-q'}$ will be present. These will disappear in the double q-summation, as each of these summations come with a Heaviside step function $\Theta(\eta_r q)$. I will therefore ignore these terms, and compute

$$\begin{aligned}
\langle X^2 \rangle = & \overline{\sum_q} \overline{\sum_{q'}} \Big(C_j^{(1)} C_k^{(3)} \langle B_{q,j}^\dagger B_{q',k} \rangle + C_j^{(2)} C_k^{(4)} \langle B_{-q,j} B_{-q',k}^\dagger \rangle \\
& + C_j^{(3)} C_k^{(1)} \langle B_{q,j} B_{q',k}^\dagger \rangle + C_j^{(4)} C_k^{(2)} \langle B_{-q,j}^\dagger B_{-q',k} \rangle \Big) + \propto \delta_{q,-q'} \\
= & \overline{\sum_q} \overline{\sum_{q'}} \left((C_j^{(1)} C_j^{(3)} + C_j^{(2)} C_j^{(4)})(1 + 2n_B(\lambda_{q,j})) \right) \delta_{qq'} \delta_{jk} \qquad (6.53) \\
\overset{T=0}{=} & \sum_{q \neq 0} \Theta(\eta_r q) \frac{2\pi}{L|q|} \mathrm{e}^{-\xi|q|} S_j S_j^{-1} \left(\Sigma_j^2 \left(\mathrm{e}^{-iqx} \mathrm{e}^{i\lambda_{q,j}t} + \mathrm{e}^{iqx} \mathrm{e}^{-i\lambda_{q,j}t} - 2 \right) \right. \\
& \left. + \Delta_j^2 \left(\mathrm{e}^{iqx} \mathrm{e}^{i\lambda_{q,j}t} + \mathrm{e}^{-iqx} \mathrm{e}^{-i\lambda_{q,j}t} - 2 \right) \right). \qquad (6.54)
\end{aligned}$$

I now evaluate Z as

$$\begin{aligned}
Z &= \frac{1}{2}\langle X^2\rangle + \frac{1}{2}Y + [\phi_0, \phi_0^\dagger] \\
&= \frac{1}{2}\sum_{q\neq 0}\Theta(\eta_r q)\frac{2\pi}{L|q|}\mathrm{e}^{-\xi|q|}S_j S_j^{-1} \\
&\quad \times \left\{\Sigma_j^2\left(\mathrm{e}^{-iqx}\mathrm{e}^{i\lambda_{q,j}t} + \mathrm{e}^{iqx}\mathrm{e}^{-i\lambda_{q,j}t} - 2 + \mathrm{e}^{iqx}\mathrm{e}^{-i\lambda_{q,j}t} - \mathrm{e}^{-iqx}\mathrm{e}^{i\lambda_{q,j}t}\right)\right. \\
&\quad \left. +\Delta_j^2\left(\mathrm{e}^{iqx}\mathrm{e}^{i\lambda_{q,j}t} + \mathrm{e}^{-iqx}\mathrm{e}^{-i\lambda_{q,j}t} - 2 - \mathrm{e}^{iqx}\mathrm{e}^{i\lambda_{q,j}t} + \mathrm{e}^{-iqx}\mathrm{e}^{-i\lambda_q t}\right) + 2\right\} \\
&= \sum_{q\neq 0}\sum_{j=1,2}\Theta(\eta_r q)\frac{2\pi}{L|q|}\mathrm{e}^{-\xi|q|}S_j S_j^{-1}\left\{\Sigma_j^2\mathrm{e}^{iqx}\mathrm{e}^{-i\lambda_{q,j}t} + \Delta_j^2\mathrm{e}^{-iqx}\mathrm{e}^{-i\lambda_{q,j}t} - 2\Delta_j^2\right\},
\end{aligned} \tag{6.55}$$

where I reinstated the j-summation over hybridized density-phonon bands for clarity. I can now insert Z in eq. (6.7) to obtain the real space Green's function. The quantity Z in eq. (6.55) is on the same form as found by Meden et al. [31], and I now express the exact form of the coefficients to show that the result is indeed identical.

Explicit Form of Coefficients

With the matrix M_q on the form of eq. (6.46), the eigenvalues are

$$\lambda_{q,1}^2 = \frac{1}{2}\left(\varepsilon_q^2 + \omega_q^2 + \sqrt{(\varepsilon_q^2 - \omega_q^2)^2 + 4\tilde{G}_q^2}\right) \tag{6.56a}$$

$$\lambda_{q,2}^2 = \frac{1}{2}\left(\varepsilon_q^2 + \omega_q^2 - \sqrt{(\varepsilon_q^2 - \omega_q^2)^2 + 4\tilde{G}_q^2}\right) \tag{6.56b}$$

and the transformation matrices S and S^{-1} is given by

$$S = \frac{1}{\tilde{G}_q}\begin{pmatrix} \lambda_{q,1}^2 - \omega_q^2 & \lambda_{q,2}^2 - \omega_q^2 \\ \tilde{G}_q & \tilde{G}_q \end{pmatrix} \tag{6.57a}$$

$$S^{-1} = \frac{1}{\sqrt{Q_q}}\begin{pmatrix} \tilde{G}_q & -\lambda_{q,2}^2 + \omega_q^2 \\ -\tilde{G}_q & \lambda_{q,1}^2 - \omega_q^2 \end{pmatrix} \tag{6.57b}$$

where $Q_q \equiv (\varepsilon_q^2 - \omega_q^2)^2 + 4\tilde{G}_q^2$. The weight of each normal bosonic mode in the fermionic density-bosons are given by the matrix elements

$$S_1 S_1^{-1} = \frac{1}{\sqrt{Q_q}}(\lambda_{q,1}^2 - \omega_q^2) \tag{6.58}$$

$$S_2 S_2^{-1} = \frac{-1}{\sqrt{Q_q}}(\lambda_{q,2}^2 - \omega_q^2). \tag{6.59}$$

The coefficients appearing in Z is therefore

$$S_1 S_1^{-1}\Sigma_1^2 = \frac{(\varepsilon_q + \lambda_{q,1})^2\left(\lambda_{q,1}^2 - \omega_q^2\right)}{4\sqrt{Q_q}\lambda_{q,1}\varepsilon_q} \quad S_1 S_1^{-1}\Delta_1^2 = \frac{(\varepsilon_q - \lambda_{q,1})^2\left(\lambda_{q,1}^2 - \omega_q^2\right)}{4\sqrt{Q_q}\lambda_{q,1}\varepsilon_q}$$

$$S_2 S_2^{-1}\Sigma_2^2 = \frac{(\varepsilon_q + \lambda_{q,2})^2\left(\omega_q^2 - \lambda_{q,2}^2\right)}{4\sqrt{Q_q}\lambda_{q,2}\varepsilon_q} \quad S_2 S_2^{-1}\Delta_2^2 = \frac{(\varepsilon_q - \lambda_{q,2})^2\left(\omega_q^2 - \lambda_{q,2}^2\right)}{4\sqrt{Q_q}\lambda_{q,2}\varepsilon_q}, \tag{6.60}$$

which can be put in shorthand notation as

$$c_{j,\pm} = \frac{(\varepsilon_q \pm \lambda_{q,j})^2|\lambda_{q,j}^2 - \omega_q^2|}{4\lambda_{q,j}\varepsilon_q\sqrt{Q_q}}, \qquad j = 1, 2. \tag{6.61}$$

These coefficients is the same as those found by Meden et al. [31], who considered an Einstein model for a single phonon branch. The expression holds for arbitrary phonon dispersion, and the coefficients satisfy the sum rule

$$\sum_{j=1,2}(c_{j,+} - c_{j,-}) = 1 \quad \forall\, q \neq 0. \tag{6.62}$$

Closed Form Approximation

I will now bring the Green's function to a closed form by solving the q-integral in eq. (6.55). This is done by approximating the electron-phonon coupling as

$$g_q = \alpha q \tag{6.63}$$

for sufficiently small scattering momenta q. The coupling that appears in the energy eigenvalues of eq. (6.56) is

$$\begin{aligned} 4\tilde{G}_q^2 &= 4\left(g_q\left(\frac{L|q|}{2\pi}\right)^{\frac{1}{2}}\sqrt{2\varepsilon_q}\right)^2 \\ &= 4\alpha^2|q|^2\frac{v_F L|q|^2}{\pi} \equiv \beta|q|^4, \end{aligned} \tag{6.64}$$

where I defined the effective coupling constant β. In this approximation, the eigenenergies are

$$\lambda_{q,1}^2 = \frac{|q|^2}{2}\left(v_F^2 + v_s^2 + \sqrt{(v_F^2 - v_s^2)^2 + \beta}\right) \equiv u_1^2|q|^2 \tag{6.65a}$$

$$\lambda_{q,2}^2 = \frac{|q|^2}{2}\left(v_F^2 + v_s^2 - \sqrt{(v_F^2 - v_s^2)^2 + \beta}\right) \equiv u_2^2|q|^2 \tag{6.65b}$$

If the coupling is sufficiently large, the energies become imaginary. The proper lattice vibrations are then unstable, and the system breaks down, as first pointed out by Wentzel [28]. In the general discussion of electrons coupled to lattice vibrations in one, Bardeen [29] gave a remark that the application of the Tomonaga model sets a constraint on coupling strength which is identical (up to a factor of 2) to the criterion of superconductivity in Fröhlich's theory [81]. The requirement of real energy eigenvalues is fulfilled if

$$\beta < 4v_F^2 v_s^2, \tag{6.66}$$

or equivalently

$$\alpha < \sqrt{\frac{\pi v_F v_s^2}{L}}. \tag{6.67}$$

In this approximation of the coupling strength, the coefficients $c_{j,\pm}$ given in eq. (6.61) are constants

$$c_{j,\pm} = \frac{(v_F \pm u_j)^2 |u_j^2 - v_s^2|}{4u_j v_F \sqrt{(v_F^2 - v_s^2)^2 + \beta}}. \tag{6.68}$$

These are plotted in fig. 6.1 for different coupling strengths β up to the critical value in eq. (6.66) where the system breaks down. The phonon velocity is assumed to be smaller than the Fermi velocity.

With the energy eigenvalues $\lambda_{q,j} = u_j|q|$ linear in q, I can represent the total greater Green's function in eq. (6.7) by solving the integrals in eq. (6.55) analytically. Denoting $\mathrm{e}^Z = \mathrm{e}^{Z_1}\mathrm{e}^{Z_2}$, I compute

$$\begin{aligned}
Z_j &= \sum_{q\neq 0} \Theta(\eta_r q) \frac{2\pi}{L|q|} \mathrm{e}^{-\xi|q|} \left\{ c_{j,+} \mathrm{e}^{iqx} \mathrm{e}^{-iu_j|q|t} + c_{j,-} \mathrm{e}^{-iqx} \mathrm{e}^{-iu_j|q|t} - 2c_{j,-} \right\} \\
&= c_{j,+} \sum_{q>0} \frac{2\pi}{Lq} \mathrm{e}^{-\xi q} \mathrm{e}^{i\eta_r qx} \mathrm{e}^{-iu_j qt} + c_{j,-} \sum_{q>0} \frac{2\pi}{Lq} \mathrm{e}^{-\xi q} \mathrm{e}^{-i\eta_r qx} \mathrm{e}^{-iu_j qt} \\
&\qquad - 2c_{j,-} \sum_{q>0} \frac{2\pi}{L|q|} \mathrm{e}^{-\xi q} \\
&= -c_{j,+} \ln\left(1 - \exp\left(\frac{2\pi}{L}(-\xi + i\eta_r x - iu_j t)\right)\right) \\
&\qquad - c_{j,-} \ln\left(1 - \exp\left(\frac{2\pi}{L}(-\xi - i\eta_r x - iu_j t)\right)\right), \\
&\qquad + 2c_{j,-} \ln\left(1 - \exp\left(-\frac{2\pi\xi}{L}\right)\right),
\end{aligned} \tag{6.69}$$

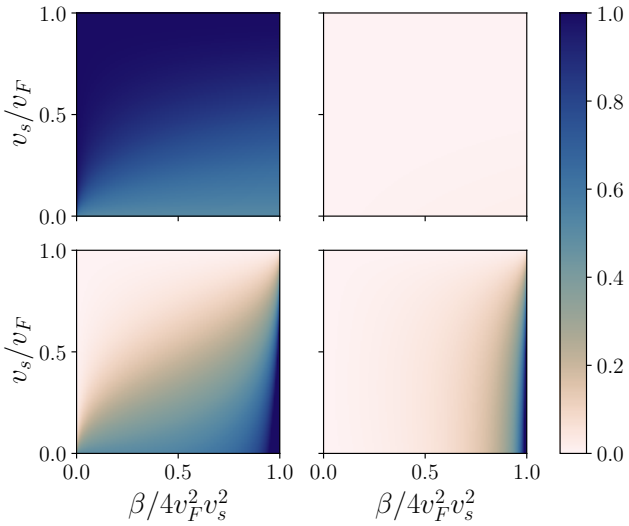

Figure 6.1: Dimensionless coefficients $c_{j,\pm}$ in eq. (6.68) for different values of the acoustic phonon velocity v_s and electron-phonon coupling strength β (see eq. (6.64)). Top row: $c_{1,+}$ (left) and $c_{1,-}$ (right). Bottom row: $c_{2,+}$ (left) and $c_{2,-}$ (right). The coefficients satisfy the sum rule in eq. (6.62).

which is now evaluated in the large L-limit, where

$$1 - \exp\left(\frac{2\pi}{L}A\right) \simeq -\frac{2\pi}{L}A \tag{6.70}$$

for $|A| \ll L$. The greater Green's function $G_r^>(x,t)$ may then be written in closed form as

$$\begin{aligned} iG_r^>(x,t)\mathrm{e}^{i\mu t} = \frac{i\eta_r}{2\pi}\frac{\mathrm{e}^{ik_F\eta_r x}}{(\eta_r x - u_1 t + i\xi)^{c_{1,+}}}\left(\frac{\xi^2}{\eta_r x + u_1 t - i\xi}\right)^{c_{1,-}} \\ \times \frac{1}{(\eta_r x - u_2 t + i\xi)^{c_{2,+}}}\left(\frac{\xi^2}{\eta_r x + u_2 t - i\xi}\right)^{c_{2,-}}. \end{aligned} \tag{6.71}$$

This representation is on a more familiar form and is less impenetrable than $G^> \sim \exp(Z(x,t))$ for acquiring physical insight. In this approximation, the effect of phonons is more visible; The characteristic velocities of the system are renormalized, and the peaks appearing in the Green's function are no longer simple poles, but rather algebraic singularities. This closed form approximation is neglecting the q-dependence of the interactions, whose details are known to be of great importance for the resulting power-law Luttinger behavior of spectral peaks [33, 34, 36]. Note that the limit $\xi \to 0$ is now difficult without resulting in a vanishing correlation function. This is avoided by keeping the "effective" bandwidth ξ finite, and noticing that the coefficients $c_{j,-}$ are very small compared to $c_{j,+}$, as can be seen in fig. 6.1. The weight of the factors $\sim \xi^{2c_{j,-}}$ is nonvanishing.

6.2.2 Spinless Fermions With Density-Interactions

In section 5.3.2, I diagonalized interacting fermion-densities as a Bogoliubov transformation. By repeating eqs. (5.70), (5.71) and (5.73), the starting point of the calculations of $G_r^>(x,t)$ is the Hamiltonian

$$H = \sum_q \tilde{\varepsilon}_q \beta_q^\dagger \beta_q + H_{\mathrm{ph}} + H_{\mathrm{int}}, \tag{6.72}$$

where H_{ph} and H_{int} is given in eqs. (6.42) and (6.43). The density wave ρ_q appearing in the interaction term is given in terms of eq. (5.50). To find a representation in terms of the Bogoliubov transformed operators β_q, I insert

eq. (5.73) and find

$$\begin{aligned}\rho_{-q} &= \left(\frac{L|q|}{2\pi}\right)^{\frac{1}{2}} (a_q^\dagger + a_{-q}) \\ &= \left(\frac{L|q|}{2\pi}\right)^{\frac{1}{2}} \left(v_q\beta_{-q} + u_q\beta_q^\dagger + u_q\beta_{-q} + v_q\beta_q^\dagger\right) \\ &= \left(\frac{L|q|}{2\pi}\right)^{\frac{1}{2}} \mathrm{e}^{\theta_q}(\beta_q^\dagger + \beta_{-q}),\end{aligned} \tag{6.73}$$

where u_q and v_q are parameters that diagonalize the electron Hamiltonian through eq. (5.70). By inserting this relation into the interaction term of the Hamiltonian, the Bogoliubov mixing parameter θ_q effectively renormalizes the electron phonon coupling strength through

$$g_q \to g_q \mathrm{e}^{\theta_q}, \tag{6.74}$$

where θ_q is given in eq. (5.72). Thus the coupling to lattice vibrations is either enhanced or suppressed, depending if the interaction is attractive or repulsive for a given q.

Other terms representing a constant shift of the energy is disregarded. Following the same lines as in section 6.2.1, the creation and annihilation operators in eqs. (6.36) and (6.38) now read

$$\beta_q = S_{1j}\left(\Sigma_{1j}B_{q,j} + \Delta_{1j}B_{-q,j}^\dagger\right) \tag{6.75a}$$

$$\beta_q^\dagger = S_{j1}^{-1}\left(\Sigma_{1j}B_{q,j}^\dagger + \Delta_{1j}B_{-q,j}\right) \tag{6.75b}$$

for the uncoupled density modes, and

$$b_q = S_{2j}\left(\Sigma_{2j}B_{q,j} + \Delta_{2j}B_{-q,j}^\dagger\right) \tag{6.76a}$$

$$b_q^\dagger = S_{j2}^{-1}\left(\Sigma_{2j}B_{q,j}^\dagger + \Delta_{2j}B_{-q,j}\right) \tag{6.76b}$$

for the single phonon mode present. In the spinless case, the basis is two-dimensional, and I am only interested in the single mode β_q corresponding to the Bogoliubov transformed density operators, since the phonon operator b_q does not appear in the electron propagator. The a_q-bosons appearing in $\phi_r(x,t)$ can be represented through eq. (5.73). With implied summation over

j and dropping the index $i = 1$, these are

$$\begin{aligned} a_q &= u_q\beta_q + v_q\beta^\dagger_{-q} \\ &= u_q S_j \left(\Sigma_j B_{q,j} + \Delta_j B^\dagger_{-q,j}\right) + v_q S_1^{-1} \left(\Sigma_j B^\dagger_{-q,j} + \Delta_j B_{q,j}\right) \\ &= \left(u_q S_j \Sigma_j + v_q S_j^{-1}\Delta_j\right) B_{q,j} + \left(u_q S_j \Delta_j + v_q S_j^{-1}\Sigma_j\right) B^\dagger_{-q,j} \\ &\equiv \sum_j \left(U_j B_{q,j} + V_j B^\dagger_{-q,j}\right) \end{aligned} \tag{6.77}$$

$$\begin{aligned} a^\dagger_q &= v_q\beta_{-q} + u_q\beta^\dagger_q. \\ &= \left(v_q S_j \Sigma_j + u_q S_j^{-1}\Delta_j\right) B_{-q,j} + \left(v_q S_j \Delta_j + u_q S_j^{-1}\Sigma_j\right) B^\dagger_{q,j} \\ &\equiv \sum_j \left(V_j^\dagger B_{-q,j} + U_j^\dagger B^\dagger_{q,j}\right), \end{aligned} \tag{6.78}$$

where I introduced the matrix quantities $U(q)$ and $V(q)$ by (no implicit summation)

$$U_j = u_q S_j \Sigma_j + v_q S_j^{-1}\Delta_j \qquad U_j^\dagger = u_q S_j^{-1}\Sigma_j + v_q S_j \Delta_j \tag{6.79a}$$

$$V_j = u_q S_j \Delta_j + v_q S_j^{-1}\Sigma_j \qquad V_j^\dagger = u_q S_j^{-1}\Delta_j + v_q S_j \Sigma_j. \tag{6.79b}$$

Inserting the property $u_q^2 - v_q^2 = 1$, these matrix quantities satisfy

$$\begin{aligned} U_j U_j^\dagger - V_j V_j^\dagger &= (u_q S_j \Sigma_j + v_q S_j^{-1}\Delta_j)(v_q S_j \Delta_j + u_q S_j^{-1}\Sigma_j) \\ &\quad - (u_q S_j \Delta_j + v_q S_j^{-1}\Sigma_j)(v_q S_j \Sigma_j + u_q S_j^{-1}\Delta_j) \\ &= u_q S_j \Sigma_j v_q S_j \Delta_j - u_q S_j \Delta_j v_q S_j \Sigma_j + v_q S_j^{-1}\Delta_j u_q S_j^{-1}\Sigma_j - v_q S_j^{-1}\Sigma_j u_q S_j^{-1}\Delta_j \\ &\quad + u_q^2 S_j S_j^{-1}(\Sigma_j^2 - \Delta_j^2) + v_q^2 S_j^{-1} S_j (\Delta_j^2 - \Sigma_j^2) \\ &\overset{(6.39)}{=} S_j S_j^{-1}, \end{aligned} \tag{6.80}$$

which implies the sum rule

$$\sum_j \left(U_j U_j^\dagger - V_j V_j^\dagger\right) = 1. \tag{6.81}$$

The time evolution of the B-bosons may now enter, and I compute the

commutation relations for the fermion density bosons, yielding

$$\begin{aligned}
[a_q(t), a^\dagger_{q'}(t')] &= [U_j B_{q,j}(t) + V_j B^\dagger_{-q,j}(t), V^\dagger_k B_{-q',k}(t') + U^\dagger_k B^\dagger_{q',k}(t')] \\
&= U_j V^\dagger_k \underbrace{[B_{q,j}(t), B_{-q',k}(t')]}_{=0} + U_j U^\dagger_k [B_{q,j}(t), B^\dagger_{q',k}(t')] \\
&\quad + V_j V^\dagger_k [B^\dagger_{-q,j}(t), B_{-q',k}(t')] + V_j U^\dagger_k \underbrace{[B^\dagger_{-q,j}(t), B^\dagger_{q',k}(t')]}_{=0} \\
&= U_j U^\dagger_k \mathrm{e}^{-i\lambda_{q,j}t} \mathrm{e}^{i\lambda_{q',k}t'} \delta_{qq'}\delta_{jk} - V_j V^\dagger_k \mathrm{e}^{i\lambda_{q,j}t} \mathrm{e}^{-i\lambda_{q',k}t'} \delta_{qq'}\delta_{jk} \\
&= (U_j U^\dagger_j \mathrm{e}^{-i\lambda_{q,j}(t-t')} - V_j V^\dagger_j \mathrm{e}^{i\lambda_{q,j}(t-t')})\delta_{qq'}. \qquad (6.82)
\end{aligned}$$

As in the case with no density-interactions, eq. (6.81) that the bosons still satisfy bosonic commutation relations at equal times $[a_q(t), a^\dagger_q(t)] = 1$. The fields $\phi(x,t)$ are now given by

$$\phi_r(x,t) = -i\overline{\sum_q} \mathrm{e}^{iqx} \left(U_j B_{q,j} \mathrm{e}^{-i\lambda_{q,j}t} + V_j B^\dagger_{-q,j} \mathrm{e}^{i\lambda_{q,j}t} \right) \qquad (6.83a)$$

$$\phi^\dagger_r(x,t) = i\overline{\sum_q} \mathrm{e}^{-iqx} \left(V^\dagger_j B_{-q,j} \mathrm{e}^{-i\lambda_{q,j}t} + U^\dagger_j B^\dagger_{q,j} \mathrm{e}^{i\lambda_{q,j}t} \right) \qquad (6.83b)$$

Comparing these to the case in eq. (6.49), the cases are similar with the substitutions $S_j\Sigma_j \to U_j$ and $S_j\Delta_j \to V_j$. The fields satisfy the commutation relation

$$\begin{aligned}
[\phi_r(x,t), \phi^\dagger_{r'}(x',t')] &= \overline{\sum_q} \overline{\sum_{q'}} \mathrm{e}^{iqx} \mathrm{e}^{-iq'x'} [a_q(t), a^\dagger_{q'}(t')] \\
&= \delta_{rr'} \sum_{q\neq 0} \Theta(\eta_r q) \frac{2\pi}{L|q|} \mathrm{e}^{-\xi|q|} \mathrm{e}^{iq(x-x')} \sum_{j=1,2} \left(U_j U^\dagger_j \mathrm{e}^{-i\lambda_{q,j}(t-t')} - V_j V^\dagger_j \mathrm{e}^{i\lambda_{q,j}(t-t')} \right). \qquad (6.84)
\end{aligned}$$

Computing Z

As a reminder, Z is given in eq. (6.8). The commutator $[\phi_0, \phi^\dagger_0]$ is unchanged compared to eq. (6.51) without density-interactions, but X and Y appearing

in Z will be affected. I now compute these, starting with X which is

$$\begin{aligned}
X &= i(\phi^\dagger + \phi) - i(\phi_0^\dagger + \phi_0) \\
&= \overline{\sum_q} \Big\{ \mathrm{e}^{-iqx} \left(V_j^\dagger B_{-q,j} \mathrm{e}^{-i\lambda_{q,j}t} + U_j^\dagger B_{q,j}^\dagger \mathrm{e}^{i\lambda_{q,j}t} \right) - \left(V_j^\dagger B_{-q,j} + U_j^\dagger B_{q,j}^\dagger \right) \\
&\qquad + \left(U_j B_{q,j} + V_j B_{-q,j}^\dagger \right) - \mathrm{e}^{iqx} \left(U_j B_{q,j} \mathrm{e}^{-i\lambda_{q,j}t} + V_j B_{-q,j}^\dagger \mathrm{e}^{i\lambda_{q,j}t} \right) \Big\} \\
&= \overline{\sum_q} \Big(U_j^\dagger B_{q,j}^\dagger \left(\mathrm{e}^{-iqx} \mathrm{e}^{i\lambda_{q,j}t} - 1 \right) + V_j^\dagger B_{-q,j} \left(\mathrm{e}^{-iqx} \mathrm{e}^{-i\lambda_{q,j}t} - 1 \right) \\
&\qquad + U_j B_{q,j} \left(1 - \mathrm{e}^{iqx} \mathrm{e}^{-i\lambda_{q,j}t} \right) + V_j B_{-q,j}^\dagger \left(1 - \mathrm{e}^{iqx} \mathrm{e}^{i\lambda_{q,j}t} \right) \Big) ,
\end{aligned} \tag{6.85}$$

whose form is equivalent with that of eq. (6.52). I can therefore at once write down the expectation values $\langle X^2 \rangle$ at once, using the form in eq. (6.53). The result is

$$\begin{aligned}
\langle X^2 \rangle &= \overline{\sum_q} \overline{\sum_{q'}} \Big\{ \Big[U_j^\dagger \left(\mathrm{e}^{-iqx} \mathrm{e}^{i\lambda_{q,j}t} - 1 \right) U_j \left(1 - \mathrm{e}^{iqx} \mathrm{e}^{-i\lambda_{q,j}t} \right) \\
&\quad + V_j^\dagger \left(\mathrm{e}^{-iqx} \mathrm{e}^{-i\lambda_{q,j}t} - 1 \right) V_j \left(1 - \mathrm{e}^{iqx} \mathrm{e}^{i\lambda_{q,j}t} \right) \Big] \left(1 + 2 n_B(\lambda_{q,j}) \right) \Big\} \delta_{qq'} \\
&\overset{T=0}{=} \sum_q \Theta(\eta_r q) \frac{2\pi}{L|q|} \mathrm{e}^{-\xi|q|} \Big\{ U_j U_j^\dagger \left(\mathrm{e}^{-iqx} \mathrm{e}^{i\lambda_{q,j}t} + \mathrm{e}^{iqx} \mathrm{e}^{-i\lambda_{q,j}t} - 2 \right) \\
&\qquad + V_j^\dagger V_j \left(\mathrm{e}^{iqx} \mathrm{e}^{i\lambda_{q,j}t} + \mathrm{e}^{-iqx} \mathrm{e}^{-i\lambda_{q,j}t} - 2 \right) \Big\} .
\end{aligned} \tag{6.86}$$

Y is given in eq. (6.4b) as

$$\begin{aligned}
Y &= [\phi, \phi_0^\dagger] - [\phi_0, \phi^\dagger] \\
&= \sum_{q \neq 0} \Theta(\eta_r q) \frac{2\pi}{L|q|} \mathrm{e}^{-\xi|q|} \Big\{ \mathrm{e}^{iqx} \left(U_j U_j^\dagger \mathrm{e}^{-i\lambda_{q,j}t} - V_j V_j^\dagger \mathrm{e}^{i\lambda_{q,j}t} \right) \\
&\qquad - \mathrm{e}^{-iqx} \left(U_j U_j^\dagger \mathrm{e}^{i\lambda_{q,j}t} - V_j V_j^\dagger \mathrm{e}^{-i\lambda_{q,j}t} \right) \Big\}
\end{aligned} \tag{6.87}$$

I can now compute Z as

$$\begin{aligned}
Z &= \frac{1}{2}\langle X^2\rangle + \frac{1}{2}Y + [\phi_0, \phi_0^\dagger] \\
&= \frac{1}{2}\sum_q \Theta(\eta_r q)\frac{2\pi}{L|q|}\mathrm{e}^{-\xi|q|} \\
&\quad \times \Big\{U_j U_j^\dagger \left(\mathrm{e}^{-iqx}\mathrm{e}^{i\lambda_{q,j}t} + \mathrm{e}^{iqx}\mathrm{e}^{-i\lambda_{q,j}t} - 2 + \mathrm{e}^{iqx}\mathrm{e}^{-i\lambda_{q,j}t} - \mathrm{e}^{-iqx}\mathrm{e}^{i\lambda_{q,j}t}\right) \\
&\quad + V_j V_j^\dagger \left(\mathrm{e}^{iqx}\mathrm{e}^{i\lambda_{q,j}t} + \mathrm{e}^{-iqx}\mathrm{e}^{-i\lambda_{q,j}t} - 2 - \mathrm{e}^{iqx}\mathrm{e}^{i\lambda_{q,j}t} + \mathrm{e}^{-iqx}\mathrm{e}^{-i\lambda_{q,j}t}\right) + 2\Big\} \\
&= \sum_q \Theta(\eta_r q)\frac{2\pi}{L|q|}\mathrm{e}^{-\xi|q|}\left(U_j U_j^\dagger(\mathrm{e}^{iqx}\mathrm{e}^{-i\lambda_{q,j}t} - 1) + V_j V_j^\dagger\left(\mathrm{e}^{-iqx}\mathrm{e}^{-i\lambda_{q,j}t} - 1\right) + 1\right) \\
&= \sum_q \sum_{j=1,2} \Theta(\eta_r q)\frac{2\pi}{L|q|}\mathrm{e}^{-\xi|q|}\left\{\left(U_j U_j^\dagger \mathrm{e}^{iqx} + V_j V_j^\dagger \mathrm{e}^{-iqx}\right)\mathrm{e}^{-i\lambda_{q,j}t} - 2V_j V_j^\dagger\right\},
\end{aligned} \tag{6.88}$$

where the j-summation is reinserted for explicitness. The exact Green's function is given in terms of Z in eq. (6.7). This integral can in most cases not be computed analytically, however some approximations can be made to bring $G_r^>$ to a form for which physical interpretations are easier to extract.

Explicit Form of Coefficients

The eigenvalues of the combined problem with density-density interactions are equivalent to those in eq. (6.56), but with an altered coupling constant given by the transformation

$$\tilde{G}_q \to \mathrm{e}^{\theta_q}\tilde{G}_q, \tag{6.89}$$

where θ_q is determined by the Bogoliubov transformation that decouples the density-density interaction in eq. (5.72). Hence, the S-matrices has the same form as in eq. (6.57), and by inserting these in eq. (6.79), I find

$$\begin{aligned}
V_j V_j^\dagger &= (u_q S_j \Delta_j + v_q S_j^{-1}\Sigma_j)(u_q S_j^{-1}\Delta_j + v_q S_j \Sigma_j) \\
&= u_q^2 S_j S_j^{-1}\Delta_j^2 + v_q^2 S_j S_j^{-1}\Sigma_j^2 + u_q v_q \Delta_j \Sigma_j((S_j)^2 + (S_j^{-1})^2) \\
&\equiv c_{j,-} + v_q^2(c_{j,+} + c_{j,-}) + u_q v_q d_j.
\end{aligned} \tag{6.90}$$

Here, I defined the coefficients

$$d_j \equiv \Delta_j \Sigma_j((S_j)^2 + (S_j^{-1})^2). \tag{6.91}$$

Since these coefficients do not include terms on the form $S_j S_j^{-1}$, the normalization of S require extra care. By ensuring that determinants of the matrices

in eq. (6.57) are equal, the coefficients are found to be

$$d_j = \frac{\left(\varepsilon_q^2 - \lambda_{q,j}^2\right)}{4\lambda_{q,j}\varepsilon_q}\left(\frac{(\lambda_{q,j}^2 - \omega_q^2)^2}{\tilde{G}_q\sqrt{Q_q}} + \frac{\tilde{G}_q}{\sqrt{Q_q}}\right), \tag{6.92}$$

where I have inserted the definitions of Σ_j and Δ_j in eq. (6.37).

$U_jU_j^\dagger$ is similarly found to be

$$U_jU_j^\dagger = c_{j,+} + v_q^2(c_{j,+} + c_{j,-}) + u_qv_qd_j. \tag{6.93}$$

The first two terms of $VV^\dagger$ and $UU^\dagger$ involves the coefficients $c_{j,\pm}$ from eq. (6.61). Note that in the limit of zero coupling, i.e. $\beta \to 0$, and with the assumed form of the coupling $4\tilde{G}_q^2 = \beta|q|^4$, the coefficients d_j in eq. (6.92) goes as

$$d_1 = -\frac{\sqrt{\beta}}{8v_F^2} + \mathcal{O}\left(\beta^{\frac{3}{2}}\right) \tag{6.94a}$$

$$d_2 = \frac{\sqrt{\beta}}{8v_sv_F} + \mathcal{O}\left(\beta^{\frac{3}{2}}\right). \tag{6.94b}$$

Closed Form Approximation

In the case of non-interacting fermions in section 6.2.1, I considered a coupling $g_q = \alpha q$ to the acoustic phonon branch. I will approximate $\mathrm{e}^{\theta_q} \simeq \mathrm{e}^{\theta_0}$ and absorb this into the interaction strength. Repeating the assumption of the electron phonon coupling in the present case, the coefficients d_j in eq. (6.92) become q-independent as well as $c_{j,\pm}$. The fermion interaction introduces new quantities u_q and v_q satisfying $u_q^2 - v_q^2 = 1$. These quantities are dependent on the specific interaction. The most common method of continuing analytic investigations [32–34, 82] is by replacing the potential with an exponential cutoff resulting in

$$\sinh^2(\theta_q) = v_q^2 = \nu\mathrm{e}^{-\Lambda|q|}. \tag{6.95}$$

Unlike the normal geology models, phonon interactions introduces an anomalous term with the product u_qv_q of both Bogoliubov weights. Using the approximation in eq. (6.95), this term can for small coupling strengths ν be written

$$\begin{aligned} u_qv_q &= \sqrt{(1+\nu\mathrm{e}^{-\Lambda|q|})\nu\mathrm{e}^{-\Lambda|q|}} \\ &= \nu^{\frac{1}{2}}\mathrm{e}^{-\frac{\Lambda|q|}{2}}\left(1 + \frac{\nu}{2}\mathrm{e}^{-\Lambda|q|} + \mathcal{O}\left(\nu^2\right)\right) \\ &\simeq \nu^{\frac{1}{2}}\mathrm{e}^{-\frac{\Lambda|q|}{2}} + \frac{\nu^{\frac{3}{2}}}{2}\mathrm{e}^{-\frac{3\Lambda|q|}{2}}. \end{aligned} \tag{6.96}$$

The resulting greater Green's function is by eq. (6.7)

$$G_r^>(x,t)\mathrm{e}^{i\mu t} = \frac{\mathrm{e}^{ik_F\eta_r x}}{L}\mathrm{e}^{Z_1+Z_2}, \tag{6.97}$$

with $Z = Z_1 + Z_2$ given in eq. (6.88). Inserting eq. (6.90) in the expression for Z and the above approximations for the density-density interactions, I find in the large L-limit

$$\begin{aligned}\mathrm{e}^Z = \prod_{j=1,2}\Bigg\{ &\left(\frac{1}{\frac{2\pi}{L}(\xi - i\eta_r x + iu_j t)}\right)^{c_{j,+}} \left(\frac{\left(\frac{2\pi}{L}\xi\right)^2}{\frac{2\pi}{L}(\xi + i\eta_r x + iu_j t)}\right)^{c_{j,-}} \\ &\times \left(\frac{\Lambda^2}{(\Lambda - i\eta_r x + iu_j t)(\Lambda + i\eta_r x + iu_j t)}\right)^{\nu(c_{j,+}+c_{j,-})} \\ &\times \left(\frac{\frac{1}{4}\Lambda^2}{(\frac{1}{2}\Lambda - i\eta_r x + iu_j t)(\frac{1}{2}\Lambda + i\eta_r x + iu_j t)}\right)^{\nu^{\frac{1}{2}}d_j} \\ &\times \left(\frac{\frac{9}{4}\Lambda^2}{(\frac{3}{2}\Lambda - i\eta_r x + iu_j t)(\frac{3}{2}\Lambda + i\eta_r x + iu_j t)}\right)^{\frac{1}{2}\nu^{\frac{3}{2}}d_j}\end{aligned} \tag{6.98}$$

with the approximation $\xi + \Lambda \simeq \Lambda$. This form of the Green's function is hardly any more convenient to work with than the exact expression using Z in eq. (6.88). Moreover, this approximation puts a strong restriction on the strength of the scattering potential, whose assumed form is already dubious. This restriction can be avoided[1] by including more terms of the Taylor expansion in eq. (6.96), which will appear as cloud factors in eq. (6.98) with decreasing singularities. The analytic expression for Z given in eq. (6.88) still hold, where I do not assume the specific interaction nor the approximate form of the electron-phonon coupling, which is known to be important for the shape of spectral peaks [34].

By setting the density-interaction to zero, i.e. $\nu = 0$, I recover the same expression for $G_r^>$ as in eq. (6.71). Correspondingly, I can turn off the electron-phonon interaction by letting $\beta \to 0$. The coefficients d_j follow eq. (6.94) and is 0 in this limit. The remaining constants $c_{j\pm}$ defined in eq. (6.61) is $c_{j+} = \delta_{j1}$ and $c_{j-} = 0$. Lastly, u_1 is the unperturbed Fermi velocity v_F. By inserting these in eq. (6.98), the resulting Green's function in the limit of no electron-phonon coupling is

$$iG_r^>(x,t)\mathrm{e}^{i\mu t} = \frac{i\eta_r}{2\pi}\mathrm{e}^{ik_F\eta_r x}\frac{1}{x - \eta_r v_F t + i\eta_r\xi}\left(\frac{\Lambda^2}{x^2 - (v_F t - i\Lambda)^2}\right)^\nu. \tag{6.99}$$

[1] I still assume ν to be less than one, such that the Taylor series converges.

This is the expected result, as it is the closed form approximation of eq. (5.86) under the same assumptions [32].

6.2.3 Spinful Fermions

As shown in section 5.3.1, the dynamics of the spinful system can be split into independent degrees of freedom for separate quantum numbers. In the problem of electron-phonon interactions, this is particularly useful since the interaction term

$$\sum_{q,\sigma} g_q \rho_{-q,\sigma} u_q \tag{6.100}$$

is spin independent. The charge and spin-parts of the density waves $\rho_r(q)$ and $\sigma_r(q)$ are defined in eq. (5.58). The corresponding boson operators $a_{q,c}$ and $a_{q,s}$ are defined in eq. (5.59), describing charge (c) and spin (s) density wave fluctuations. The bosons $a_{q,\sigma}$ is related to these by eq. (5.60). The total density wave excitation appearing in the interaction term can be represented in terms of $\rho(q), \sigma(q)$ through

$$\sum_r \rho_{r,\sigma}(q) = \frac{1}{2} \sum_r \left(\rho_r(q) + \sigma \sigma_r(q) \right). \tag{6.101}$$

Summing over spins thus cancels out the spin-density wave $\sigma_r(q)$ if there is no other spin-dependency, and the density wave interacting with phonons is

$$\rho_{-q} = \left(\frac{\pi}{L|q|} \right)^{\frac{1}{2}} \left(a^\dagger_{q,c} + a_{-q,c} \right). \tag{6.102}$$

The interaction term of the Hamiltonian is therefore

$$H_{\text{int}} = \sum_q g_q \left(\frac{\pi}{L|q|} \right)^{\frac{1}{2}} (a^\dagger_{q,c} + a_{-q,c}) u_q, \tag{6.103}$$

and the total Hamiltonian for the dynamics of the system is

$$H = \sum_q \varepsilon_q (a^\dagger_{q,c} a_{q,c} + a^\dagger_{q,s} a_{q,s}) + H_{\text{ph}} + H_{\text{int}}, \tag{6.104}$$

where H_{ph} is given in eq. (6.19) and $\varepsilon_q = v_F|q|$. That one of the normal modes of this model is a spin wave oscillating with the unperturbed dispersion was pointed out by Engelsberg and Varga [30] analyzing the eigenmodes of the system. This is already evident from the Hamiltonian in eq. (6.104),which is already diagonal in the spin-operators. The diagonalization procedure of

the charge terms is identical to the spinless case in section 6.2.1, with the replacement

$$\tilde{G}_q \to \sqrt{2}\tilde{G}_q. \tag{6.105}$$

By inserting the representation of charge-density bosons found in eqs. (6.36) and (6.38) into the spin dependent operators in eq. (5.60), the resulting time evolved operators are

$$a_{q,\sigma}(t) = \frac{1}{\sqrt{2}}\left(S_j\left(\Sigma_j B_{q,j}(t) + \Delta_j B^\dagger_{-q,j}(t)\right) + \sigma a_{q,s}(t)\right) \tag{6.106a}$$

$$a^\dagger_{q,\sigma}(t) = \frac{1}{\sqrt{2}}\left(S_j^{-1}\left(\Sigma_j B^\dagger_{q,j}(t) + \Delta_j B_{-q,j}(t)\right) + \sigma a^\dagger_{q,s}(t)\right), \tag{6.106b}$$

and the commutation relations are

$$\begin{aligned}[a_{q,\sigma}(t), a^\dagger_{q',\sigma'}(t')] &= \frac{1}{2}\Big(S_j S_k^{-1}\Big(\Sigma_j\Sigma_k[B_{q,j}(t), B^\dagger_{q',k}(t')] \\ &\quad + \Delta_j\Delta_k[B^\dagger_{-q,j}, B_{-q',k}(t')]\Big) + \sigma\sigma'[a_{q,s}(t), a^\dagger_{q',s}(t')]\Big) \\ &= \frac{1}{2}\left(S_j S_j^{-1}\left(\Sigma_j^2 \mathrm{e}^{-i\lambda_{q,j}(t-t')} - \Delta_j^2 \mathrm{e}^{i\lambda_{q,j}(t-t')}\right) + \sigma\sigma' \mathrm{e}^{-i\varepsilon_q(t-t')}\right)\delta_{qq'}. \end{aligned} \tag{6.107}$$

At $t = t'$, eq. (6.107) reduces to the normal commutator

$$[a_{q,\sigma}(t), a^\dagger_{q',\sigma'}(t)] = \delta_{\sigma\sigma'}\delta_{qq'}. \tag{6.108}$$

The spin-dependent fields $\phi_{r,\sigma}(x,t)$ are now given by

$$\begin{aligned}\phi_{r,\sigma}(x,t) = \frac{-i}{\sqrt{2}}\overline{\sum_q} \mathrm{e}^{iqx}\Big\{S_j\left(\Sigma_j B_{q,j}\mathrm{e}^{-i\lambda_{q,j}t} + \Delta_j B^\dagger_{-q,j}\mathrm{e}^{i\lambda_{q,j}t}\right) \\ + \sigma a_{q,s}\mathrm{e}^{-i\varepsilon_q t}\Big\}\end{aligned} \tag{6.109a}$$

$$\begin{aligned}\phi^\dagger_{r,\sigma}(x,t) = \frac{i}{\sqrt{2}}\overline{\sum_q} \mathrm{e}^{-iqx}\Big\{S_j^{-1}\left(\Sigma_j B^\dagger_{q,j}\mathrm{e}^{i\lambda_{q,j}t} + \Delta_j B_{-q,j}\mathrm{e}^{-i\lambda_{q,j}t}\right) \\ + \sigma a^\dagger_{q,s}\mathrm{e}^{i\varepsilon_q t}\Big\},\end{aligned} \tag{6.109b}$$

which includes the quantum number σ. However, this quantum number only serves a purpose in the calculations of correlation functions involving fermion fields with opposite spin. For the computation of Green's functions, the spins

are of the two fields are taken to be equal. The commutator of the fields is

$$\begin{aligned}
[\phi_{r,\sigma}(x,t),\phi^\dagger_{r',\sigma'}(x',t')] &= \overline{\sum_q}\overline{\sum_{q'}} \mathrm{e}^{i(qx-q'x')}[a_{q,\sigma}(t),a_{q',\sigma'}(t')] \\
&= \delta_{rr'}\sum_{q\neq 0}\Theta(\eta_r q)\frac{\pi}{L|q|}\mathrm{e}^{-\xi|q|}\mathrm{e}^{iq(x-x')} \\
&\quad\times\left(S_jS_j^{-1}\left(\Sigma_j^2\mathrm{e}^{-i\lambda_{q,j}(t-t')}-\Delta_j^2\mathrm{e}^{i\lambda_{q,j}(t-t')}\right)+\sigma\sigma'\mathrm{e}^{-i\varepsilon_q(t-t')}\right). \quad (6.110)
\end{aligned}$$

For helical states, the delta-function $\delta_{rr'}$ for left / right branches is equivalent to $\delta_{\sigma\sigma'}$, as right-moving electrons carry spin opposite to that of left-movers.

Computing Z

With the explicit form of ϕ for the spinful case, I can proceed with the calculations of the greater Green's function which is on the form $G_r^> \sim \exp(Z)$, where Z is defined in eq. (6.8) and its constituent operators X, Y in eq. (6.4). For equal coordinates, the commutator of the ϕ-fields remain unchanged compared to eq. (6.51) by the inclusion of spin,

$$[\phi_0,\phi_0^\dagger] = \sum_{q\neq 0}\Theta(\eta_r q)\frac{2\pi}{L|q|}\mathrm{e}^{-\xi|q|}, \quad (6.111)$$

but both X and Y gain additional terms corresponding to the spin-degrees. Y is

$$\begin{aligned}
Y &\equiv [\phi,\phi_0^\dagger]-[\phi_0,\phi^\dagger] \\
&= \delta_{rr'}\sum_q\Theta(\eta_r q)\frac{\pi}{L|q|}\mathrm{e}^{-\xi|q|}\left\{\mathrm{e}^{iqx}\left(S_jS_j^{-1}\left(\Sigma_j^2\mathrm{e}^{-i\lambda_{q,j}t}-\Delta_j^2\mathrm{e}^{i\lambda_{q,j}t}\right)+\mathrm{e}^{-i\varepsilon_q t}\right)\right. \\
&\quad\left.-\mathrm{e}^{-iqx}\left(S_jS_j^{-1}\left(\Sigma_j^2\mathrm{e}^{i\lambda_{q,j}t}-\Delta_j^2\mathrm{e}^{-i\lambda_{q,j}t}\right)+\mathrm{e}^{i\varepsilon_q t}\right)\right\}, \quad (6.112)
\end{aligned}$$

and X is computed as

$$\begin{aligned}
X &\equiv i(\phi^\dagger+\phi)-i(\phi_0^\dagger+\phi_0) \\
&= \overline{\sum_q}\left(\mathrm{e}^{-iqx}a^\dagger_{q,\sigma}(t)-a^\dagger_{q,\sigma}(0)+(a_{q,\sigma}(0)-\mathrm{e}^{iqx}a_{q,\sigma}(t)\right) \\
&\overset{(6.106)}{=} \frac{1}{\sqrt{2}}\overline{\sum_q}\left\{\mathrm{e}^{-iqx}\left(S_j^{-1}\left(\Sigma_jB^\dagger_{q,j}\mathrm{e}^{i\lambda_{q,j}t}+\Delta_jB_{-q,j}\mathrm{e}^{-i\lambda_{q,j}t}\right)+\sigma a^\dagger_{q,s}\mathrm{e}^{i\varepsilon_q t}\right)\right. \\
&\quad-\left(S_j^{-1}\left(\Sigma_jB^\dagger_{q,j}+\Delta_jB_{-q,j}\right)+\sigma a^\dagger_{q,s}\right)+\left(S_j\left(\Sigma_jB_{q,j}+\Delta_jB^\dagger_{-q,j}\right)+\sigma a_{q,s}\right) \\
&\quad\left.-\mathrm{e}^{iqx}\left(S_j\left(\Sigma_jB_{q,j}\mathrm{e}^{-i\lambda_{q,j}t}+\Delta_jB^\dagger_{-q,j}\mathrm{e}^{i\lambda_{q,j}t}\right)+\sigma a_{q,s}\mathrm{e}^{-i\varepsilon_q t}\right)\right. . \quad (6.113)
\end{aligned}$$

The expectation value $\langle X^2 \rangle$ can now be computed using the commutation properties of the bosonic operators in X. Since most operators commute, only terms with one creation- and one destruction operator will survive when taking the expectation value, and I obtain

$$\begin{aligned}\langle X^2 \rangle = \frac{1}{2}\overline{\sum_q}\overline{\sum_{q'}}\Big\{ &\langle B^\dagger_{q,j} B_{q',k}\rangle S_j^{-1}\Sigma_j \left(\mathrm{e}^{-iqx}\mathrm{e}^{i\lambda_{q,j}t} - 1\right) S_k \Sigma_k \left(1 - \mathrm{e}^{iq'x}\mathrm{e}^{-i\lambda_{q',k}t}\right) \\ &+ \langle B_{-q,j} B^\dagger_{-q',k}\rangle S_j^{-1}\Delta_j \left(\mathrm{e}^{-iqx}\mathrm{e}^{-i\lambda_{q,j}t} - 1\right) S_k \Delta_k \left(1 - \mathrm{e}^{iq'x}\mathrm{e}^{i\lambda_{q',k}t}\right) \\ &+ \langle B^\dagger_{-q,j} B_{-q',k}\rangle S_j \Delta_j \left(1 - \mathrm{e}^{iqx}\mathrm{e}^{i\lambda_{q,j}t}\right) S_k^{-1}\Delta_k \left(\mathrm{e}^{-iqx}\mathrm{e}^{-i\lambda_{q',k}t} - 1\right) \\ &+ \langle B_{q,j} B^\dagger_{q',k}\rangle S_j \Sigma_j \left(1 - \mathrm{e}^{iqx}\mathrm{e}^{-i\lambda_{q,j}t}\right) S_k^{-1}\Sigma_k \left(\mathrm{e}^{-iq'x}\mathrm{e}^{i\lambda_{q',k}t} - 1\right) \\ &+ \langle a^\dagger_{q,s} a_{q',s}\rangle \left(\mathrm{e}^{-iqx}\mathrm{e}^{i\varepsilon_q t} - 1\right)\left(1 - \mathrm{e}^{iq'x}\mathrm{e}^{-i\varepsilon_{q'}t}\right) \\ &+ \langle a_{q,s} a^\dagger_{q',s}\rangle \left(1 - \mathrm{e}^{iqx}\mathrm{e}^{-i\varepsilon_q t}\right)\left(\mathrm{e}^{-iq'x}\mathrm{e}^{i\varepsilon_{q'}t} - 1\right). \end{aligned} \tag{6.114}$$

At zero temperature, the Bose distribution is zero for all $q \neq 0$, such that

$$\begin{aligned}\langle X^2 \rangle \overset{T=0}{=} \frac{1}{2}\sum_q \Theta(\eta_r q)\frac{2\pi}{L|q|}\mathrm{e}^{-\xi|q|}\Big\{ S_j S_j^{-1}\Big[\Sigma_j^2(\mathrm{e}^{iqx}\mathrm{e}^{-i\lambda_{q,j}t} + \mathrm{e}^{-iqx}\mathrm{e}^{i\lambda_{q,j}t} - 2) \\ + \Delta_j^2(\mathrm{e}^{iqx}\mathrm{e}^{i\lambda_{q,j}t} + \mathrm{e}^{-iqx}\mathrm{e}^{-i\lambda_{q,j}t} - 2)\Big] + (\mathrm{e}^{iqx}\mathrm{e}^{-i\varepsilon_q t} + \mathrm{e}^{-iqx}\mathrm{e}^{i\varepsilon_q t} - 2)\Big\}. \end{aligned} \tag{6.115}$$

The function Z can now be evaluated as

$$\begin{aligned} Z &= \frac{1}{2}\langle X^2\rangle + \frac{1}{2}Y + [\phi_0, \phi_0^\dagger] \\ &= \frac{1}{4}\sum_{q\neq 0}\Theta(\eta_r q)\frac{2\pi}{L|q|}\mathrm{e}^{-\xi|q|}\Big\{c_{j,+}\left(2\mathrm{e}^{iqx}\mathrm{e}^{-i\lambda_{q,j}t} - 2\right) + c_{j,-}\left(2\mathrm{e}^{-iqx}\mathrm{e}^{-i\lambda_{q,j}t} - 2\right) \\ &\qquad + (2\mathrm{e}^{iqx}\mathrm{e}^{-i\varepsilon_q t} - 2) + 4.\Big\} \\ &\equiv Z_s + Z_c, \end{aligned} \tag{6.116}$$

with

$$Z_s = \frac{1}{2}\sum_{q\neq 0}\Theta(\eta_r q)\frac{2\pi}{L|q|}\mathrm{e}^{-\xi|q|}\mathrm{e}^{iqx}\mathrm{e}^{-iv_F|q|t} \tag{6.117}$$

and

$$Z_c = \frac{1}{2}\sum_{q,j}\Theta(\eta_r q)\frac{2\pi}{L|q|}\mathrm{e}^{-\xi|q|}\left\{\left(c_{j,+}\mathrm{e}^{iqx} + c_{j,-}\mathrm{e}^{-iqx}\right)\mathrm{e}^{-i\lambda_{q,j}t} - 2c_{j,-}\right\}, \tag{6.118}$$

where I use the same notation as in eq. (6.61) for the coefficients $S_j S_j^{-1} \Sigma_j^2$ and $S_j S_j^{-1} \Delta_j^2$ appearing in eq. (6.115). I have for clarity reinstated the summation over j. Notice the similarity of Z_c with Z in the spinless case given in eq. (6.55). The only difference is a factor $1/2$ corresponding to a reduction of eventual singularities appearing in closed form approximations of the Green's function. Z_s represents a non-interacting system with a square root singularity at $\eta_r x = v_F t$. Denoting the interacting spinless Green's function by $G_r^>(x,t;g)$, the spinful Green's function is therefore

$$iG_{r\sigma}^>(x,t)\mathrm{e}^{i\mu t} = \frac{\mathrm{e}^{ik_F\eta_r x}}{L}\mathrm{e}^{Z_s+Z_c} = \left(iG_r^>(x,t,0)iG_r^>(x,t,\sqrt{2}g)\right)^{\frac{1}{2}}, \quad (6.119)$$

also pointed out by Meden et al. [31] and announced in eq. (6.9).

Closed Form Approximation

As for the spinless case, I approximate the electron-phonon coupling as $g_q \simeq \alpha q$. The charge-part of the Hamiltonian reduces to eq. (6.71) with all exponents reduced by a factor 2. Inserting eq. (6.119), I obtain

$$\begin{aligned} iG_{r\sigma}^>(x,t)\mathrm{e}^{i\mu t} = {} & \frac{i\eta_r \mathrm{e}^{i\eta_r k_F x}}{2\pi}\left(\frac{1}{\eta_r x - v_F t + i\xi}\right)^{\frac{1}{2}}\left(\frac{1}{\eta_r x - u_1 t + i\xi}\right)^{c_{1,+}/2} \\ & \times \left(\frac{1}{\eta_r x - u_2 t + i\xi}\right)^{c_{2,+}/2}\left(\frac{\xi^2}{\eta_r x + u_1 t - i\xi}\right)^{c_{1,-}/2}\left(\frac{\xi^2}{\eta_r x + u_2 t - i\xi}\right)^{c_{2,-}/2}. \end{aligned} \quad (6.120)$$

This propagator involves square root correlations in the spin-channel, and can not be explained as a Fermi liquid quasiparticle. Moreover, since $v_F \neq u_j$ for $\alpha \neq 0$, the Green's function shows that the system exhibit spin-charge separation caused by phonon interactions alone.

6.2.4 Conclusions, Single Branch Correction

I have in this section computed the real space single particle greater Green's function for multiple interacting systems, and found explicit formulas for the function $Z(x,t)$ appearing as $iG^> \sim \exp(Z)$. Several closed form expressions has been found for an assumed linear coupling $g_q = \alpha q$.

For the spinless case with density-density-interactions, additional coefficients d_j is introduced. These scale as $d_j \sim \alpha$ for small couplings. The closed form approximation in eq. (6.98) is dubious because of a suppressed Taylor expansion and restriction on the scattering potential. I check that the zero

coupling limit of this representation reproduces earlier results. With the addition of electron density interactions, I generalize the results of Meden et al. [31] by the integral representation in eq. (6.88).

For a general q-dependent interaction potential that cannot be approximated by $\sinh^2(\theta_q) \sim \nu e^{-\Lambda|q|}$, obtaining a closed form expression for the Green's function is difficult. Obtaining analytic spectral properties of the system requires a double Fourier transform of the Green's function. At one of the edges of a QSH insulator, the right-movers carry spin up, and left-movers spin down. The correlation functions for both is known through the parameter $\eta_r = \eta_{r\sigma}$ which is $\eta_{R\uparrow} = -\eta_{L\downarrow} = 1$. This describes helicity as a single quantum number, which is modeled as a spinless Luttinger liquid [57, 58].

6.3 Multibranch Nanoribbon Phonons

In this section, I extend the theory to consider the interaction with several phonon branches. The procedure follows the theory described in section 6.1.1, but the explicit diagonalization and integration is performed numerically. I will denote the number of independent phonon branches with n_ν, for which each phonon branch has dispersion $\omega_{q,\nu}$ and couples to density waves with the coupling strength g_q^ν. The effective coupling element $\tilde{G}_q$ from eq. (6.47) is plotted in fig. 6.2 over half the Brillouin zone for the five lowest energetically lying energy eigenstates. For small q, the effective coupling behaves as $|\tilde{G}_q| \sim q^2$, demonstrating that the approximations made in the single phonon branch case is qualitatively correct. In fig. 6.3, the phonon spectrum is plotted with the effective coupling constant marked. For the acoustic branches, the effective coupling constant correlates with the localization shown in fig. 4.10. This is not the case for the localized optical branches, but these are more important for sufficiently small q.

Since the diagonalization procedure follows the same lines as for a single phonon branch, the Green's $G_r^>$ function may immediately be written on the same form as in eq. (6.7), where Z depends on the specific system. Unless otherwise stated, I will set the Fermi velocity to $v_F = 4\text{eV}\frac{a}{\hbar}$ as in eq. (4.56). The resulting Green's functions are computed for small N_y. I will from here only consider right-moving electrons, i.e. $r = R$ and $\eta_R = 1$. If spin degrees are accounted for, a spin-up projection is assumed. The Fermi momentum is set to $k_F = \pi/6a$, and the effective bandwidth is in all calculations taken to be $\xi = 1/k_F$. The system length L is determined by the desired discretization resolution. In these calculations, this is set to $L = 1500a$.

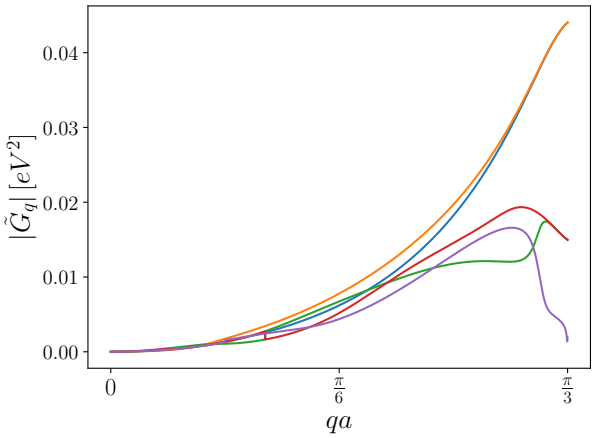

Figure 6.2: The effective coupling parameter $\tilde{G}_q^\nu$ for the five energetically lowest lying phonon modes ν. The width of the system is $N_y = 31$. The coupling for the remaining modes are not qualitatively different, and the acoustic modes marked in blue and orange are the modes with strongest coupling at the Brillouin zone boundary.

6.3.1 Spinless Fermions Without Density-Interactions

In the single branch case, the combined coefficients $S_j S_j^{-1}\Sigma_j$ and $S_j S_j^{-1}\Sigma_j$ was introduced for $j = 1, 2$. For the multi-branch case on an armchair edge graphene nanoribbon with n_ν independent phonon modes, the index j takes the values

$$j = 1, \ldots, n_\nu + 1 = 1, \ldots, 4N_y + 1, \tag{6.121}$$

where N_y is the number of carbon atoms of the nanoribbon along its width, These coefficients are shown for a small system size and small q in fig. 6.4. They satisfy the same sum rule as in eq. (6.62), whose generalization is to the multibranch case is

$$\sum_{j=1}^{4N_y+1} S_j S_j^{-1}(\Sigma_j^2 - \Delta_j^2) = 1, \tag{6.122}$$

which is numerically fulfilled with high precision for all values of q. I recapitulate the coefficients that were introduced in section 6.1. The quantities $S_j = S_{j1}$ are components of the first column in the matrix S that diagonalize the boson Hamiltonian. Written in terms of generalized coordinates and conjugate momenta, the diagonalization is a similarity transform $M = SDS^{-1}$.

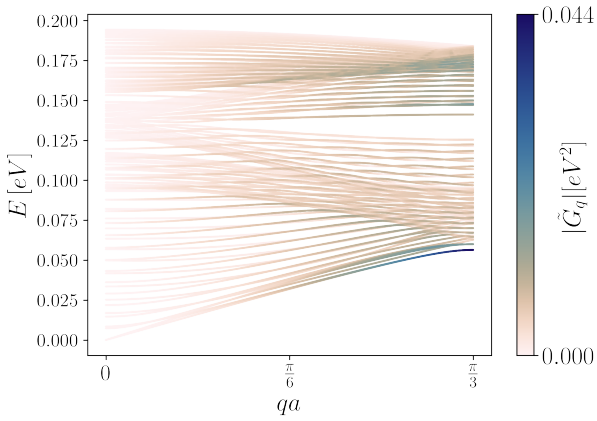

Figure 6.3: Phonon spectrum and effective coupling constant $\tilde{G}_q$ for a system of width $N_y = 31$. For all phonon modes, the coupling goes to zero as $q \to 0$.

Thus, S_j picks out the projection of normal modes onto the fermionic density bosons which I have conveniently put on index 1 in the chosen basis. The coefficients Σ_j and Δ_j are defined in eq. (6.37) and relates the energy of the non-interacting excitations to the ones in the interacting system. These satisfy the relation $\Sigma_j^2 - \Delta_j^2 = 1\,\forall j$ and can hence be associated with hyperbolic functions which is expected in an exactly solvable interacting boson system. This relation also makes the sum rule in eq. (6.122) evident.

For the spinless case without density-density interactions, the form of Z follows eq. (6.55), which in the multi-branch case is given by

$$Z = \sum_{q>0} \sum_{j=1}^{4N_y+1} \frac{2\pi}{Lq} \mathrm{e}^{-\xi q} S_j S_j^{-1} \left\{ \Sigma_j^2 \mathrm{e}^{iqx} \mathrm{e}^{-i\lambda_{q,j} t} + \Delta_j^2 \mathrm{e}^{-iqx} \mathrm{e}^{-i\lambda_{q,j} t} - 2\Delta_j^2 \right\}. \tag{6.123}$$

The hybridized energy spectrum $\lambda_{q,j}$ for a system of width $N_y = 31$ is show in fig. 6.5, where the projection onto density-bosons is shown. The fingerprints of density-bosons are small if the effective coupling is smaller than the energy gap between phonon modes. For $v_F|q| > \omega_\Gamma \simeq 0.2\text{eV}$, the fermions are close to unaltered by the phonons. This is also evident from the form of the coefficients shown in fig. 6.4, which is completely dominated by a single value close to 1 for $qa > 0.05$. As noted, the coupling with the highest energy level optical branches is strong, and the hybridization almost erase the fingerprints of density-oscillations.

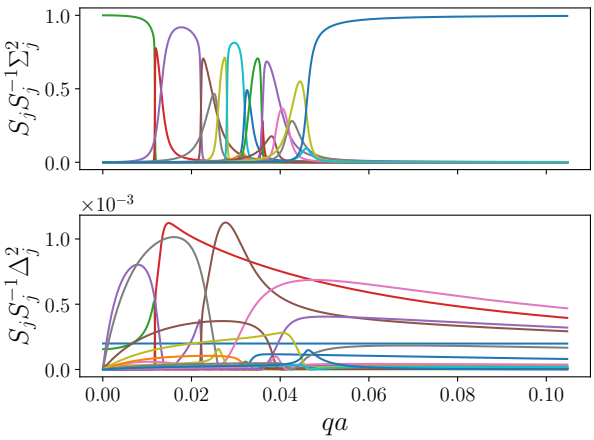

Figure 6.4: The q-dependent factors appearing in Z for a system with width $N_y = 5$ corresponding to $j = 1, \ldots, 21$. Notice that for larger q, only one coefficient dominates in the upper plot. The coefficients in the bottom panel are three orders of magnitude smaller than those in the upper panel.

The relative correction to the real space Green's function is shown in fig. 6.6 for a small system $N_y = 6$, and the effect of phonon interactions to the otherwise non-interacting system is apparent. The singularity in the vicinity of $x = v_F t$ is reduced, and a cloud of particle-hole excitations caused by phonon interactions lagging behind the electron density wave gets increasingly visible for larger x, t. Since the characteristic singularity at $x = v_F t$ is reduced compared to the free propagator G_0, it is expected that this will appear as a broadening of spectral peaks. For Landau quasiparticles, this corresponds to a finite lifetime τ_k.

6.3.2 Spinless Fermions With Density-Interactions

As shown by comparing eqs. (6.55) and (6.88), the change of $Z(x,t)$ when adding density interactions is represented by the transformation

$$S_j S_j^{-1} \Sigma_j^2 \to U_j U_j^\dagger \tag{6.124a}$$

$$S_j S_j^{-1} \Delta_j^2 \to V_j V_j^\dagger, \tag{6.124b}$$

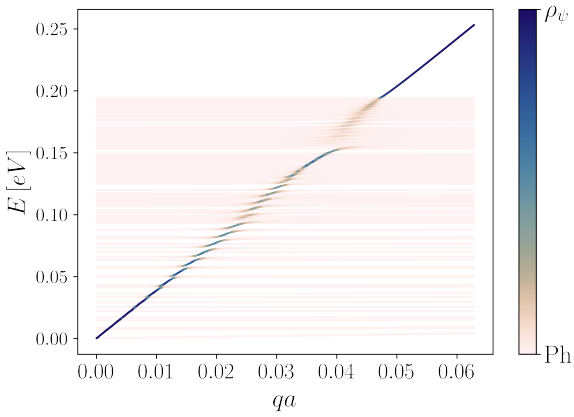

Figure 6.5: Hybridization of phonons and density on the armchair edges for a system with $N_y = 31$ at small values of qa. The color of the branches is determined by the projection onto density-bosons ρ_ψ which transitions close to avoided crossings.

where U_j and V_j are defined in eq. (6.79) and satisfy the sum rule

$$\sum_{j=1}^{4N_y+1} \left(U_j U_j^\dagger - V_j V_j^\dagger \right) = 1. \tag{6.125}$$

Hence, Z states for the spinless case

$$Z = \sum_{q>0} \sum_{j=1}^{4N_y+1} \frac{2\pi}{Lq} \mathrm{e}^{-\xi q} \left\{ \left(U_j U_j^\dagger \mathrm{e}^{iqx} + V_j V_j^\dagger \mathrm{e}^{-iqx} \right) \mathrm{e}^{-i\lambda_{q,j} t} - 2 V_j V_j^\dagger \right\}. \tag{6.126}$$

For a repulsive interaction, such as for instance the Coulomb interaction between electrons, the Bogoliubov mixing parameter θ_q given in eq. (5.72) is negative. As in eq. (6.74), the density-density interaction renormalize the electron-phonon coupling through $g_q \to g_q \mathrm{e}^{\theta_q}$, which means that the phonon interactions are suppressed for repulsive interactions.

In the numerical calculations, I have taken the density-density interaction to be on the form of a Coulomb interaction

$$V_q = \frac{\nu}{q^2}, \tag{6.127}$$

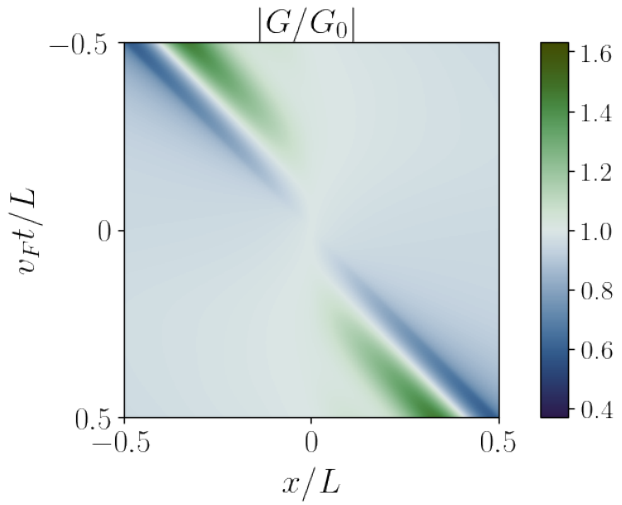

Figure 6.6: The absolute relative correction to the spinless Green's function G_0 caused by phonon interactions in the spinless case without density-interactions.

where ν is some coupling scale which I can vary. The renormalized Fermi dispersion is then given by eq. (5.68) as

$$\tilde{\varepsilon}_q = |q| v_F \sqrt{1 + \frac{\nu}{\pi v_F q^2}}. \tag{6.128}$$

Requiring that the Bogoliubov mixing parameter θ_q and energy is real puts a restriction on the interaction strength. All $\nu > 0$ is allowed, however the strength of attractive potentials are bounded by

$$\nu > -\frac{4\pi^3 v_F}{L^2} \equiv -\nu_0, \tag{6.129}$$

which is vanishing in the continuum limit $L \to \infty$. The excitation spectrum of the combined electron-phonon system is affected due to both the renormalized coupling constant and dispersion. In the low q limit, the spectrum goes as

$$\tilde{\varepsilon}_q = \omega_P + \frac{1}{2m^*} q^2 + \mathcal{O}(q^4), \tag{6.130}$$

where the effective mass is given by

$$m^* \equiv \frac{1}{v_F} \sqrt{\frac{\nu}{\pi v_F}}, \tag{6.131}$$

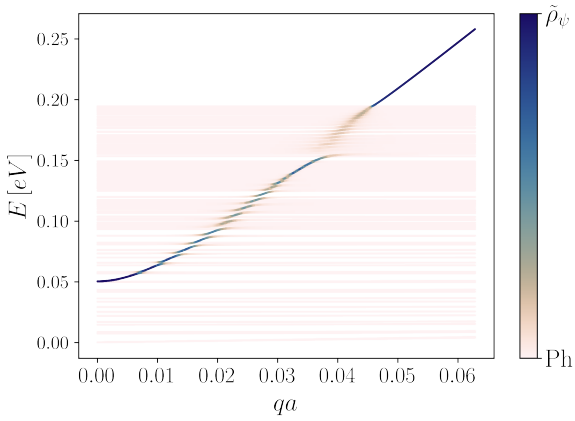

Figure 6.7: Hybridized bosonic excitation spectrum with Coulomb-like interaction and strength $\nu = \nu_0$ for a system of width $N_y = 31$. The colors is determined by the projection of eigenstates onto Bogoliubov transformed density-bosons $\tilde{\rho}_\psi$. The plasma frequency of this system is $\omega_P \simeq 0.05$eV.

and the plasma frequency is

$$\omega_P \equiv \sqrt{\frac{\nu v_F}{\pi}}. \tag{6.132}$$

This non-zero frequency describes oscillations in the electron density with zero propagation. As also pointed out by Tomonaga [25], ω_P is independent on the system length for a repulsive Coulomb-like interaction and only depends on the strength ν. The onset of density-interactions thus causes the excitation of oscillations in the long distance limit to cost a finite amount of energy, and also acquire a mass.

The hybridization between phonons and Bogoliubov transformed density-bosons in the presence of Coulomb-interaction is shown in fig. 6.7 for the same system as in fig. 6.5. If the plasma frequency ω_P is greater than the phonon scale ω_Γ, the presence of phonons will not affect the resulting fermion propagation as the fermions and phonons will not hybridize.

Since the low-energy limit of the density-bosons behaves different from for the case without density-density interactions, the behavior of momentum resolved Green's functions near the Fermi points $q = k - \eta_r k_F$ is expected to be qualitatively different from the $\nu = 0$ case. This is expected, as any interaction in the "g-ology"-models are known to destroy the discontinuity at the Fermi level, even at zero temperature [23], and the characteristic power-law behavior

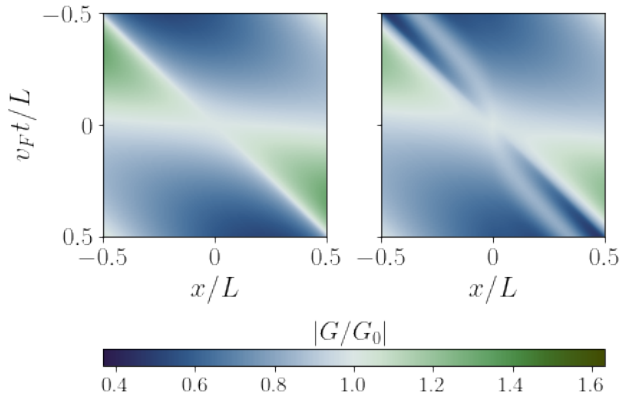

Figure 6.8: Relative correction to the non-interacting Green's function $G_0(x,t)$ without (left) and with (right) electron phonon coupling present. The interaction strength is in both panels $\nu = 0.1\nu_0$, and the system size is $N_y = 6$.

of the spectral function is known highly dependent of the specific interaction [34].

The relative correction including density-density interactions is shown for a small system size in fig. 6.8 both with and without electron-phonon corrections present. The coupling scale is set to $\nu = 0.1\nu_0$.

At this coupling strength, the Coulomb interaction is the most apparent contribution to the relative difference. This is consistent with Tomonaga [25], who pointed out that the effect of external perturbations to the plasma frequency is negligible for small q. The cone-like shape appears due to the non-vanishing plasma frequency ω_P and nonlinear spectrum in this finite system. However, the presence of phonons reduces the sharpness of the cone edges near $x = v_F t$, and partly recovers the amplitude reduction in the Green's function by electron interactions, as seen by the inverse "S"-like shape in the right panel of fig. 6.8.

6.3.3 Spinful Fermions

For the spinful case, Z is given by the constituent spin and charge sectors $Z_s + Z_c$ shown in eqs. (6.116) to (6.118). Since Z_s is independent of the phonon coupling, the relative correction to the Green's function will therefore only be dependent on Z_c, which for the spinless case has a rescaled electron-phonon coupling constant $g \to \sqrt{2}g$. The coefficients appearing in Z_c is shown in fig. 6.9 for the same parameters as fig. 6.4.

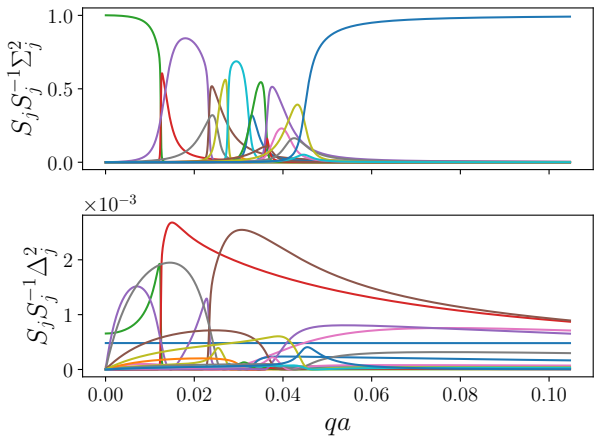

Figure 6.9: The same coefficients as in fig. 6.4, but with a rescaled coupling $g \to \sqrt{2}g$ which appears in the spin-dependent Green's functions. The coefficients $S_j S_j^{-1} \Delta_j^2$ reach values over twice the largest value in the spinless case, but is still multiple orders of magnitude smaller than $S_j S_j^{-1} \Sigma_j^2$.

In the case of no electron-electron interaction, the spin-sector is unaltered by the onset of electron-phonon coupling, and propagates with the free Fermi velocity v_F. In the charge sector, the hybridization of density bosons and phonons appears as a cloud of particle-hole excitations away from the characteristic singularity at $x = v_F t$. As pointed out, this suggests that spin-charge separation occur in the absence of spin-dependent interactions.

I now add a spin-dependent potential as in eq. (5.63). I take the shift from the Coulomb interaction in eq. (6.127) to be a constant on the form

$$U_q = U \equiv \nu_s \frac{\pi}{2} v_F, \tag{6.133}$$

where ν_s is dimensionless and sets the coupling scale for the spin sector. The renormalized dispersion for Bogoliubov spin-density bosons is then

$$\tilde{\varepsilon}_{s,q} = |q| v_F \sqrt{1 + \nu_s} \equiv \tilde{v}_s |q| \tag{6.134}$$

which means that the constant shift to the Coulomb interaction is restricted to

$$U \geq -\frac{\pi}{2} v_F, \tag{6.135}$$

and the Bogoliubov mixing parameter $\theta_{q,s}$ is constant and determined by

$$\tanh(2\theta_{q,s}) = \frac{-\nu_s}{\nu_s + 2}. \tag{6.136}$$

The generalization of $Z_s(x,t)$ to include spin-dependent interactions is completely equivalent to the spinless case without density-interactions in eq. (5.86), and states

$$Z_s = \sum_{q>0} \frac{\pi}{Lq} \mathrm{e}^{-\xi q} \left(\mathrm{e}^{iqx} \mathrm{e}^{-i\tilde{v}_F q t} + 2\sinh^2(\theta_{q,s}) \left(\cos(qx) \mathrm{e}^{-i\tilde{v}_F q t} - 1 \right) \right). \tag{6.137}$$

With the assumed spin-dependent potential, this integral can be solved analytically, and the spin-part of the Green's function is on the form

$$G_s \sim \left(\frac{1}{x - \tilde{v}_s t + i\xi} \right)^{\frac{1}{2}} \left(\frac{\xi^2}{(x - \tilde{v}_s t + i\xi)(-x - \tilde{v}_s t + i\xi)} \right)^{\frac{\gamma_s}{4}}, \tag{6.138}$$

where I have skipped prefactors, and introduced the constant$\gamma_s \equiv \sinh^2(\theta_{q,s})$ which for $|\nu_s| \ll 1$ is $\gamma_s \simeq \frac{\nu_s^2}{16}$. The relative correction to the spin sector is for weak interactions therefore dominated by

$$\frac{G_s}{G_s^0} \sim \left(\frac{x - v_F t + i\xi}{x - v_F \sqrt{1 + \nu_s} t + i\xi} \right)^{\frac{1}{2}}, \tag{6.139}$$

since the "cloud" factor in eq. (6.138) is very close to unity for small couplings. As seen in eqs. (6.134) and (6.139), a finite ν_s causes spin-densities to propagate with a velocity different than the unperturbed Fermi velocity. The charge-sector remains unaffected by the inclusion of spin dependency, apart from the aforementioned normalization of density-operators and rescaling of the electron-phonon coupling strength.

The relative correction to the Green's function is shown in fig. 6.10 for an armchair ribbon of width $N_y = 6$ where electron-phonon coupling and spin-interaction is turned on individually. The strength of the Coulomb interactions is $\nu = 0.1\nu_0$ and the spin-dependent shift is taken to be $\nu_s = 0.01$. For the case without Coulomb or spin-interaction, the addition of spin degrees of freedom in the system only appears as a renormalization of coupling g, and the relative correction is as expected very similar to the equivalent quantity in fig. 6.6 for the spinless case. By increasing the spin-interaction scale ν_s, the relative correction to the Green's function is dominated by the poles of eq. (6.139). By comparing the top row of fig. 6.10 with the spinless case in fig. 6.8, the cone-shape has a visible reduced sharpness at its edges. This is expected as all exponents are reduced by a factor 2 by including spin degrees of freedom.

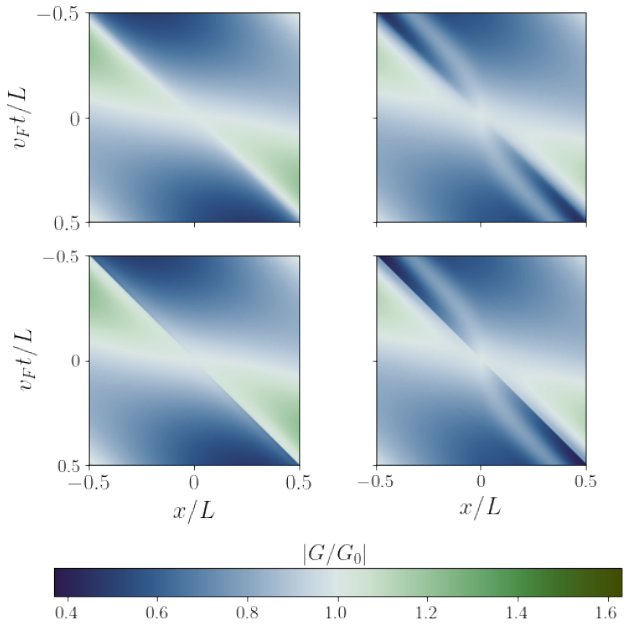

Figure 6.10: Relative correction to the spinful Green's function without (left column) and with (right column) electron phonon coupling. For the top row, spin-interaction is set to zero. For the bottom row, the spin coupling is determined by eq. (6.133) with $\nu_s = 0.01$. G_0 denotes the noninteracting Green's function where $g_q = V_q = U_q = 0$.

6.3.4 Conclusions, Multibranch Corrections

I have in this section numerically computed phonon corrections to the single particle Green's function. By utilizing the theory described in section 6.1.1, I can immediately write down the generalizations of the results in section 6.2 for the different cases I consider.

The electron-phonon coupling behave as $g_q \sim \alpha q$ for small q, which justifies the approximations made in section 6.2, and is found by projecting phonon eigenstates onto the edge of a graphene nanoribbon. The coupling is only relevant for energy scales $v_F|q| < \omega_\Gamma$, and the long distance physics is dominated by the coupling as $q \to 0^+$.

The effect of phonons has been demonstrated to dampen the singularity in $G(x,t)$ at $x = v_F t$ as x and t increases, which will appear as a broadening of δ-peaks in the spectral function. The inclusion of a Coulomb-like interac-

tions result in a non-zero plasma frequency ω_q. This is seen to appear as a precocious cloud of particle-hole excitations. Repulsive interactions suppress the electron-phonon coupling, and the lattice vibrations become irrelevant if $\omega_P > \omega_\Gamma$. Including spin degrees of freedom, adding a spin-dependent interaction renormalize the velocity of the spin-sector.

Chapter 7.
Summary and Extensions

7.1 Summary

Starting with a brief re capitulation of many-body quantum mechanics and an introduction to topological insulators, I have in this thesis studied the effect of phonons coupled to a fermionic density waves residing on the edge of a Quantum Spin Hall (QSH) insulator. More specifically, I have had the aim of computing one-particle correlation functions in the presence of quantized lattice vibrations on a graphene nanoribbon with armchair edge geometry. Gapless states residing in the bulk gap of a simple topological model is shown to be localized at the edges. A one-dimensional electron theory with linear dispersion is then used to model these close to the Fermi momentum. To obtain the phonon dynamics of the system, I follow the derivation of Thingstad et al. [69], Falkovsky [72] for the bulk bands, and apply the couplings to the finite width nanoribbon.

Following von Delft and Schoeller [76], I derive the bosonization identity for electrons in one dimension. This is used to compute the explicit forms of the single particle propagator in an interacting system.

I rederive the resulting form for the Green's function found by Meden et al. [31], and proceed to find a closed form approximation for a system with a linear electron-phonon coupling and a single acoustic phonon branch. I expand upon this framework, and derive equivalent forms of the correlation function in presence of a possibly spin-dependent two-electron interaction.

The resulting theory generalizes naturally to include several phonon branches, and by projecting phonon eigenstates onto the edges I numerically compute the single electron Green's function in their presence. This is then compared with the noninteracting Green's function G_0, and the relative correction induced by phonons is discussed for different scenarios.

In the spinless case without Coulomb interaction, the electron phonon coupling result in a cloud of particle-hole excitations lagging after a reduced singularity at $x = v_F t$, where v_F is the Fermi velocity. Adding a Coulomb-type interaction results in a plasma frequency in the infrared limit, whose effect on the relative correction to the Green's function is apparent, although phonon interactions partly suppresses this effect in the vicinity of the aforementioned particle-hole cloud. I show that density-density interactions renormalize the electron-phonon coupling strength which is suppressed for repulse interactions. Adding spin degrees of freedom to the system scales this coupling with a factor $\sqrt{2}$, and spin-charge separation occur as a consequence of phonon interactions. This is not realized by QSH insulators as the states are described by a single helicity quantum number and is equivalent to a spinless Luttinger liquid.

7.2 Extensions

Although the real space correlation functions give necessary physical insights to the system, the connection to experiments is usually found by considering the spectral function $A(k, \omega)$. To find this, a double Fourier transform of $G(x, t)$ needs to be performed. These are hard to obtain analytically, since the closed form approximations found (see for instance eq. (6.120)) involve branch cuts. The Fourier transform of the exact form for the propagator is worse, since the integral appearing in the quantity $Z(x, t)$ is generally difficult to compute other than in a few simple cases. One way to proceed with analytic investigations is by recursively expanding $G(x, t)$ in its Laurent series and using the Cauchy product of series to analytically perform the x-integration. The time integral can then be performed by replacing δ-functions by narrow Lorentzian functions [33, 34]. To my knowledge, this approach has neither been applied to an acoustic phonon branch nor to the combined problem with both density-interactions and coupling to quantized lattice vibrations present.

The calculations I have presented deals with the electron-phonon coupling in a non-perturbative fashion, although several crude approximate simplifications have been made. It would therefore be interesting to compare the results with the perturbative analysis by Apostol and Baldea [83], which I was only made aware of at a late stage in this work.

In topological insulators, spin-orbit interactions are known to be important. By the addition of such interactions, or even external magnetic fields, the lattice symmetry $z \to -z$ can be broken, and the assumption that out of plane phonon modes do not couple to fermions no longer hold. Crude estimates for the coupling to these modes can be calculated. Transverse out of plane phonons can also give rise to a spin-phonon coupling [61] which can be included in the computation of Green's functions.

Lastly, the effect of phonon interactions on top of $2k_F$ electron-electron scatterings is not considered in this work. At the edges of QSH insulators, such a scattering event requires a spin-flipping mechanism and is in the "g-ology"-models known as the $g_{1\perp}$ scattering process. In the presence of a Rashba impurity, it has been shown that transverse phonons can induce such scattering terms [62], and that the quantized spin Hall conductance is conserved to leading order in order.

Bibliography

[1] M. Konig, S. Wiedmann, C. Brune, A. Roth, H. Buhmann, L. W. Molenkamp, X.-L. Qi, and S.-C. Zhang. Quantum Spin Hall Insulator State in HgTe Quantum Wells. *Science*, 318(5851):766–770, nov 2007. doi:10.1126/science.1148047.

[2] O. Gröning, S. Wang, X. Yao, C. A. Pignedoli, G. Borin Barin, C. Daniels, A. Cupo, V. Meunier, X. Feng, A. Narita, K. Müllen, P. Ruffieux, and R. Fasel. Engineering of robust topological quantum phases in graphene nanoribbons. *Nature*, 560(7717):209–213, aug 2018. doi:10.1038/s41586-018-0375-9.

[3] C. Nayak, S. H. Simon, A. Stern, M. Freedman, and S. Das Sarma. Non-Abelian anyons and topological quantum computation. *Reviews of Modern Physics*, 80(3):1083–1159, sep 2008. doi:10.1103/RevModPhys.80.1083.

[4] X.-L. Qi and S.-C. Zhang. Topological insulators and superconductors. *Reviews of Modern Physics*, 83(4):1057–1110, oct 2011. doi:10.1103/RevModPhys.83.1057.

[5] M. Z. Hasan and C. L. Kane. Colloquium : Topological insulators. *Reviews of Modern Physics*, 82(4):3045–3067, nov 2010. doi:10.1103/RevModPhys.82.3045.

[6] D. J. Thouless, M. Kohmoto, M. P. Nightingale, and M. den Nijs. Quantized Hall Conductance in a Two-Dimensional Periodic Potential. *Physical Review Letters*, 49(6):405–408, aug 1982. doi:10.1103/PhysRevLett.49.405.

[7] K. V. Klitzing, G. Dorda, and M. Pepper. New Method for High-Accuracy Determination of the Fine-Structure Constant Based on Quantized Hall Resistance. *Physical Review Letters*, 45(6):494–497, aug 1980. doi:10.1103/PhysRevLett.45.494.

[8] F. D. M. Haldane. Model for a Quantum Hall Effect without Landau Levels: Condensed-Matter Realization of the "Parity Anomaly". *Physical Review Letters*, 61(18):2015–2018, oct 1988. doi:10.1103/PhysRevLett.61.2015.

[9] The Nobel Prize in Physics 2016, `https://www.nobelprize.org/prizes/physics/2016/summary/`.

[10] C. L. Kane and E. J. Mele. Quantum Spin Hall Effect in Graphene. *Physical Review Letters*, 95(22):226801, nov 2005. doi:10.1103/PhysRevLett.95.226801.

[11] B. A. Bernevig, T. L. Hughes, and S.-C. Zhang. Quantum Spin Hall Effect and Topological Phase Transition in HgTe Quantum Wells. *Science*, 314 (5806):1757–1761, dec 2006. doi:10.1126/science.1133734.

[12] E. Thingstad, A. Kamra, A. Brataas, and A. Sudbø. Chiral Phonon Transport Induced by Topological Magnons. *Physical Review Letters*, 122 (10):107201, mar 2019. doi:10.1103/PhysRevLett.122.107201.

[13] L. N. Cooper. Bound Electron Pairs in a Degenerate Fermi Gas. *Physical Review*, 104(4):1189–1190, nov 1956. doi:10.1103/PhysRev.104.1189.

[14] J. Bardeen, L. N. Cooper, and J. R. Schrieffer. Theory of Superconductivity. *Physical Review*, 108(5):1175–1204, dec 1957. doi:10.1103/PhysRev.108.1175.

[15] L. M. Cangemi, A. S. Mishchenko, N. Nagaosa, V. Cataudella, and G. De Filippis. Topological Quantum Transition Driven by Charge-Phonon Coupling in the Haldane Chern Insulator. *Physical Review Letters*, 123(4): 046401, jul 2019. doi:10.1103/PhysRevLett.123.046401.

[16] R. Stühler, F. Reis, T. Müller, T. Helbig, T. Schwemmer, R. Thomale, J. Schäfer, and R. Claessen. Tomonaga–Luttinger liquid in the edge channels of a quantum spin Hall insulator. *Nature Physics*, 16(1):47–51, jan 2020. doi:10.1038/s41567-019-0697-z.

[17] J. Strunz, J. Wiedenmann, C. Fleckenstein, L. Lunczer, W. Beugeling, V. L. Müller, P. Shekhar, N. T. Ziani, S. Shamim, J. Kleinlein, H. Buhmann, B. Trauzettel, and L. W. Molenkamp. Interacting topological edge channels. *Nature Physics*, 16(1):83–88, jan 2020. doi:10.1038/s41567-019-0692-4.

[18] H. A. Fertig and L. Brey. Luttinger Liquid at the Edge of Undoped Graphene in a Strong Magnetic Field. *Physical Review Letters*, 97(11): 116805, sep 2006. doi:10.1103/PhysRevLett.97.116805.

[19] L. D. Landau. The Theory of a Fermi Liquid. *Sov. Phys. JETP*, 3(6): 920–925, 1956.

[20] F. D. M. Haldane. 'Luttinger liquid theory' of one-dimensional quantum fluids. I. Properties of the Luttinger model and their extension to the general 1D interacting spinless Fermi gas. *Journal of Physics C: Solid State Physics*, 14(19):2585–2609, jul 1981. doi:10.1088/0022-3719/14/19/010.

[21] J. Voit. One-dimensional Fermi liquids. *Reports on Progress in Physics*, 58(9):977–1116, sep 1995. doi:10.1088/0034-4885/58/9/002.

[22] T. Giamarchi. *Quantum Physics in One Dimension*. Oxford University Press, dec 2003. ISBN 9780198525004. doi:10.1093/acprof:oso/9780198525004.001.0001.

[23] T. Giamarchi. One-dimensional physics in the 21st century. *Comptes Rendus Physique*, 17(3-4):322–331, mar 2016. doi:10.1016/j.crhy.2015.11.009.

[24] J. Voit. Charge-spin separation and the spectral properties of Luttinger liquids. *Physical Review B*, 47(11):6740–6743, mar 1993. doi:10.1103/PhysRevB.47.6740.

[25] S.-i. Tomonaga. Remarks on Bloch's Method of Sound Waves applied to Many-Fermion Problems. *Progress of Theoretical Physics*, 5(4):544–569, jul 1950. doi:10.1143/ptp/5.4.544.

[26] J. M. Luttinger. An Exactly Soluble Model of a Many-Fermion System. *Journal of Mathematical Physics*, 4(9):1154–1162, sep 1963. doi:10.1063/1.1704046.

[27] H. Gutfreund and M. Schick. Momentum Distribution in the Tomonaga Model. *Physical Review*, 168(2):418–425, apr 1968. doi:10.1103/PhysRev.168.418.

[28] G. Wentzel. The Interaction of Lattice Vibrations with Electrons in a Metal. *Physical Review*, 83(1):168–169, jul 1951. doi:10.1103/PhysRev.83.168.

[29] J. Bardeen. Electron-Vibration Interactions and Superconductivity. *Reviews of Modern Physics*, 23(3):261–270, jul 1951. doi:10.1103/RevModPhys.23.261.

[30] S. Engelsberg and B. B. Varga. One-Dimensional Electron-Phonon Model. *Physical Review*, 136(6A):A1582–A1598, dec 1964. doi:10.1103/PhysRev.136.A1582.

[31] V. Meden, K. Schönhammer, and O. Gunnarsson. Electron-phonon interaction in one dimension: Exact spectral properties. *Physical Review B*, 50(15):11179–11182, oct 1994. doi:10.1103/PhysRevB.50.11179.

[32] V. Meden and K. Schönhammer. Spectral functions for the Tomonaga-Luttinger model. *Physical Review B*, 46(24):15753–15760, dec 1992. doi:10.1103/PhysRevB.46.15753.

[33] V. Meden. Nonuniversality of the one-particle Green's function of a Luttinger liquid. *Physical Review B*, 60(7):4571–4575, aug 1999. doi:10.1103/PhysRevB.60.4571.

[34] L. Markhof and V. Meden. Spectral function of the Tomonaga-Luttinger model revisited: Power laws and universality. *Physical Review B*, 93(8): 085108, feb 2016. doi:10.1103/PhysRevB.93.085108.

[35] K. Schönhammer and V. Meden. Nonuniversal spectral properties of the Luttinger model. *Physical Review B*, 47(24):16205–16215, jun 1993. doi:10.1103/PhysRevB.47.16205.

[36] K. Schönhammer and V. Meden. Spectral sum rules for the Tomonaga-Luttinger model. *Physical Review B*, 48(15):11390–11393, oct 1993. doi:10.1103/PhysRevB.48.11390.

[37] T.-C. Hsieh, Y.-Z. Chou, and L. Radzihovsky. Finite-temperature spectroscopy of dirty helical Luttinger liquids. *Physical Review B*, 102(8): 085152, aug 2020. doi:10.1103/PhysRevB.102.085152.

[38] A. A. Abrikosov, L. P. Gorkov, and I. E. Dzyaloshinski. *Methods of Quantum Field Theory in Statistical Physics*. Dover Publications, rev. eng. edition, 1975. ISBN 0486632288.

[39] A. L. Fetter and J. D. Walecka. *Quantum theory of many-particle systems*. Dover Books on Physics. Dover, New York, NY, 2003. ISBN 9780486428277, https://cds.cern.ch/record/1985988.

[40] J. W. Negele and H. Orland. *Quantum many-particle systems*. Westview, 1988. ISBN 9780738200521.

[41] A. Altland and B. D. Simons. *Condensed Matter Field Theory*. Cambridge University Press, Cambridge, 2 edition, 2010. ISBN 9780511789984. doi:10.1017/CBO9780511789984.

[42] I. Žutić, J. Fabian, and S. Das Sarma. Spintronics: Fundamentals and applications. *Reviews of Modern Physics*, 76(2):323–410, apr 2004. doi:10.1103/RevModPhys.76.323.

[43] J. Linder and J. W. A. Robinson. Superconducting spintronics. *Nature Physics*, 11(4):307–315, apr 2015. doi:10.1038/nphys3242.

[44] X.-L. Qi and S.-C. Zhang. The quantum spin Hall effect and topological insulators. *Physics Today*, 63(1):33–38, jan 2010. doi:10.1063/1.3293411.

[45] C. L. Kane and E. J. Mele. Z2 topological order and the quantum spin hall effect. *Physical Review Letters*, 95(14):146802, sep 2005. doi:10.1103/PhysRevLett.95.146802.

[46] B. A. Bernevig and S.-C. Zhang. Quantum Spin Hall Effect. *Physical Review Letters*, 96(10):106802, mar 2006. doi:10.1103/PhysRevLett.96.106802.

[47] L. Fu and C. L. Kane. Topological insulators with inversion symmetry. *Physical Review B*, 76(4):045302, jul 2007. doi:10.1103/PhysRevB.76.045302.

[48] A. Rubio-García and J. J. García-Ripoll. Topological phases in the Haldane model with spin–spin on-site interactions. *New Journal of Physics*, 20(4):043033, apr 2018. doi:10.1088/1367-2630/aabb1a.

[49] J. de Lisle, S. De, E. Alba, A. Bullivant, J. J. Garcia-Ripoll, V. Lahtinen, and J. K. Pachos. Detection of Chern numbers and entanglement in topological two-species systems through subsystem winding numbers. *New Journal of Physics*, 16(8):083022, aug 2014. doi:10.1088/1367-2630/16/8/083022.

[50] G. Jotzu, M. Messer, R. Desbuquois, M. Lebrat, T. Uehlinger, D. Greif, and T. Esslinger. Experimental realization of the topological Haldane model with ultracold fermions. *Nature*, 515(7526):237–240, nov 2014. doi:10.1038/nature13915.

[51] P. W. Anderson. Absence of Diffusion in Certain Random Lattices. *Physical Review*, 109(5):1492–1505, mar 1958. doi:10.1103/PhysRev.109.1492.

[52] W. Zheng, H. Shen, Z. Wang, and H. Zhai. Magnetic-order-driven topological transition in the Haldane-Hubbard model. *Physical Review B*, 91 (16):161107, apr 2015. doi:10.1103/PhysRevB.91.161107.

[53] T.-W. Chen, Z.-R. Xiao, D.-W. Chiou, and G.-Y. Guo. High Chern number quantum anomalous Hall phases in single-layer graphene with Haldane orbital coupling. *Physical Review B*, 84(16):165453, oct 2011. doi:10.1103/PhysRevB.84.165453.

[54] S. A. Owerre. Topological honeycomb magnon Hall effect: A calculation of thermal Hall conductivity of magnetic spin excitations. *Journal of Applied Physics*, 120(4):043903, jul 2016. doi:10.1063/1.4959815.

[55] S. A. Owerre. A first theoretical realization of honeycomb topological magnon insulator. *Journal of Physics: Condensed Matter*, 28(38):386001, sep 2016. doi:10.1088/0953-8984/28/38/386001.

[56] L. Privitera, N. T. Ziani, I. Safi, and B. Trauzettel. Backscattering off a driven Rashba impurity at the helical edge. *Physical Review B*, 102(19): 195413, nov 2020. doi:10.1103/PhysRevB.102.195413.

[57] C. Wu, B. A. Bernevig, and S.-C. Zhang. Helical Liquid and the Edge of Quantum Spin Hall Systems. *Physical Review Letters*, 96(10):106401, mar 2006. doi:10.1103/PhysRevLett.96.106401.

[58] B. Braunecker, C. Bena, and P. Simon. Spectral properties of Luttinger liquids: A comparative analysis of regular, helical, and spiral Luttinger liquids. *Physical Review B*, 85(3):035136, jan 2012. doi:10.1103/PhysRevB.85.035136.

[59] P. Thalmeier. Surface phonon propagation in topological insulators. *Physical Review B*, 83(12):125314, mar 2011. doi:10.1103/PhysRevB.83.125314.

[60] I. Garate. Phonon-Induced Topological Transitions and Crossovers in Dirac Materials. *Physical Review Letters*, 110(4):046402, jan 2013. doi:10.1103/PhysRevLett.110.046402.

[61] S. Groenendijk, G. Dolcetto, and T. L. Schmidt. Fundamental limits to helical edge conductivity due to spin-phonon scattering. *Physical Review B*, 97(24):241406, jun 2018. doi:10.1103/PhysRevB.97.241406.

[62] J. C. Budich, F. Dolcini, P. Recher, and B. Trauzettel. Phonon-Induced Backscattering in Helical Edge States. *Physical Review Letters*, 108(8): 086602, feb 2012. doi:10.1103/PhysRevLett.108.086602.

[63] K. S. Novoselov. Electric Field Effect in Atomically Thin Carbon Films. *Science*, 306(5696):666–669, oct 2004. doi:10.1126/science.1102896.

[64] C. Lee, X. Wei, J. W. Kysar, and J. Hone. Measurement of the elastic properties and intrinsic strength of monolayer graphene. *Science*, 321 (5887):385–388, jul 2008. doi:10.1126/science.1157996.

[65] B. A. Bernevig and T. L. Hughes. *Topological insulators and topological superconductors*. Princeton University Press, 2013. ISBN 069115175X.

[66] A. H. Castro Neto, F. Guinea, N. M. R. Peres, K. S. Novoselov, and A. K. Geim. The electronic properties of graphene. *Reviews of Modern Physics*, 81(1):109–162, jan 2009. doi:10.1103/RevModPhys.81.109.

[67] P. Roushan, C. Neill, Y. Chen, M. Kolodrubetz, C. Quintana, N. Leung, M. Fang, R. Barends, B. Campbell, Z. Chen, B. Chiaro, A. Dunsworth, E. Jeffrey, J. Kelly, A. Megrant, J. Mutus, P. J. O'Malley, D. Sank, A. Vainsencher, J. Wenner, T. White, A. Polkovnikov, A. N. Cleland, and J. M. Martinis. Observation of topological transitions in interacting quantum circuits. *Nature*, 515(7526):241–244, nov 2014. doi:10.1038/nature13891.

[68] G. W. Semenoff. Condensed-Matter Simulation of a Three-Dimensional Anomaly. *Physical Review Letters*, 53(26):2449–2452, dec 1984. doi:10.1103/PhysRevLett.53.2449.

[69] E. Thingstad, A. Kamra, J. W. Wells, and A. Sudbø. Phonon-mediated superconductivity in doped monolayer materials. *Physical Review B*, 101 (21):214513, jun 2020. doi:10.1103/PhysRevB.101.214513.

[70] B. A. Bernevig, T. L. Hughes, S.-C. Zhang, H. D. Chen, and C. Wu. Band Collapse and the Quantum Hall Effect in Graphene. *International Journal of Modern Physics B*, 20(22):3257–3278, sep 2006. doi:10.1142/S0217979206035448.

[71] C. Kittel. *Introduction to solid state physics*. John Wiley & Sons Inc, 8 edition, 2004. ISBN 978-0-471-41526-8.

[72] L. A. Falkovsky. Phonon dispersion in graphene. *Journal of Experimental and Theoretical Physics*, 105(2):397–403, aug 2007. doi:10.1134/S1063776107080122.

[73] M. Bockrath, D. H. Cobden, J. Lu, A. G. Rinzler, R. E. Smalley, L. Balents, and P. L. McEuen. Luttinger-liquid behaviour in carbon nanotubes. *Nature*, 397(6720):598–601, feb 1999. doi:10.1038/17569.

[74] M. Dressel, K. Petukhov, B. Salameh, P. Zornoza, and T. Giamarchi. Scaling behavior of the longitudinal and transverse transport in quasi-one-dimensional organic conductors. *Physical Review B*, 71(7):075104, feb 2005. doi:10.1103/PhysRevB.71.075104.

[75] T. Li, P. Wang, H. Fu, L. Du, K. A. Schreiber, X. Mu, X. Liu, G. Sullivan, G. A. Csáthy, X. Lin, and R. R. Du. Observation of a Helical Luttinger Liquid in InAs/GaSb Quantum Spin Hall Edges. *Physical Review Letters*, 115(3):136804, sep 2015. doi:10.1103/PhysRevLett.115.136804.

[76] J. von Delft and H. Schoeller. Bosonization for beginners - refermionization for experts. *Annalen der Physik*, 7(4):225–305, nov 1998. doi:10.1002/(SICI)1521-3889(199811)7:4<225::AID-ANDP225>3.0.CO;2-L.

[77] D. C. Mattis and E. H. Lieb. Exact Solution of a Many-Fermion System and Its Associated Boson Field. *Journal of Mathematical Physics*, 6(2): 304–312, feb 1965. doi:10.1063/1.1704281.

[78] C. Tsallis. Diagonalization methods for the general bilinear Hamiltonian of an assembly of bosons. *Journal of Mathematical Physics*, 19(1):277–286, jan 1978. doi:10.1063/1.523549.

[79] E. J. Villaseñor. *Introduction to Quantum Mechanics*, volume 1023. Cambridge University Press, 2008. ISBN 9780735405462. doi:10.1063/1.2958160.

[80] P. A. M. Dirac. *The principles of quantum mechanics*. Oxford university press, 4th edition, 1981. ISBN 9780198520115.

[81] H. Fröhlich. Theory of the Superconducting State. I. The Ground State at the Absolute Zero of Temperature. *Physical Review*, 79(5):845–856, sep 1950. doi:10.1103/PhysRev.79.845.

[82] A. Luther and I. Peschel. Single-particle states, Kohn anomaly, and pairing fluctuations in one dimension. *Physical Review B*, 9(7):2911–2919, apr 1974. doi:10.1103/PhysRevB.9.2911.

[83] M. Apostol and I. Baldea. One-electron Green function for electrons coupled with acoustical phonons in one dimension. *Physics Letters A*, 88 (2):73–76, feb 1982. doi:10.1016/0375-9601(82)90594-1.

Appendix A.

A.1 Rashba Spin-Orbit Coupling on an Armchair Nanoribbon

In appendix I show the explicit matrix form of a Rashba spin-orbit coupling on an armchair nanoribbon. Beginning with the Hamiltonian

$$H_{SOC} = i\lambda_{SOC} \sum_{\langle i,j \rangle} \sum_{\sigma,\sigma'} c^\dagger_{i\sigma} (\boldsymbol{\delta}_{ij} \times \boldsymbol{\sigma})_z c_{j\sigma'}, \tag{A.1}$$

the same transformations as in section 4.2 is carried out. Here, the intrinsic spin degrees of freedom of the lattice fermions is not neglected, and I compute

$$\begin{aligned} H_{SOC} &= i\lambda_{SOC} \sum_D \sum_{i\in D} \sum_{\sigma,\sigma'} \sum_{\boldsymbol{\delta}} c^\dagger_{i,\sigma,D} \left(\delta_x \sigma_y - \delta_y \sigma_x\right) c_{i+\boldsymbol{\delta},\sigma',D'} \\ &= i\lambda_{SOC} \sum_D \sum_{(x,y)\in D} \sum_{\sigma,\sigma'} \sum_{\boldsymbol{\delta}} \frac{1}{N_x} \\ &\qquad \times \sum_{k_1,k_2} \mathrm{e}^{-ik_1 x} c^\dagger_{k_1,y,\sigma,D} \left(\delta_x \sigma_y - \delta_y \sigma_x\right) \mathrm{e}^{ik_2(x+\delta_x)} c_{k_2,y+\delta_y,\sigma',D'} \\ &= i\lambda_{SOC} \sum_D \sum_y \sum_{\sigma,\sigma'} \sum_{\boldsymbol{\delta}} \sum_k c^\dagger_{k,y,\sigma,D} \left(\delta_x \sigma_y - \delta_y \sigma_x\right) \mathrm{e}^{ik\delta_x} c_{k,y+\delta_y,\sigma',D'}. \end{aligned}$$

By using the familiar spinor representation for the fermion spins, $\sigma \in (\uparrow, \downarrow)$ where $|\uparrow\rangle = \begin{pmatrix} 1 \\ 0 \end{pmatrix}, |\downarrow\rangle = \begin{pmatrix} 0 \\ 1 \end{pmatrix}$, the relevant matrix elements are

$$\langle\uparrow|\sigma_x|\downarrow\rangle = 1 \qquad \langle\uparrow|\sigma_y|\downarrow\rangle = -i \tag{A.2a}$$

$$\langle\downarrow|\sigma_x|\uparrow\rangle = 1 \qquad \langle\downarrow|\sigma_y|\uparrow\rangle = i \tag{A.2b}$$

while other combinations of spins yield 0. For simplicity, I now use the notation $a_{k,y,\sigma} \equiv c_{k,y,\sigma,A}$ and $b_{k,y,\sigma} \equiv c_{k,y,\sigma,B}$. Using these relations and the nearest-neighbor vectors in fig. 4.9, the spin-interaction term is

$$\begin{aligned} H_{SOC} = ia\lambda_{SOC} \sum_y \sum_k \Big(& a^\dagger_{k,y,\uparrow} \left(-ib_{k,y,\downarrow} - \omega^* \theta_k b_{k,y+1,\downarrow} + \omega b_{k,y-1,\downarrow}\right) \\ & + a^\dagger_{k,y,\downarrow} \left(ib_{k,y,\uparrow} - \omega \theta_k b_{k,y+1,\uparrow} + \omega^* b_{k,y-1,\uparrow}\right) \\ & + b^\dagger_{k,y,\uparrow} \left(ia_{k,y,\downarrow} + \omega^* \theta^*_k a_{k,y-1,\downarrow} - \omega a_{k,y+1,\downarrow}\right) \\ & + b^\dagger_{k,y,\downarrow} \left(-ia_{k,y,\uparrow} + \omega \theta^*_k a_{k,y-1,\uparrow} - \omega^* a_{k,y-1,\uparrow}\right) \Big), \end{aligned}$$

with $\omega = \frac{1}{2}(i + \sqrt{3}) = \mathrm{e}^{i\frac{\pi}{6}}$. Introducing the spinful basis

$$\psi_k = (a_{k,1,\uparrow}, a_{k,1,\downarrow}, b_{k,1,\uparrow}, b_{k,1,\downarrow}, \ldots, a_{k,N_y,\uparrow}, a_{k,N_y,\downarrow}, b_{k,N_y,\uparrow}, b_{k,N_y,\downarrow}) \tag{A.3}$$

and $\alpha \equiv i\omega$ leads to the matrix representation

$$H_{SOC} = \lambda_{SOC} \begin{pmatrix} & & & 1 & & & & \alpha^*\theta_k & \\ & & -1 & & & & -\alpha\theta_k & & \\ & -1 & & & & -\alpha & & & \\ 1 & & & & \alpha^* & & & & \\ & & & \alpha & & & & 1 & \\ & & -\alpha^* & & & & -1 & & \\ & -\alpha^*\theta_k^* & & & & -1 & & & \\ \alpha\theta_k^* & & & & 1 & & & & \\ & & & & & & & & \ddots \end{pmatrix}. \tag{A.4}$$

A.2 Mathematical Identities

Lattice Summation

When introducing discrete Fourier transformed operators into a lattice Hamiltonian, the identity

$$\sum_i \mathrm{e}^{i(k-k')r_i} = N\delta(k-k') \tag{A.2.1}$$

is often used, where N is the number of lattice sites covered in the summation over i.

Hilbert Space Operator Identities

Consider two operators A and B acting on a Hilbert space, $\mathcal{H}$. The Baker-Campbell-Hausdorff formula states

$$\mathrm{e}^A\mathrm{e}^B = \mathrm{e}^{A+B+\frac{1}{2}[A,B]+\text{Higher order commutators}}. \tag{A.2.2}$$

An alternative, and equivalent representation of this is

$$\mathrm{e}^{iB\lambda}A\mathrm{e}^{-iB\lambda} = A + i\lambda[B,A] + \frac{(i\lambda)^2}{2!}[B,[B,A]] + \ldots. \tag{A.2.3}$$

Thus, if the commutator $[B,A] = \alpha A$. where $\alpha \in \mathbb{C}$ is a complex number, then this relation implies

$$\mathrm{e}^{iB\lambda}A\mathrm{e}^{-iB\lambda} = A\mathrm{e}^{i\lambda\alpha}. \tag{A.2.4}$$

If $C \equiv [A,B]$ with $[C,A] = [C,B] = 0$, i.e. that C is a (complex) number, then the relation

$$\mathrm{e}^{-B}f(A)\mathrm{e}^{-B} = f(A+C) \tag{A.2.5}$$

holds for a function f. Both f and the exponential function is here defined by its Taylor series representation.

If the Hamiltonian is on the form $H = \sum_i \omega_i b_i^\dagger b_i$, describing free bosons, and $X = \sum_i(\alpha_i b_i + \beta_i b_i^\dagger)$ with $\alpha_i, \beta_i \in \mathbb{C}$ is an operator, then [76]

$$\left\langle \mathrm{e}^X \right\rangle = \mathrm{e}^{\frac{1}{2}\left\langle X^2 \right\rangle}. \tag{A.2.6}$$

Karl Kristian Ladegård Lockert

Phonon Coupled Luttinger Liquids in a Haldane Armchair Nanoribbon

NTNU
Norwegian University of
Science and Technology